



HAL
open science

Towards a Deeper Understanding of Preferential Enrichment. A Case Study: DL Arginine Fumarate in Ethanol-Water 50-50 Mixture

Clément De Saint Jores

► **To cite this version:**

Clément De Saint Jores. Towards a Deeper Understanding of Preferential Enrichment. A Case Study : DL Arginine Fumarate in Ethanol-Water 50-50 Mixture. Cristallography. Normandie Université, 2019. English. NNT : 2019NORMR007 . tel-02132142

HAL Id: tel-02132142

<https://theses.hal.science/tel-02132142>

Submitted on 16 May 2019

HAL is a multi-disciplinary open access archive for the deposit and dissemination of scientific research documents, whether they are published or not. The documents may come from teaching and research institutions in France or abroad, or from public or private research centers.

L'archive ouverte pluridisciplinaire **HAL**, est destinée au dépôt et à la diffusion de documents scientifiques de niveau recherche, publiés ou non, émanant des établissements d'enseignement et de recherche français ou étrangers, des laboratoires publics ou privés.



Normandie Université

THÈSE

Pour obtenir le diplôme de doctorat

Spécialité Chimie

Préparée au sein de l'Université de Rouen Normandie

**Towards a Deeper Understanding of Preferential Enrichment.
A Case Study: DL Arginine Fumarate in Ethanol-Water 50-50 Mixture**

**Présentée et soutenue par
Clément DE SAINT JORES**

**Thèse soutenue publiquement le 27 février 2019
devant le jury composé de**

M. Rui TAMURA	Pr Kyoto University	Rapporteur
M. Alain BERTHOD	DR Université Claude Bernard Lyon I	Rapporteur
M. Frédéric GUILLEN	Pr Université Toulouse III - Paul Sabatier	Président
Mme Najla GHARBI	MCF Université de Rouen Normandie	Examineur
M. Pascal CARDINAEL	Pr Université de Rouen Normandie	Directeur de thèse
M. Gérard COQUEREL	Pr Université de Rouen Normandie	Codirecteur de thèse

Thèse dirigée par Pascal CARDINAEL et Gérard COQUEREL professeurs des universités au laboratoire Sciences et Méthodes Séparatives (EA3233 SMS)





Normandie Université

THÈSE

Pour obtenir le diplôme de doctorat

Spécialité Chimie

Préparée au sein de l'Université de Rouen Normandie

**Vers une meilleure compréhension de l'enrichissement préférentiel.
Un cas d'étude : le Fumarate de DL Arginine dans un mélange 50/50
eau/ethanol**

**Présentée et soutenue par
Clément DE SAINT JORES**

**Thèse soutenue publiquement le 27 février 2019
devant le jury composé de**

M. Rui TAMURA	Pr Kyoto University	Rapporteur
M. Alain BERTHOD	DR Université Claude Bernard Lyon I	Rapporteur
M. Frédéric GUILLEN	Pr Université Toulouse III - Paul Sabatier	Président
Mme Najla GHARBI	MCF Université de Rouen Normandie	Examineur
M. Pascal CARDINAEL	Pr Université de Rouen Normandie	Directeur de thèse
M. Gérard COQUEREL	Pr Université de Rouen Normandie	Codirecteur de thèse

**Thèse dirigée par Pascal CARDINAEL et Gérard COQUEREL professeurs des universités au
laboratoire Sciences et Méthodes Séparatives (EA3233 SMS)**



C'est des démarches.

(Xavier "MV" Dang)

On va l'avoir cette thèse.

(Une amie)

Acknowledgments

First of all, I would like to thank my thesis director Prof. Pascal Cardinael, for his confidence in my work during the second year of my Master's and my thesis. I really appreciate our scientific discussions. During these four years you gave to me your passion for chirality.

I would like to thank Prof. Gérard Coquerel head of the laboratory for accepting me inside his laboratory and also for being the co-director of my PhD thesis.

I thank Dr. Najla Gharbi for her supervision.

I would like to thank all the members of the jury: Prof. Rui Tamura, Dr. Alain Berthod and Prof. Frédéric Guillen for having accepted to review this work.

J'aimerais remercier le Dr Clément Brandel pour son aide pendant ces trois années de thèse et tout particulièrement pour ses conseils avisés lors de la rédaction de ce manuscrit. J'aimerais également le remercier pour sa grande gentillesse.

Je souhaite remercier le Pr Jean-Philippe Bouillon d'avoir accepté d'être mon référent de thèse et de m'avoir toujours soutenu et conseillé lors de mon cursus universitaire.

Je voudrais remercier tout particulièrement Marie Vaccaro qui m'a beaucoup aidé durant mes quatre années au laboratoire. Sans elle l'ensemble de mes manipulations aurait été plus compliqué, la préparation de plus de 2000 solutions m'a beaucoup aidé. J'aimerais également la remercier pour son soutien dans mes moments difficiles, sa bonne humeur (pas tous les jours certes), pour m'avoir fait rire souvent (des fois à son insu), pour toutes nos discussions sur des sujets variés et pour son amitié.

Je remercie Lætitia Bailly pour son humour et pour le prêt de ses chaînes pendant ces quatre ans. Je remercie également Émilie Petit pour l'aide qu'elle m'a apportée lors de mes manipulations et pour toutes nos expériences en SFC. Je voudrais les remercier toutes les deux pour toutes nos discussions plus ou moins chromatographiques et le partage de Tagada. Je voudrais remercier Françoise Ringot pour les deux ans et demi à partager le même bureau à l'IRCOF et pour ses pesées à la précision remarquable. Je voudrais également remercier quelques autres personnes du Laboratoire COBRA notamment Babette (ma maman de laboratoire) et Alex (qui est parti maintenant).

Je remercie la Dr Morgane Sanselme pour son aide dans le domaine des cristaux, pour la structure de l'asparagine (un jour je te donnerai un bon monocristal) et pour nos autres activités à base de bières et de jeux de société. Je remercie aussi le Dr Nicolas Couvrat (¡El fuego!) pour ses analyses thermiques et son côté grincheux.

Je voudrais remercier la Dr Marie Hubert-Roux et la Dr Isabelle Schmitz-Afonso, pour leur aide, leurs conseils et leurs disponibilités, pour les analyses en LC-MS.

Je remercie les différents permanents du laboratoire pour nos discussions. Avec un remerciement spécial pour Lucie, Céline et Séverine, je continuerai de vous embêter.

Je remercie les étudiants que j'ai pu côtoyer pendant ces années en commençant par les anciens : Mélanie pour son aide précieuse et nos manipulations en commun qui ont été très importantes pour moi, ainsi que pour sa grande gentillesse et les congrès passés ensemble avec le petit déjeuner prêt quand on se lève ; Aurélien qui m'a supporté pendant la rédaction de sa thèse ; Émilie (27 en force) avec qui les discussions scientifiques et non-scientifiques ont été très fructueuses ; Benjamin pour sa générosité, les séances de sport et les six mois dans le même bureau ; Li Na (Hélène) pour son sourire et nos discussions bilingues à des horaires parfois improbables et Quentin le spécialiste de l'Hilic ; ainsi que les anciens qui sont encore là : Antoine (qui est de nouveau désagréable, et ça fait plaisir !) pour toutes nos discussions de chimie organique et de chromatographie et Simon (Loulou) pour sa "folie" et ses manipulations en SHG et en In-SituX.

Je remercie particulièrement mes deux collègues qui ont commencé en même temps que moi : Bienvenu pour m'avoir fait rire et avoir fait de la science incompréhensible ; F.X. (Choup') qui m'a beaucoup aidé à comprendre les diagrammes de phases et les procédés de cristallisation, je le remercie également pour les schémas de diagrammes de phases. Je vous souhaite à tous les deux de beaux projets pour la suite.

La liste des étudiants ne serait pas complète sans les petits : "La Belle" Manon une collègue super, avec qui j'ai partagé des galères du doctorat et de la rédaction ; Marine que la force l'accompagne pendant sa thèse ; Aurélien avec son humour ; Adeline la succession en chromato ; Kangli ; Aliou ; Lina 2 et Ryusei.

Je voudrais remercier deux étudiantes qui sont passées au labo et qui ont beaucoup compté pour moi : Adeline et Nihad, j'espère que vos fins de thèse se passeront bien.

Je voudrais remercier les stagiaires que j'ai pu avoir pendant mon doctorat, Marie, Ambre, Kori et Manon 2, ainsi que les stagiaires organiciens du laboratoire : François et Valentin.

Je voudrais remercier Baptiste pour nos nombreuses aventures, pour nos soirées improvisées, pour nos discussions de chimie mais pas que, ainsi que pour le prêt de sa cuisine pour la réalisation de crêpes.

Je voudrais remercier mes amis pour m'avoir permis de me changer les idées et pour leur soutien. Merci à Thomas qui a bien voulu corriger mes fautes dans ce manuscrit.

Je voudrais, pour finir, remercier ma famille qui m'a supporté et toujours soutenu. Je sais que les histoires de mains droites et de mains gauches ne sont pas évidentes pour eux.

Table of contents

Acknowledgments	1
Table of contents	4
Introduction	8
I Generalities	10
1 Chirality	11
1.1 Definition	11
1.2 Nomenclature	11
1.3 Chiral Molecule Properties	12
1.3.1 Physicochemical Properties	12
1.3.2 Biological and Pharmaceutical Properties	12
2 Crystalline State	13
2.1 Crystallization	13
2.2 Crystallography	15
3 Phase Diagrams of Chiral Molecules	15
3.1 Thermodynamics State of the Art	15
3.2 Binary Systems of Enantiomers	16
3.2.1 Racemic Compound	16
3.2.2 Conglomerate	17
3.2.3 Solid Solution	18
3.2.4 Metastable Equilibria	19
3.3 Ternary Systems	20
3.4 Higher Dimensions	21
4 Other Considerations about Solid State	22
4.1 Polymorphism	22
4.2 Salt, Co-crystal, Solvate	23
5 Access to Pure Enantiomer	24
5.1 Non-enantioselective Synthesis from the Chiral Pool	25
5.2 Asymmetric Synthesis	25

5.3	Chiral Chromatography	25
5.3.1	Liquid Chromatography (HPLC)	26
5.3.2	Other Chromatographic Techniques	27
5.3.2.1	Simulated Moving Bed (SMB)	27
5.3.2.2	Supercritical Fluid Chromatography (SFC)	27
5.3.2.3	Gas Chromatography (GC)	28
5.4	Crystallization	28
5.4.1	Pasteurian Resolution	28
5.4.2	Preferential Crystallization	29
5.4.3	Deracemization	30
6	Preferential Enrichment	31
6.1	Presentation of the Phenomenon	31
6.2	Mechanisms	35
6.2.1	Mechanism of 2002, Proposed on the Basis of the First Generation of Compounds	35
6.2.2	Mechanism of 2016 Proposed on the Basis of the First Generation of Compounds and Adapted to the Second Generation of Compounds	39
6.3	Criteria for the Establishment of Preferential Enrichment	41
II	Analytical Methods	42
1	Introduction	43
2	Method for the Impurity Profile Determination	43
3	Quantification and Determination of Enantiomeric Excess Using HPLC-UV Method	49
3.1	Method Development	49
3.2	Method Validation	54
3.2.1	Specificity	55
3.2.2	Linearity	55
3.2.3	Precision	56
3.2.3.1	Repeatability	56
3.2.3.2	Ruggedness and Intermediate Precision	57
3.2.4	Accuracy	58
3.2.5	Limit of Detection and Limit of Quantification	60
3.2.6	Conclusion of the validation	60

4	Quantification Method of the ¹³C₆L-Arginine: HPLC-MS/MS	61
4.1	Method Development	61
4.1.1	Analytical Conditions	61
4.1.2	Fragmentation	61
4.2	Quantification	63
5	Conclusion	65
III Mechanism of Preferential Enrichment for Second Generation Compounds – Case Study of Arginine Fumarate		
1	Introduction	67
2	Presentation of the Preferential Enrichment Process of Arginine Fumarate and Effects of its Parameters	67
2.1	The Arginine Fumarate System	67
2.2	Presentation of the Preferential Enrichment Process of Arginine Fumarate	72
2.3	Statistical study	73
2.4	Effect of the Parameters	75
2.4.1	Overall Composition Effect	75
2.4.1.1	Effect of Starting Enantiomeric Excess	75
2.4.1.2	Effect of starting supersaturation	76
2.4.2	Equilibrium state	77
2.4.2.1	Influence of Agitation: Use of a Rocking plate	78
2.4.2.2	Evolution of a System after PE	79
3	Monitoring of the Preferential Enrichment Process of Arginine Fumarate	80
3.1	Monitoring of Preferential Enrichment <i>versus</i> Time	80
3.2	Successive Dissolution of the Solid Phase	82
3.2.1	Protocol	83
3.2.2	Results of Successive Dissolution of Solid Phase	83
4	Study of the Mechanism of Arginine Fumarate Preferential Enrichment	86
4.1	Addition of Labeled Arginine	86
4.1.1	Addition during PE experiments starting with an initial e.e. of D	87
4.1.1.1	Addition after 2.5 h of PE	87
4.1.1.2	Addition after 6 h of PE	89
4.1.1.3	Addition after 6 days of PE	90

4.1.2	Addition during PE experiments starting with an initial e.e. of L	92
4.1.2.1	Addition after 2.5 h of PE	92
4.1.2.2	Addition after 6 days of PE	93
4.1.3	Comparison between addition during PE experiments starting with an initial e.e. of D and starting with an initial e.e. of L . . .	95
4.2	About the Occurrence of Phase Transitions during PE of Arg-Fum . . .	96
4.2.1	Observation of the Deposited Crystals during PE Process by Microscopy	96
4.2.2	In-situ X-Ray Powder Diffraction: In-SituX	98
4.3	Molecular modeling of the solid solution	102
4.3.1	Modeling Solid Solution from Arginine Fumarate Structure . . .	102
4.3.2	Modeling Solid Solution for DL-Tryptophan Ethyl Ester Hydrochloride	103
4.3.3	Modeling Solid Solution for Other Compounds of First and Second Generations	105
4.4	Further Preferential Enrichment after the End of the Process	106
5	Conclusion	106
General Conclusion: About the Mechanism of Preferential Enrichment and Revision of the Required Criteria		108
Bibliography		117
Appendices		126
A	Experimental part	127
B	Bravais Lattices and Number of Associated Space Groups	131
C	Method validation supplementary tables and figures	132
D	Case of tryptophan ethyl ester hydrochloride	135
E	PE without Supersaturation	138

Introduction

An important part of active pharmaceutical ingredients are chiral. Since two opposite enantiomers may have different and sometimes opposite biological properties, chiral separation is mandatory to know their biological effects.

Among the available methods to obtain pure enantiomer from a racemic mixture, chiral resolution by means of crystallization is often the cheapest method and therefore the most used for industrial applications. There are several crystallization techniques, the most encountered being Pasteurian resolution which consists in resolving diastereomeric salts. In the cases of conglomerate forming systems, resolution is possible by preferential crystallization, or for racemizable systems, via deracemization. Another method developed by Prof. Tamura's group in the late 90's is Preferential Enrichment.

Preferential Enrichment is an out of equilibrium process, performed with a high initial supersaturation (4 to 25 fold supersaturated). Starting with a slightly enriched solution, this unusual spontaneous symmetry breaking phenomenon occurs in stagnant conditions, and generates at the end of the process (*i.e.* several days) a mother liquor highly enriched in one enantiomer and deposited crystals slightly enriched in the opposite enantiomer. Preferential Enrichment can achieve enantiomeric excess up to 95% in the mother liquor with a moderate yield, depending on the system. Prof. Tamura proposed a mechanism in 2002, and improved it in 2016. Based on this mechanism, various criteria have been defined in order to identify systems which can perform Preferential Enrichment.

The objective of this thesis is to get a deeper understanding of the mechanism of preferential enrichment and also confirm Tamura's criteria, using the case study of arginine fumarate salt in water/ethanol mixture described by Prof. Tamura's group in 2014.

In order to accurately analyze the mother liquor and the deposited crystals, different HPLC methods are developed. Two chromatographic methods are developed: one achiral to evaluate the purity and the other one, chiral for the quantification of the concentration of enantiomers and the determination of the enantiomeric excess. In addition the operating conditions are chosen in order to be compatible with mass spectrometry detection.

In order to get a clearer picture of the mechanism of preferential enrichment, the influence of different parameters are studied: the overall composition (*i.e.* supersaturation and initial enantiomeric excess), the hydrodynamics of the solution and the duration of experiments. Then a time based monitoring of the mass balance in the mother liquor and

in the deposited crystals is performed as well as successive redissolutions of the deposited crystals. These experiments are performed to measure the evolution of the enantiomeric excess of the solid phase during the crystallization process.

Fine tuned experiments are then performed to understand the key points of the mechanism and consist in the addition of labeled-L-Arginine in order to observe the possible exchanges of enantiomers between solid and liquid phases. In-situ X-Ray powder diffraction is used to observe phase transitions and their influence on preferential enrichment. Theoretical solid solutions are modeled on systems which perform Preferential Enrichment and compared with a system which presents all requirements for PE but failed to show the phenomenon.

To conclude this PhD work, we propose an update of the criteria required to select a system to perform Preferential Enrichment. A revised mechanism accounting for all experimental results presented therein is also given.

Chapter I

Generalities

1 Chirality

1.1 Definition

The word “chiral” was firstly used for molecules by Lord Kelvin in 1884:¹ “*I call any geometrical figure, or group of points, chiral and say that it has chirality if its image in a plane mirror, ideally realized, cannot be brought to coincide with itself.*”

“Chiral” comes from Greek “ $\chi\epsilon\iota\rho$ ” (cheir) which means hand (FIGURE I.1). For a chemical substance, a molecule and its mirror image are called enantiomers, if they are not superimposable.²

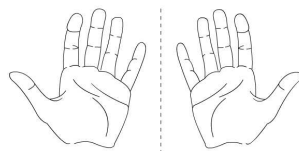


FIGURE I.1 – A right hand and a left hand are mirror images but they are not superimposable

1.2 Nomenclature

Different descriptors can be used to determine the chirality of a molecule.

- In order to describe the direction of deviation of a polarized light, (+) and (–) notations are used for a clockwise deviation and for a counterclockwise deviation respectively. Descriptors (+) and (–) can also be called *d* or *l* for dextrogyre and levogyre. However the rotation direction depends on experimental conditions (*i.e.* solvent, concentration, temperature, wavelength...)
- CIP system (Cahn, Ingold, Prelog) allows us to determine the absolute configuration of a chiral molecule.³ Stereodescriptors R (*Rectus*) and S (*Sinister*) describe the configuration of a stereogenic center (FIGURE I.2).
- Nomenclature D and L, used mainly for the description of natural molecules such as amino acids, or sugars, gives the position of the priority group on the penultimate carbon of the molecule represented in Fischer projection (FIGURE I.2).

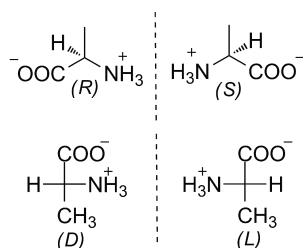


FIGURE I.2 – Structures and Fischer projections of (R)/(D)-Alanine and (S)/(L)-Alanine

Other types of chirality exist: axial chirality (atropisomerism), planar chirality and helical chirality.⁴ In these case, the two species are named antipodes.

Enantiomeric compositions of a chiral system can be described differently: a compound is enantiopure when only one enantiomer is present, if both enantiomers are present in equal quantities the mixture is called racemic mixture, and when the composition is neither racemic nor enantiopure it is called scalemic (or non racemic).

To describe a chiral composition, different expressions can be used,⁵ the most used being the enantiomeric excess (e.e.) defined by Morrison and Mosher in 1971.⁶ The ratio is defined (Eq. I.1) by the following equation with E_1 being the amount of major enantiomer and E_2 being the amount of minor enantiomer.

$$\%e.e. = \frac{E_1 - E_2}{E_1 + E_2} \times 100 \quad (\text{Eq. I.1})$$

e.e. is equal to 0% for a racemic mixture and to 100% for an enantiopure compound.

1.3 Chiral Molecule Properties

1.3.1 Physicochemical Properties

Two enantiomers of a molecule have the same scalar properties: melting point, solubility (in an achiral solvent)...

However, their vectorial properties are opposite: optical rotation or crystal packing.

1.3.2 Biological and Pharmaceutical Properties

In nature, some molecules such as sugars or amino-acids are enantiopure.⁴ Two enantiomers may not have the same properties on living organisms, on different receptors, proteins, enzymes...

In pharmacology two enantiomers with different biological activities are called eutomer for the most active one and distomer for the less active one.⁵

Examples of chiral molecules with pharmaceutical interest:⁷

- Ibuprofen (an anti inflammatory) S (+) enantiomer is more active,⁸
- Propranolol (a β -blocker) S (-) enantiomer is more active,
- Isoflurane (an anesthetic) S (+) enantiomer is more active,
- Methadone (an opioid analgesic) only R (-) enantiomer is active.

2 Crystalline State

2.1 Crystallization

In order to form a crystal lattice, molecules need to self-assemble. Crystallization is the transition from a disordered state (amorphous, liquid, gas) to an organized solid phase.⁹ If only a pure compound is used, an unary phase diagram is sufficient to highlight the crystallization process (FIGURE I.3).

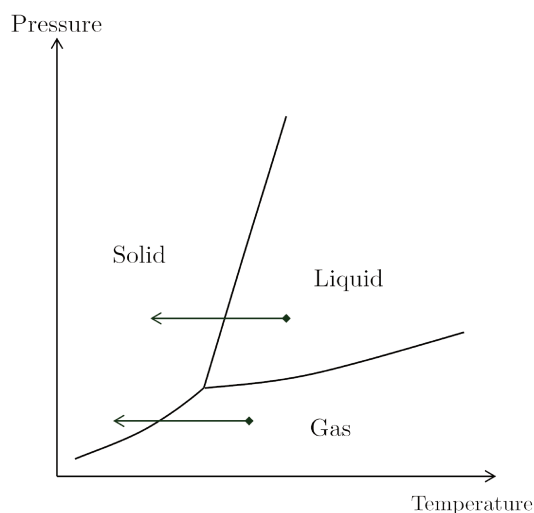


FIGURE I.3 – Representation of a unary phase diagram, arrows represent possible processes of crystallization from a liquid or a gas phase

In most cases, crystallization of a compound is performed from a solution. In this case, equilibria between solvent and the compound need to be considered. Crystallization is divided into four main steps.

1. Generation of a driving force: the supersaturation β ¹⁰ as defined in Eq. I.2 (with C being concentration of the compound in solution, and $C_{\text{saturation}}$ being concentration at saturation of the compound at a given temperature). Supersaturation is necessary to enable aggregation of molecules into clusters.¹¹

$$\beta = \frac{C}{C_{\text{saturation}}} \quad (\text{Eq. I.2})$$

2. Once the driving force is established, and first clusters created, the first step of crystallization begins: a group of molecules are assembled similarly to the crystal packing forming a *nucleus*. Two types of nucleation exist.
 - Primary nucleation,^{12,13} which corresponds to the development of nanocrystals from the medium without previous existence of a *nuclei*. It is named homogeneous if the *nucleus* appears inside the solution or named heterogeneous if it appears on the surface of a solid (reactor walls, stirrer...). Heterogeneous nucleation is less energy consuming than homogeneous nucleation.
 - Secondary nucleation,¹⁴ which corresponds to the creation of new *nuclei* from existing crystals in the system, mainly due to collisions with other crystals or reactor walls.
3. Once a *nucleus* reaches its critical radius, it grows absorbing surrounding molecules from the solution. Solvated molecules are organized on the surface of crystals.
4. The last step is Ostwald ripening.¹⁵ Since there are more than one crystal inside the solution, smaller ones are dissolved for the benefit of larger ones. Larger crystals are thermodynamically more stable than smaller ones, because they have a better ratio between surface and volume. If given sufficient time to the system, only one single crystal will remain.

In solution, two pathways are possible to obtain crystals. The first one is named *A* in FIGURE I.4, and performed by solvent evaporation at constant temperature: supersaturation increases to a threshold after which the compound nucleates. The second one, named *B* in FIGURE I.4, is performed by cooling, supersaturation is reached by solubility decrease.

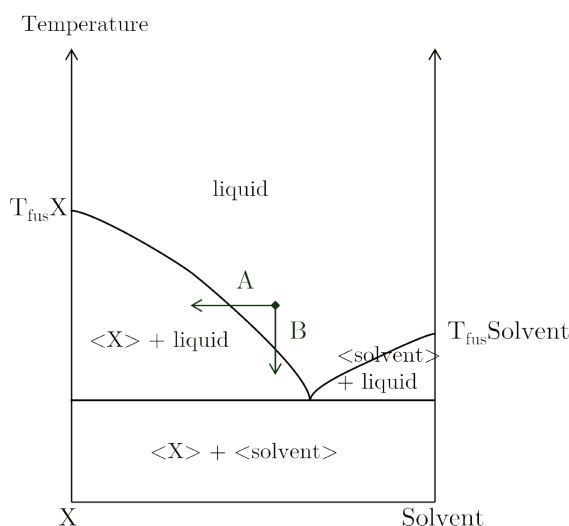


FIGURE I.4 – Representation of a binary phase diagram between a compound *X* and a solvent, arrows are representing possible processes of crystallization of compound *X* from solution

Pathway *B* (*i.e.* crystallization by cooling) has been used for the crystallization of our samples in this work.

2.2 Crystallography

The periodic nature of the molecular packing inside crystals is described by crystallography. Any crystalline substance is associated to one of the 230 space groups derived from the 14 Bravais lattices (Appendix B) which describe the symmetry of the crystal lattice.

For organic compounds, the main identified space groups correspond to triclinic (P1 or $P\bar{1}$), monoclinic ($P2_1$, $P2_1/c$) and orthorhombic systems ($P2_12_12_1$). Other systems (tetragonal, hexagonal, rhombohedral, cubic) are common in inorganic compounds.

It is possible to organize the 230 space groups in three categories:

- 92 centrosymmetric space groups; they have an inversion center thus they are SHG negative (second harmonic generation) *e.g.* $P2_1/c$; $C2/c$;
- 65 chiral space groups (Schoenke space groups) containing only first class symmetry elements which preserve the handedness of a molecule (SHG positive), *e.g.* $P2_12_12_1$; $P2_1$;
- 73 non chiral and non centrosymmetric space groups. Compatible with a racemic compound with glide mirrors or inverted axes (SHG positive), *e.g.* $Pna2_1$; $Pca2_1$; Pc ; Cc .

3 Phase Diagrams of Chiral Molecules

3.1 Thermodynamics State of the Art

A thermodynamic system is a system which is a part of the Universe, it has real or imaginary borders. Three categories of systems exist:

- *isolated*, if there are no exchanges of matter nor exchanges of energy with the exterior;
- *closed*, if the system only exchanges energy with the exterior;
- *open*, if there are exchanges of energy and matter with the exterior.

In this work, all systems used (compounds, solvents. . .) will be considered *closed*.

A phase is described as an homogeneous part of the system; it can be liquid, gas or solid. When several phases are involved in the system it is a heterogeneous equilibrium.

In order to represent the energy of a system, the Gibbs free energy G ($\text{J}\cdot\text{mol}^{-1}$) is used. It is expressed in Eq. I.3 with H being the enthalpy ($\text{J}\cdot\text{mol}^{-1}$), T being the temperature

(K) and S being the entropy ($\text{J.mol}^{-1}.\text{K}^{-1}$).

$$G = H - TS \quad (\text{Eq. I.3})$$

Equilibrium conditions are reached once free enthalpy is minimal and $\Delta G = 0$.

To know the number of changeable parameters, without any changes of the equilibrium state in a system of phases in *equilibrium*, the rule of phases of Gibbs is used. This rule defines the variance v of a system (degrees of freedom).

The variance v of a system is the number of variables that can be changed independently without altering the state of equilibrium of the system. v is expressed via the Gibbs Phase rule Eq. I.4:

$$v = n + 2 - \phi \quad (\text{Eq. I.4})$$

With n being the number of “independent” components, 2 being the number of variables (pressure and temperature) and ϕ being the number of phases. If the pressure is fixed the following equation (Eq. I.5) is obtained.

$$v = n + 1 - \phi \quad (\text{Eq. I.5})$$

3.2 Binary Systems of Enantiomers

A binary system is composed of two independent components. Two enantiomers are considered as two independent components.

Binary phase diagrams between two enantiomers are strictly symmetric with reference to the racemic composition in the center. A mixture of two enantiomers can crystallize according to three types of heterogeneous equilibria.¹⁶

3.2.1 Racemic Compound

The case of racemic compounds is the most frequent case (more than 90% of the cases). There is a defined compound made of each enantiomer at the 1:1 composition (FIGURE I.5). A defined compound is a compound that have a fixed and defined stoichiometry.

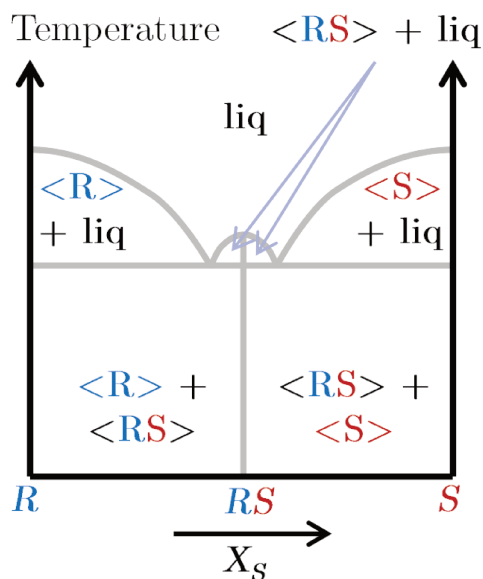


FIGURE I.5 – Theoretical binary phase diagram of a racemic compound

Melting of a racemic compound is congruent (liquid and solid phases have the same composition) and its melting point can be lower or higher than the one of the pure enantiomers. In cases where the melting temperature of the racemic compound is higher than that of the pure enantiomers, the system is referred to as an anti-conglomerate¹⁷ (FIGURE I.6).

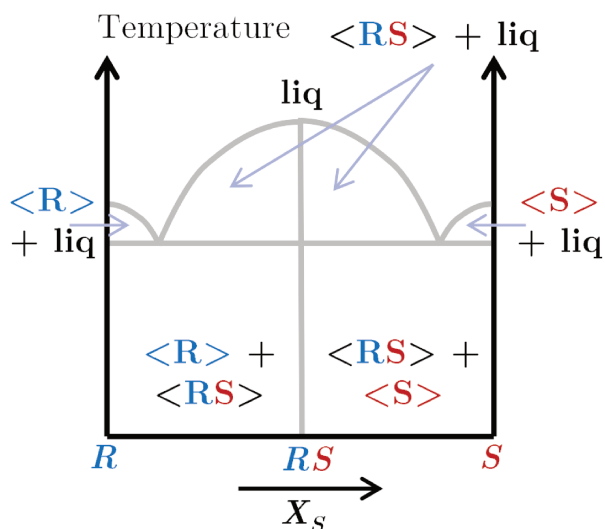


FIGURE I.6 – Theoretical binary phase diagram of an anti-conglomerate

3.2.2 Conglomerate

When both enantiomers crystallize independently, the system is a conglomerate. This case is rare compared to racemic compounds (5 - 10 % of the cases). Conglomerate systems are characterized by an eutectic invariant (FIGURE I.7).

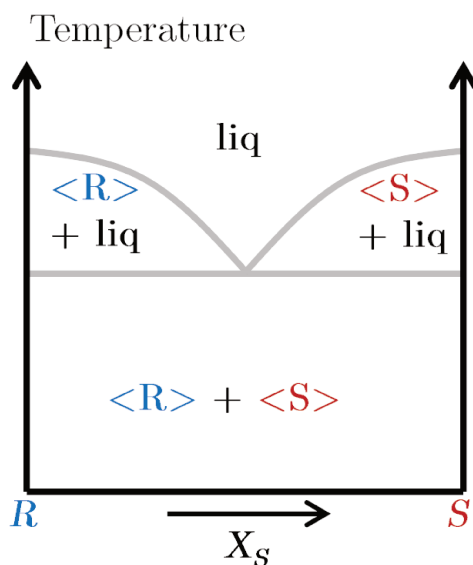


FIGURE I.7 – Theoretical binary phase diagram of a conglomerate

3.2.3 Solid Solution

In rare occurrences, it is possible to observe a complete miscibility at the solid state between the two enantiomers.¹⁸ Enantiomers are randomly distributed in the crystal lattice, each enantiomer can occupy any crystallographic sites. Solid solutions can have a maximum or minimum of melting temperature (FIGURE I.8). In an ideal case, melting temperature is the same for all compositions.

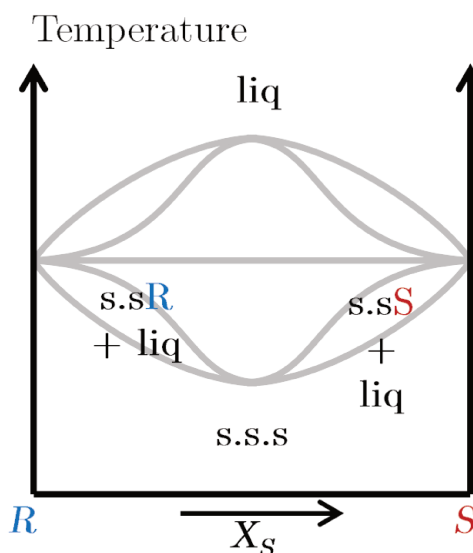


FIGURE I.8 – Theoretical binary phase diagram of solid solutions

It is also possible to observe partial solid solutions (FIGURE I.9), that is to say that only a part of the compositions allows for non stereoselective integration on crystallographic

sites.

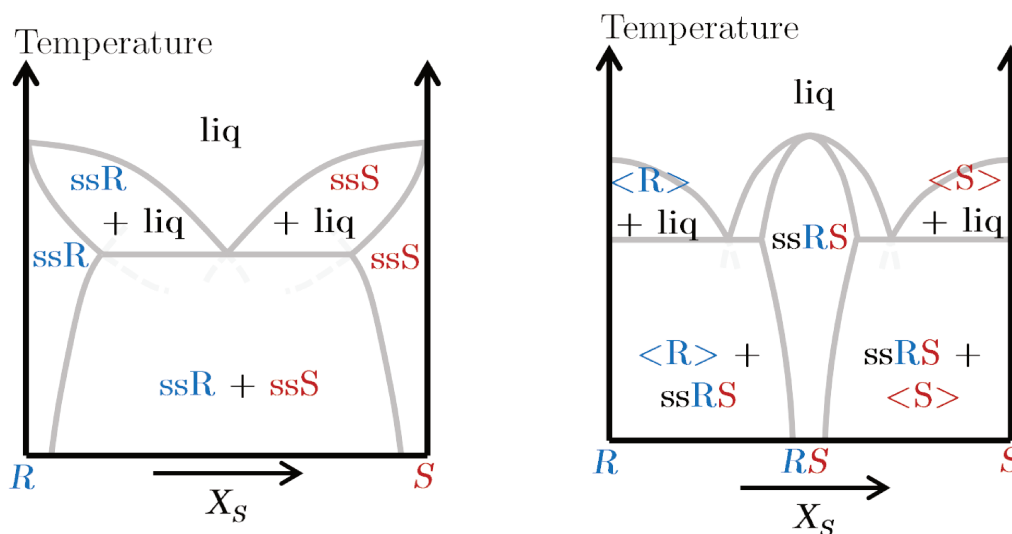


FIGURE I.9 – Partial solid solution of enantiomers (left), partial solid solution of the racemic compound (right)

3.2.4 Metastable Equilibria

A system crystallizing as a stable racemic compound can also crystallize as a metastable conglomerate (FIGURE I.10 (left)); dashed lines represent metastable equilibria. Kinetically, metastable equilibria are usually favored. Metastable equilibria are also central for the realization of preferential crystallization in the case of conglomerate (Section 5.4.2).

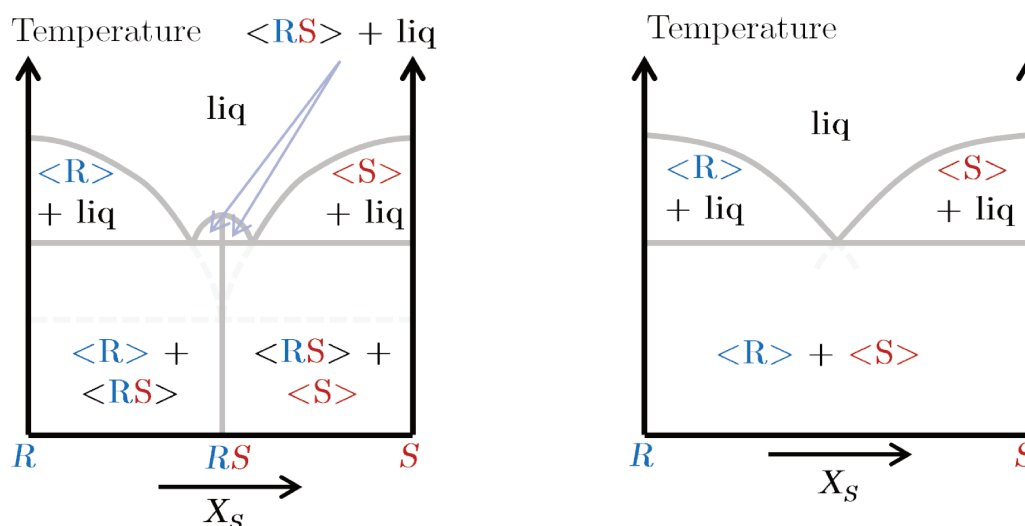


FIGURE I.10 – Metastable equilibria for a racemic compound (left) and for a conglomerate (right)

3.3 Ternary Systems

For the study of crystallization from solutions, it is central to know the evolution of the system's solubility and the different heterogeneous equilibria in the presence of solvent. To this end, isothermal sections of a polythermic ternary phase diagram (FIGURE I.11) can be determined at the relevant temperatures of the process.

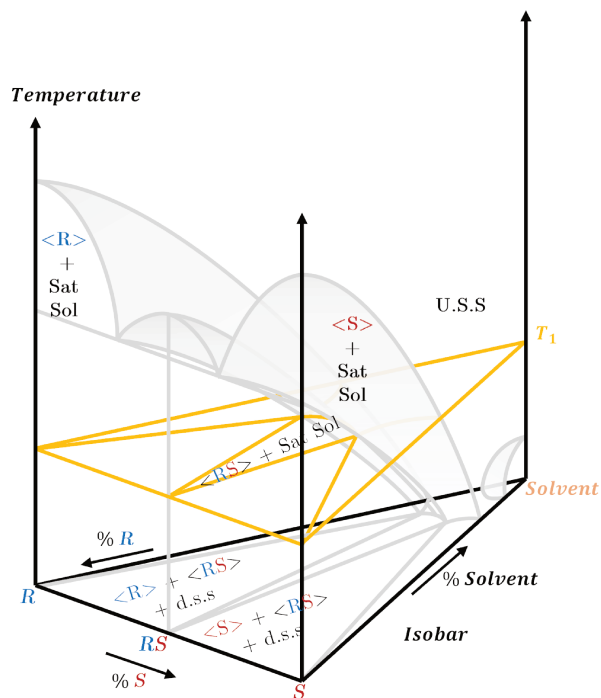


FIGURE I.11 – Polythermic ternary phase diagram of a racemic compound

The same equilibria as described in Sections 3.2.1, 3.2.2, and 3.2.3 can thus be described, using ternary phase diagrams (FIGURES I.12 to I.14).

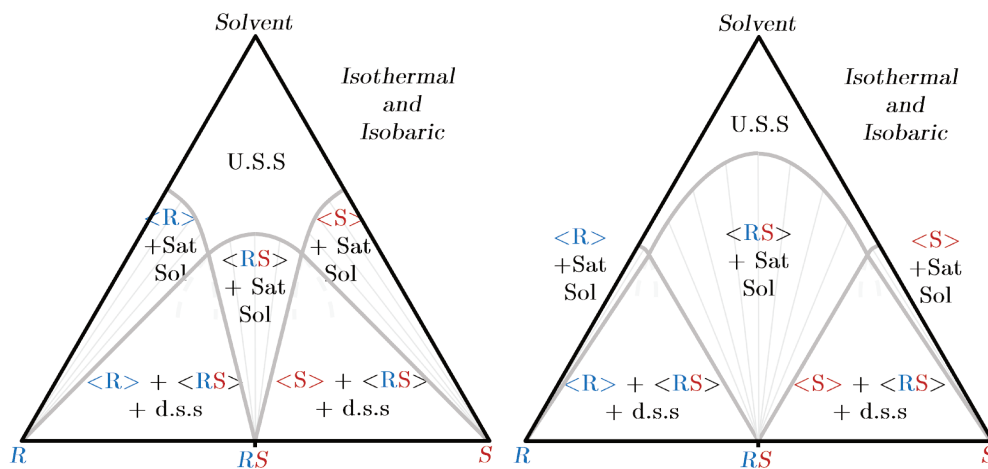


FIGURE I.12 – Theoretical ternary phase diagrams of a racemic compound (left) and an anti-conglomerate type racemic compound (right)

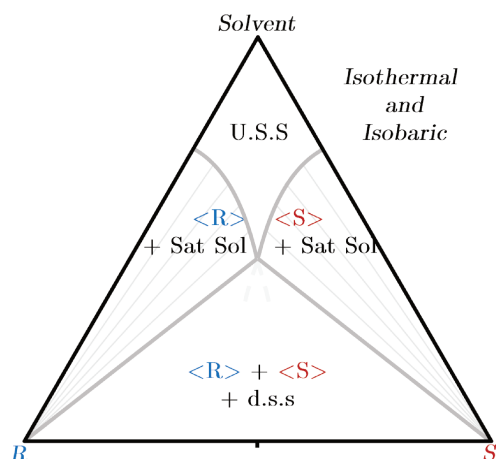


FIGURE I.13 – Theoretical ternary phase diagram of a conglomerate

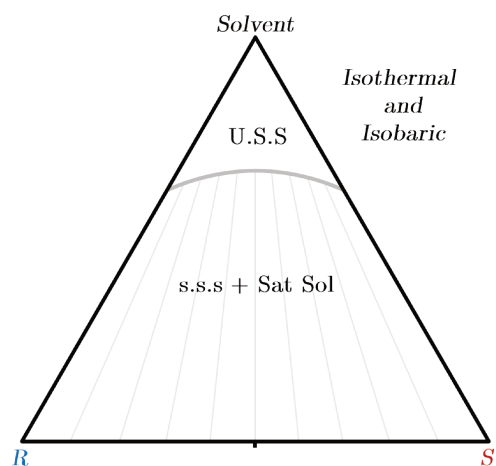


FIGURE I.14 – Theoretical ternary phase diagram of a solid solution

U.S.S, corresponds to *under saturated solution*; d.s.s, corresponds to *doubly saturated solution* (in each of the two solid phases); s.s.s, solid solution by means of substitution.

Other cases can also be observed¹⁹ with systems crystallizing in a combination of the three extreme cases through stable and metastable equilibria.

3.4 Higher Dimensions

In some processes, it is necessary to use a supplementary compound in order to resolve enantiomers (as it will be highlighted in section 5), or a mixture of solvents. For each constituent it is necessary to add a supplementary dimension to the phase diagrams.

However, for the study of chiral resolution, it is not always necessary to know the whole phase diagram, an isoplethal²⁰ and isothermal section can be sufficient, since the components which form the salt (or co-crystal), form it with both enantiomers.²¹ For mixture of solvents (as there is no evaporation) the composition remains unchanged.

For example, in the case of the process of preferential enrichment of arginine fumarate in a water/ethanol mixture²² (presented in Chapter III), five constituents are present. Normally the system should be a quinary system, however it is possible to work in a ternary isoplethal section between the salts of the two enantiomers and the fixed mixture of solvents.

4 Other Considerations about Solid State

4.1 Polymorphism

Polymorphism is the ability of a compound to crystallize according to different crystal packings, which may or may not be of the same space group. One of the forms is thermodynamically the most stable at a given temperature, others are called metastable forms.

Two types of relations between different polymorphs can be defined.

- If at any temperature, only one polymorph is stable, every other polymorph are necessarily metastable, this situation is called *monotropy* (FIGURE I.15). A metastable polymorph is monotropic with reference to the stable one.

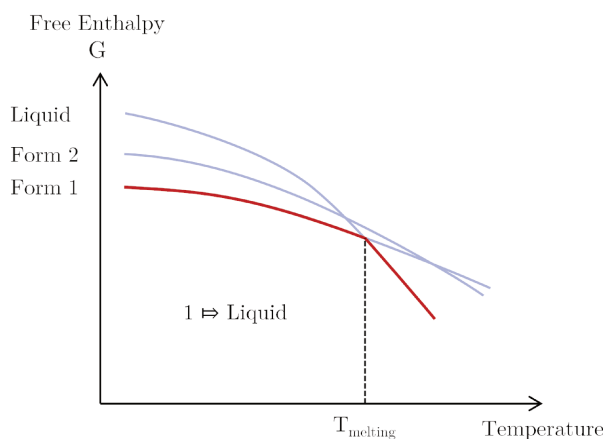


FIGURE I.15 – Monotropic system, there are no polymorphic transitions before the melting temperature of the stable polymorph (the red line represents the energy of the system as a function of the temperature)

- When a transition exists between two polymorphs before melting, this situation is referred to as *enantiotropy* (FIGURE I.16).

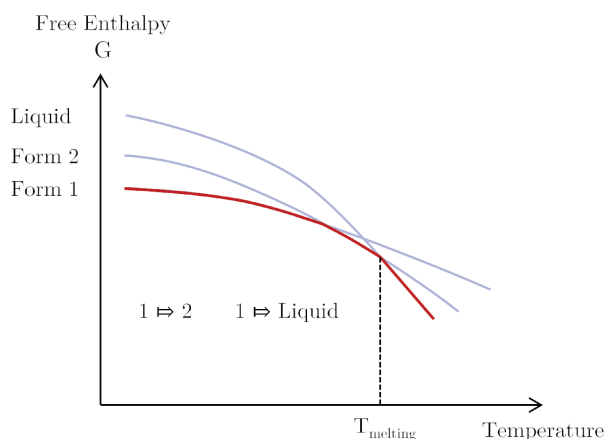


FIGURE I.16 – Enantiotropic system, a polymorphic transition is observed before melting (the red line represents the energy of the system as a function of the temperature)

One of the most simple techniques to identify the stable form is to measure the melting point, the form with the highest melting point is theoretically the most stable. If the melting of this one has the highest enthalpy, then other polymorphs are monotrope according to the stable form, else enantiotropy can happen (Burger Ramberger theorem²³).

It is also possible to mix two polymorphs in suspension at a given temperature to observe which one is present at the end of the experiment, this process is called *cross seeding*.

4.2 Salt, Co-crystal, Solvate

A salt is defined as a unique crystalline phase formed by an acid and a base with a difference of pK_a of at least 3.²⁴

A co-crystal is a unique crystalline phase formed by a mixture of two co-formers which crystallize together without exchange of hydrogen, most often encountered interactions are hydrogen bonds.²⁵

A solvate is a unique phase formed by one or more solids and one or more liquids (at 20 °C).

It is possible to obtain phases which can be described by several descriptors listed above as described by Aitipamula *et al.*²⁶ and Grothe *et al.*²⁷ (FIGURE I.17).

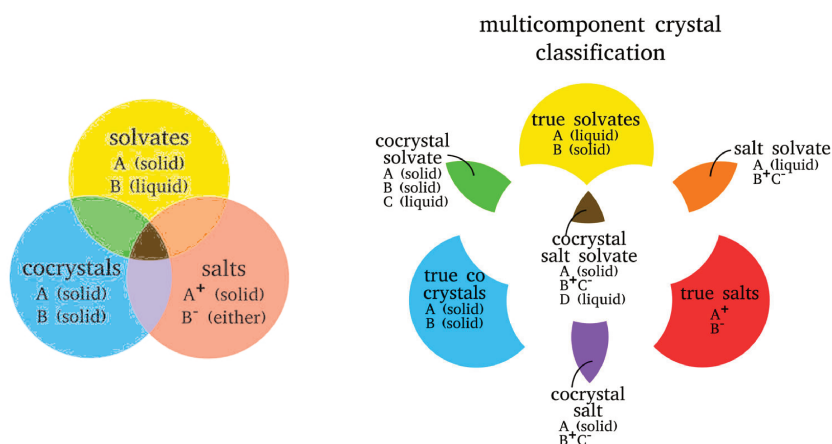


FIGURE I.17 – Distribution of salts, co-crystals and solvates and their combinations²⁷

5 Access to Pure Enantiomer

Resolution of enantiomers has been a subject of interest for a long time, and even more so in the field of active pharmaceutical ingredients. Different pathways exist to obtain pure enantiomers²⁸ (FIGURE I.18).

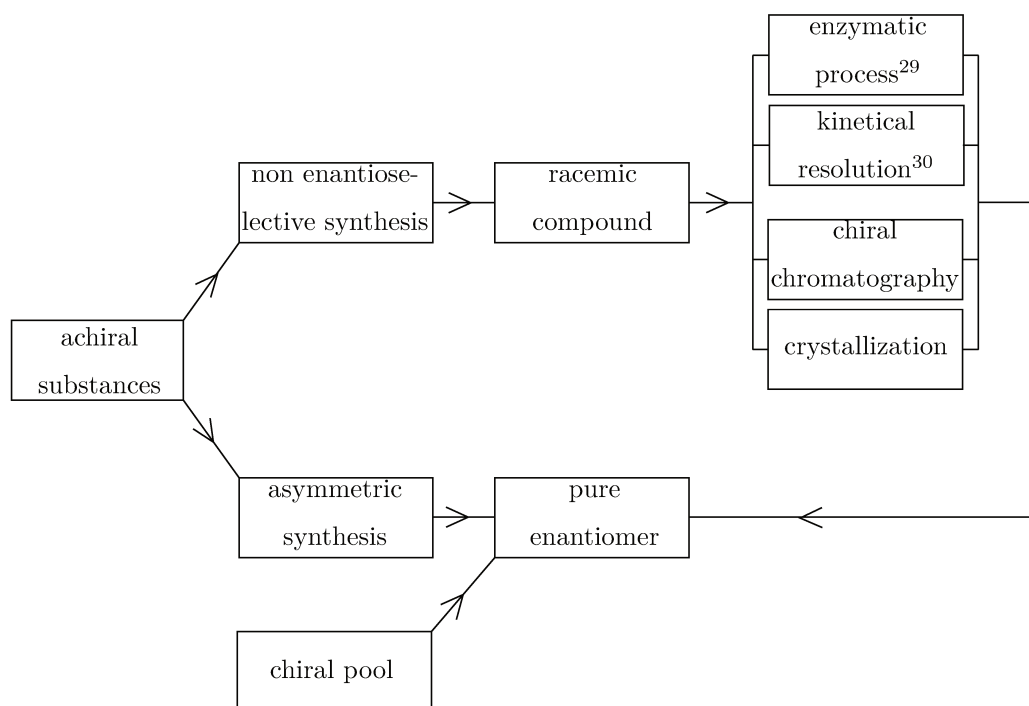


FIGURE I.18 – Possible pathways to obtain pure enantiomers

5.1 Non-enantioselective Synthesis from the Chiral Pool

In order to access enantiopure molecules, it is possible to use naturally enantiopure molecules, like sugars, amino-acids. . . They can be easily accessible, and are often inexpensive. Achiral synthetic techniques can be used, in which processes are easy to set up to obtain enantiopure materials. Nevertheless the synthesis should necessarily start with one of these synthons which might not always be compatible with the structure of the target.

5.2 Asymmetric Synthesis

If the synthesis is not possible using the chiral pool, asymmetric synthesis can be envisaged starting from achiral precursors. The objective is to obtain a stereoselectively controlled chiral center. Different strategies exist to control chirality during asymmetric synthesis.

- Usage of a chiral reactant,³¹ which is used during synthesis, but not present in the final compound.
- Usage of a chiral auxiliary,³² during a step of the synthesis a chiral compound is added to the molecule, this auxiliary induces the chirality of the center.
- Usage of a chiral catalyst,³³ which induces chirality during a transition state in which it is involved. It can be used in small quantity and can often be reused/recycled.

Asymmetric synthesis often has a prohibitive cost compared to chiral resolution by crystallization.

5.3 Chiral Chromatography

Analytical chiral chromatography permits to determine enantiomeric excess, concentrations of both enantiomers and thus quantification.

With columns of larger diameter, it is possible to preparatively separate enantiomers.

There are several chromatographic methods to separate enantiomers: direct and indirect methods.³⁴

Indirect methods were the first used to separate enantiomers by chromatography. They consist in modifying analytes with an enantiopure compound, in order to analyze diastereomers with a conventional column. These methods are easy to perform, however, modification of the sample involves a risk of racemization.

Direct methods consist in the separation without formation of diastereomers before analysis. The separation is performed with the formation of transition diastereomers during elution, either with a chiral ligand or with a chiral stationary phase. The first

mechanism of separation was the three points rule, proposed by Dalglish in 1952.³⁵ However this mechanism is not representing the real forces in presence between most of the stationary phases and analytes. Different chiral resolution mechanisms exist today to account for the different stationary phases.³⁶

5.3.1 Liquid Chromatography (HPLC)

Enantioselective liquid chromatography is widely used to determine enantiomeric excess and thus for quantification. There are two main types of direct chiral separation in HPLC,³⁴ either with chiral additive diluted in the mobile phase or using a chiral selector bonded to or immobilized in a chromatographic support.

- With chiral additives,³⁷ the analyte is eluted as a diastereomer complex. Different additive can be used such as amino-acids, sugars, cyclodextrin, crown ether... The chiral selector should not have a response to UV spectroscopy. Main limitations are the impossibility to couple with mass spectrometry, and the cost of the additives (their recovery is difficult).
- Chiral stationary phases allow usage of chiral selectors without loss after separation. There is a large variety of stationary phases^{34,38,39} (TABLE I.1).

TABLE I.1 – Chiral stationary phases for HPLC

Selector type	Examples of selectors
Polysaccharides	Amylose or cellulose derivatized by phenyl-carbamate groups
Cyclodextrins ⁴⁰	Native or derivative
Pirkle type phase ⁴¹	1-(3,5-dinitrobenzamido)-1,2,3,4-tetrahydrophenanthrene
Crown ether ⁴⁰	18-crown-6 ether
Synthetic Polymers	Polytriphenylmethyl methacrylate
Proteins	Human Serum Albumin
Macrocyclic glycopeptides ⁴²	Teicoplanin, vancomycin
Cinchona Alkaloids	Zwitterionic quinine derivatives

However, for preparative chromatography in order to obtain pure enantiomers by preparative chromatography, chiral HPLC often has a prohibitive cost in terms of solvent and stationary phases.

5.3.2 Other Chromatographic Techniques

5.3.2.1 Simulated Moving Bed (SMB)

The simulated moving bed⁴³ (SMB) uses stationary phase of conventional liquid chromatography. It simulates a continuous and reverse circulation of columns and mobile phase (FIGURE I.19). This simulation is performed with a periodical change of inlet and outlet of columns in the same direction as the solvent flow.

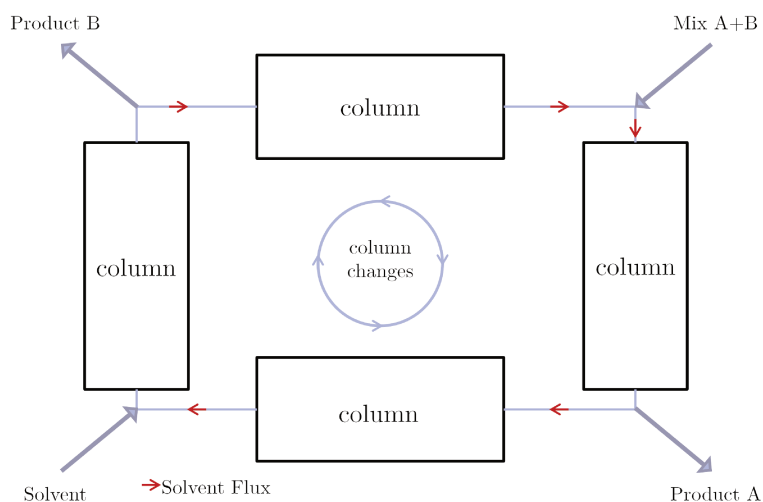


FIGURE I.19 – Representation of SMB

This technique provides continuous separation of compounds. The consumption of solvent is less important than in HPLC.

5.3.2.2 Supercritical Fluid Chromatography (SFC)

Supercritical fluid chromatography⁴⁴ (SFC) is used with most of the stationary phases used in HPLC. A pressurized mobile phase is used, this mobile phase is mainly composed of supercritical CO₂, at a temperature higher than 31 °C and a pressure higher than 73 bar (FIGURE I.20). An organic modifier and additives can be added to the mobile phase.⁴⁵

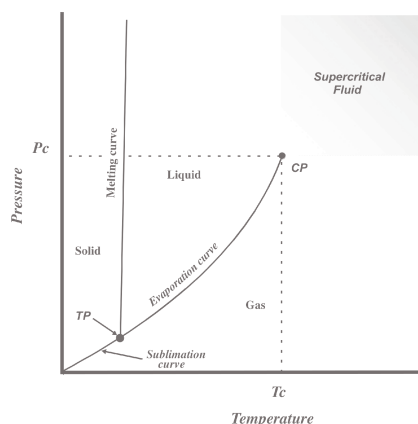


FIGURE I.20 – Unary phase diagram representing supercritical state

The main advantage of SFC is that methods can be easily transferred to preparative scale. The solvent is most often pressurized CO_2 : it evaporates upon depressurization, which allows for easy collection of the purified compound. Another advantage of SFC is the possibility to have a higher elution speed for a similar efficiency compared to the one of HPLC,⁴⁶ this elution speed can be increased up to a factor of 4, due to a lower viscosity of the mobile phase than HPLC.

5.3.2.3 Gas Chromatography (GC)

In contrast with other chromatographic techniques, gas chromatography (GC) makes product collection complicated. However, it is possible to obtain a few milligrams.^{47,48} GC is mainly used as an analytical technique only. Different stationary phases have been developed, but the most commonly used are cyclodextrin derivatives.^{49,50}

5.4 Crystallization

Chiral resolution by means of crystallization is often the preferred route in industry due to its economic advantages. Moreover crystallization can be easily applied at large scale.

5.4.1 Pasteurian Resolution

Pasteurian resolution is one of the oldest techniques to resolve enantiomers. It consists in the formation of diastereomeric salts, by adding an enantiopure acid or base to the target. Diastereomers have different physico-chemical properties,¹⁶ the most interesting here being the difference of solubility (FIGURE I.21).

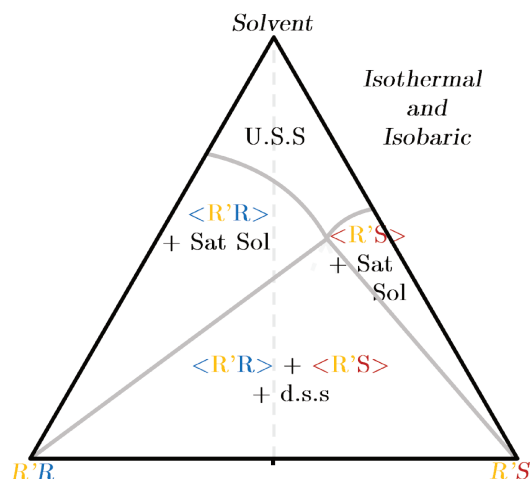


FIGURE I.21 – Ternary phase diagram highlighting solubility differences in Pasteurian resolution process

Since solubilities of these salts are different, it is possible to selectively crystallize one rather than the other. Afterwards, the resolution agent is retrieved by salting out and can be recycled. The resolution agent often comes from the chiral pool: this makes the process cheaper.

It is possible to try different resolution agents in order to optimize yield and enantiomeric excess.

5.4.2 Preferential Crystallization

Preferential crystallization^{21,51} is a chiral resolution technique discovered by Gernez, a student of Pasteur, in 1866.⁵² It has been developed in the 20th century by Secor⁵³ and Jacques.⁵⁴

Preferential crystallization relies on systems crystallizing as conglomerates (Section 3.2.2). Conglomerates provide the possibility to have a discrimination at the solid state, unlike racemic compounds.

- The oldest preferential crystallization method is SIPC (*Seeded Isothermal Preferential Crystallization*). It consists in cooling a racemic solution (or slightly enriched) under its saturation point. The saturated solution is seeded by one of the enantiomer (the one initially in excess), this permits selective crystallization of this one, with no nucleation barrier to overcome. Suspension is filtered before nucleation of the counter enantiomer.
- S3PC technique (*Seeded Polythermal Programmed Preferential Crystallization*) can also be used, it is similar to SIPC, the difference is that the solution is cooled after seeding by using a tailored cooling procedure.
- A more recent technique developed by Coquerel *et al.* in 1995⁵⁵ is the AS3PC (*Auto-*

Seeded Poythermal Programmed Preferential Crystallization). This technique is often more efficient than SIPC, it is based on continuous and controlled cooling of the mixture before nucleation of the counter-enantiomer (FIGURE I.22). It does not need any external seeding unlike the two previous methods.

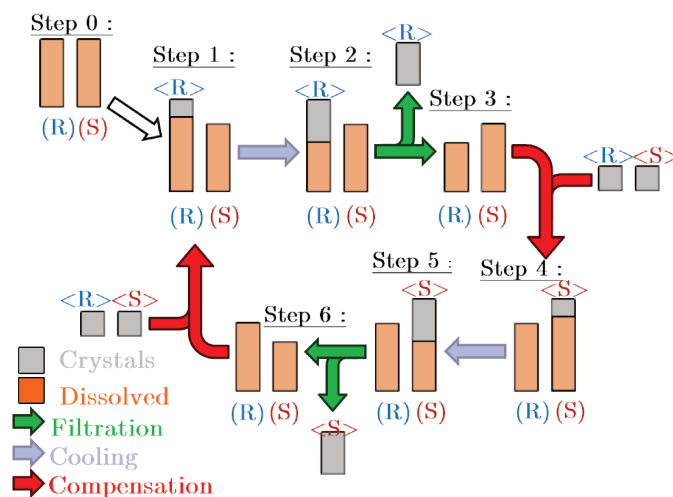


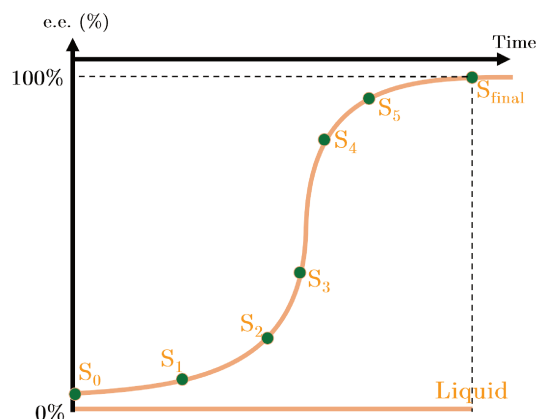
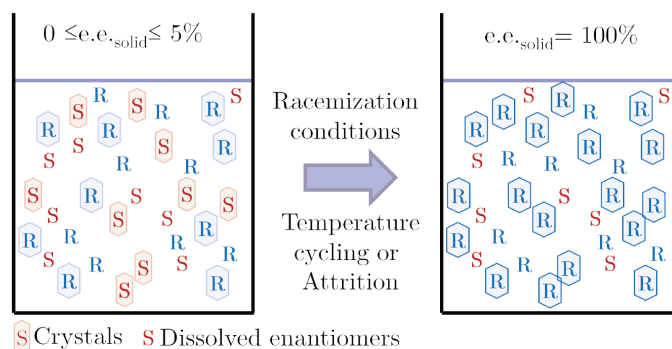
FIGURE I.22 – AS3PC process⁵¹

- Another technique developed in 2011 by Coquerel and Levillain⁵⁶ is *Auto-Seeded Preferential Crystallization Induced by Solvent Evaporation* (ASPreCISE). This technique is comparable to AS3PC but supersaturation is generated by solvent evaporation.

5.4.3 Deracemization

Using preferential crystallization, it is possible to obtain each enantiomer separately. However, if only one enantiomer is desired, the other one is an impurity, and the yield of the separation cannot be higher than 50%. Deracemization can achieve a theoretical yield of 100% in the solid phase.

Deracemization is a process which combines selective crystallization of an enantiomer and the loss of chiral information at the solvated state (*e.g.* racemization via a base).⁵⁷ Starting with a slightly enriched suspension, it is possible to obtain an enantiopure solid (FIGURE I.23).


 FIGURE I.23 – Deracemization process and variation of e.e.⁵⁷

Two conditions are necessary to achieve deracemization, a conglomerate forming system and a rapid racemization in solution.

There are two processes of deracemization.

- Deracemization by attrition or *Videma ripening*^{58–62} is historically the first technique of deracemization. Its mechanism⁶³ can be split into *four processes* 1) *racemization in the solution*, 2) *Ostwald ripening*¹⁵ *that is large crystal growing at the expense of smaller crystals*, 3) *enantioselective (partial) incorporation of clusters*^{58,64} and 4) *attrition*.
- Temperature cycles enhanced deracemization^{57,65} which can be described as a two steps process, stereoselective crystallization of the enantiomer in excess during the cooling of the solution, and dissolution of the smallest population of crystals during heating which most of the time is made of the minor enantiomer.

6 Preferential Enrichment

6.1 Presentation of the Phenomenon

The phenomenon of preferential enrichment (PE) occurs during crystallization in stagnant conditions of a racemic mixture in extreme supersaturation conditions ($4 \geq \beta \geq 25$)

and results in a high enrichment in one of the two enantiomers in the solution ($\approx 100\%$ e.e.) while deposited crystals stay approximately racemic.

This phenomenon was discovered by Prof. Tamura^{66,67} at the end of the last century for a family of compounds that consist of ammonium or sulfonium sulfonates salts (FIGURE I.24).

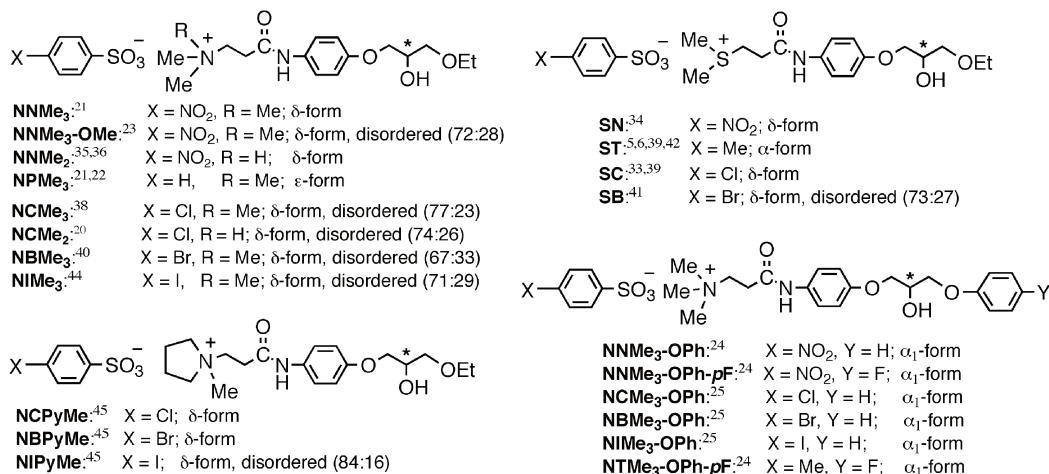


FIGURE I.24 – Ammonium or sulfonium sulfonates which exhibit PE⁶⁸

The study of the first generation of compounds prompted the development of this phenomenon as a cyclizable process of chiral separation. FIGURE I.25 explicits cyclization of the PE process for the compound NNMe₃ (FIGURE I.24).

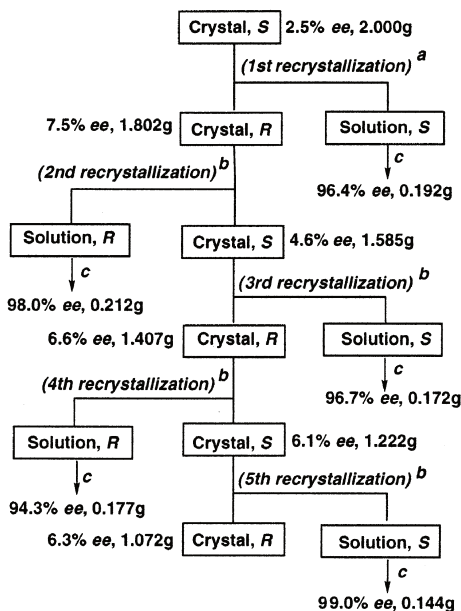


FIGURE I.25 – Cyclization of PE process for the compound NNMe₃⁶⁹

An interpretation of this phenomenon with a quasi-ternary isothermal section is necessary to grasp the unique characteristics of PE (FIGURE I.26).

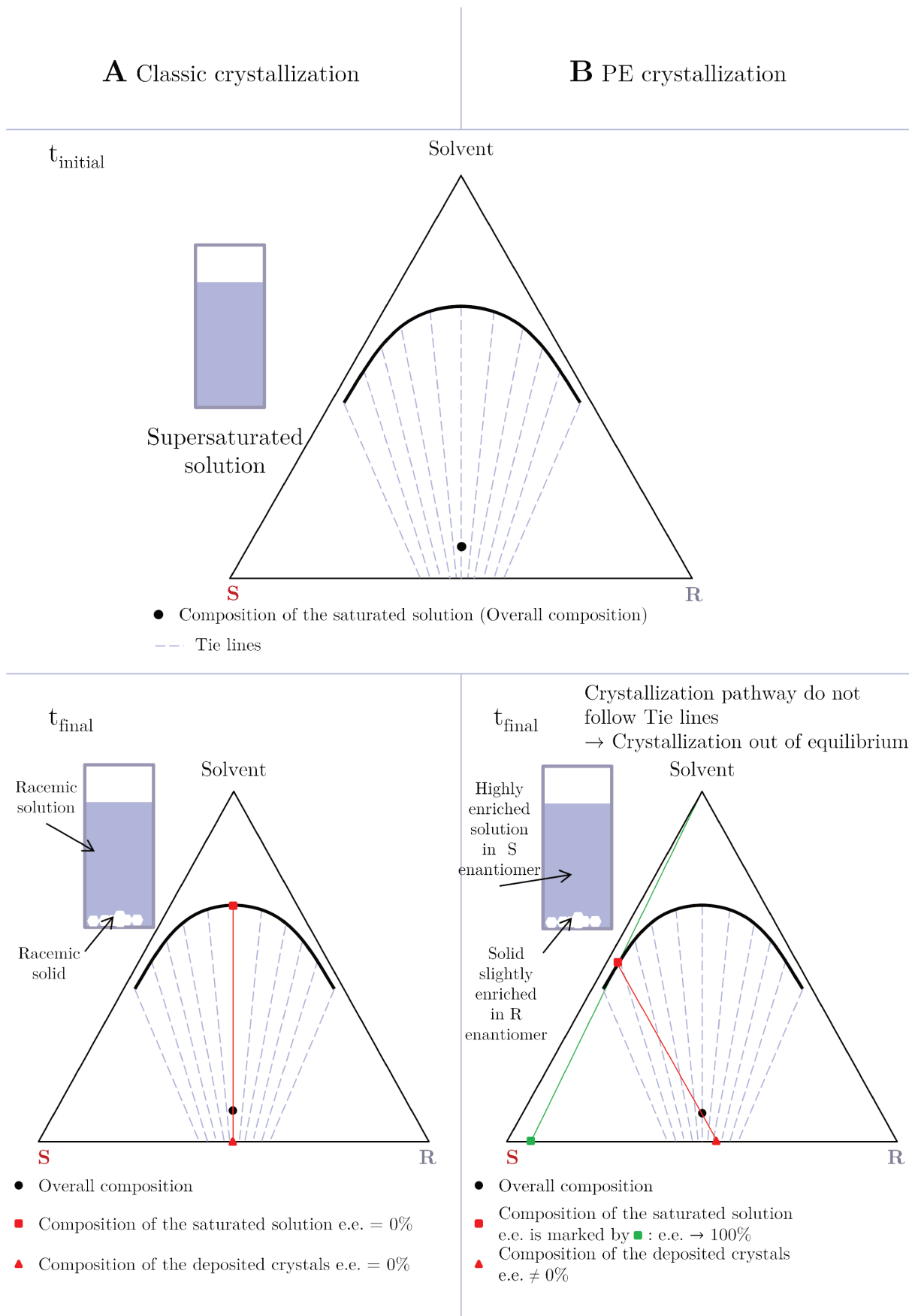


FIGURE I.26 – Comparison between classic crystallization and PE

Phase diagrams presented in FIGURE I.26 are partial and do not give information about the nature of the form of the deposited crystals (except that the solid phase must present a domain of solid solutions).

Indeed, other compounds capable of performing PE were discovered and do not crystallize as total solid solution. These compounds form the second generation: an amino-acid: alanine;⁷⁰ three salts of amino-acids: arginine fumarate,²² phenylalanine fumarate⁷¹ and leucine oxalate;⁷² and an anti-inflammatory: ketoprofen⁷³ (FIGURE I.27).

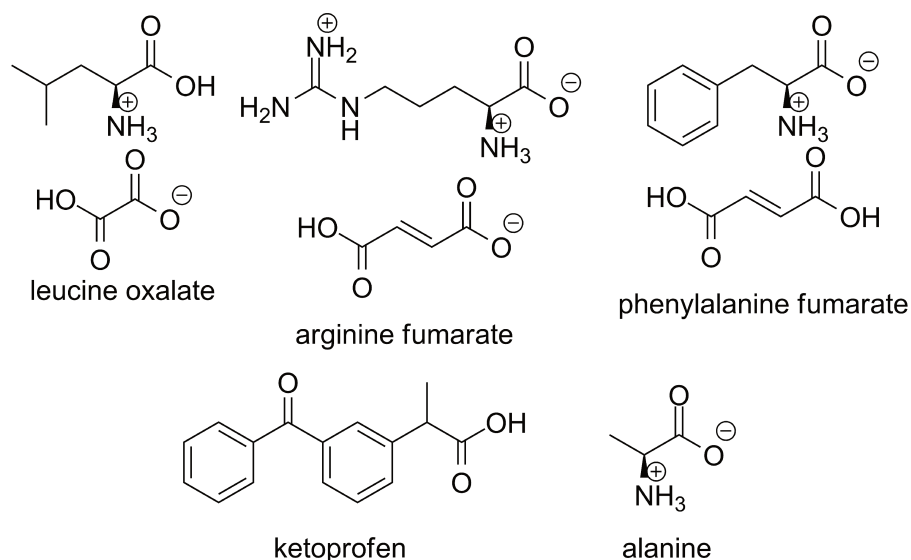


FIGURE I.27 – Compounds of second generation

Evolution of compositions in phases diagrams in FIGURE I.26 indicates that the pathways of crystallization are out of equilibrium. This is in accordance with the observation that PE do not happen when the medium is stirred (*i.e.* when the system is forced to evolve towards thermodynamic equilibrium).

PE is often defined as the opposite process of preferential crystallization:⁷⁴ for preferential crystallization, the excess is inside the solid phase, for PE the excess is in the liquid phase. Other opposite elements are listed in TABLE I.2.

TABLE I.2 – Comparison between PE and preferential crystallization⁷⁴

	Preferential enrichment	Preferential crystallization
At the end of the process	High <i>e.e.</i> in liquid phase Low <i>e.e.</i> in solid phase	Low <i>e.e.</i> in liquid phase High <i>e.e.</i> in solid phase
Behavior around overall composition Ω	Rotation around point Ω of the tie line S- Ω -L	Elongation along the S- Ω -L tie line
Heterogeneous equilibria between enantiomers	Anti-conglomerate	Conglomerate
Supersaturation	High $4 \leq \beta \leq 25$	Low to medium, to avoid spontaneous nucleation of the counter-enantiomer
Possibility to be associated with racemization in solution	No	Yes (SOAT) <i>Second Order Asymmetric Transformation</i> ²⁸
Stability	It goes through an equilibrium state (racemic composition)	It tends to reach a metastable equilibrium the metastable solubility of the enantiomer
Key step	Stereoselective dissolution or stereoselective exchange	Stereoselective nucleation and growth.
Duration	Several days under stagnant conditions	Several hours under stirring

6.2 Mechanisms

6.2.1 Mechanism of 2002, Proposed on the Basis of the First Generation of Compounds

In their publication of 2002, Prof. Tamura *et al.* proposed the first description of the mechanism of PE, based on the first generation of compounds.⁶⁹ A detailed explanation of the mechanism requires a description of these molecules which are made of a linear asymmetric backbone, with a glycerol part (containing alcohol functions), the other part containing a cationic group, ammonium or sulfonium forming ion bonds with a sulfonate anion (FIGURE I.28).

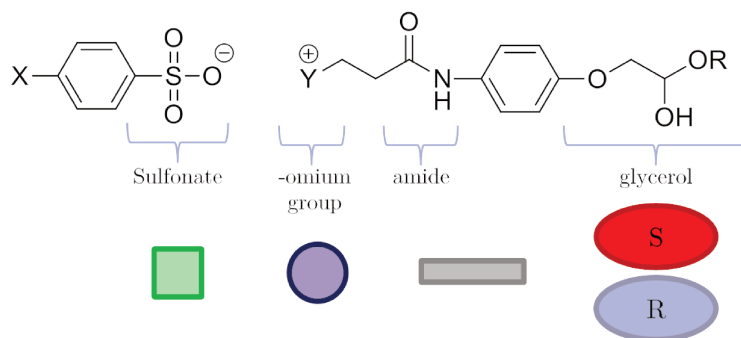


FIGURE I.28 – General structure of a first generation compound

A schematic representation (FIGURE I.29) is used for all following explanations.

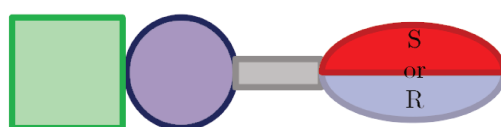


FIGURE I.29 – Schematic representation of a first generation compound

It was established that most compounds of the first generation can crystallize into two racemic polymorphic forms.

- The γ form, metastable ($P\bar{1}$)

The structure is composed of alternating alignments of homochiral antiparallel 1D chains (FIGURE I.30).

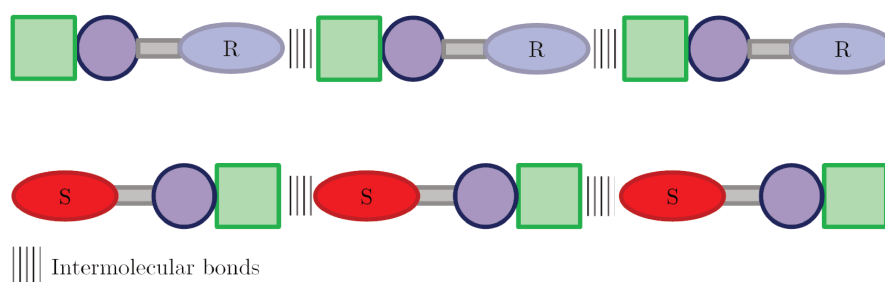


FIGURE I.30 – Schematic representation of the crystal packing of the γ form

Structural analysis reveals that intermolecular interactions between chains are weak and limited to C—H \cdots O type contacts.

- The δ form, stable ($P\bar{1}$)

The structure results from the stacking of centrosymmetric dimers and have a marked structural similarity with the γ form (FIGURE I.31).

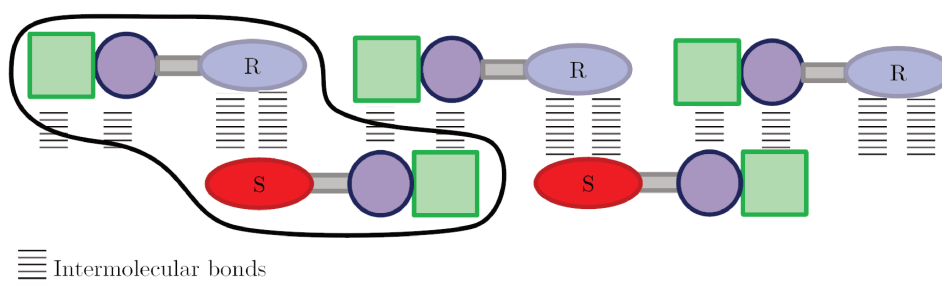


FIGURE I.31 – Schematic representation of the crystal packing of the δ form, a dimer is circled in black

A description of the mechanism proposed by Prof. Tamura in 2002^{68,69} is presented here.

1. Schematic representation of preassociations made of homochiral chains which are formed in solution (FIGURE I.32).

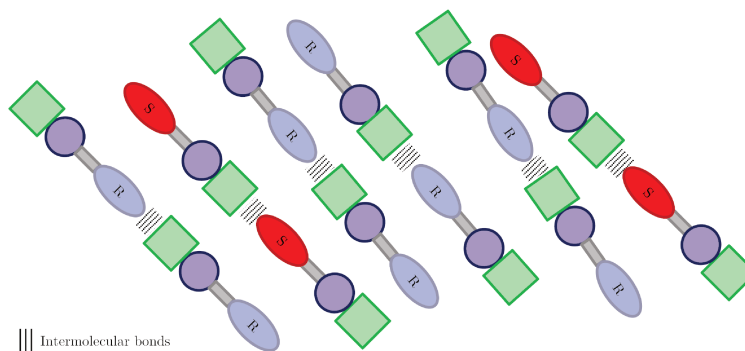


FIGURE I.32 – Schematic representation of the homochiral preassociations in solution

2. Nucleation of the γ form occurs. No chiral discrimination occurs inside this phase, domains with higher density of one enantiomer are generated (FIGURE I.33).

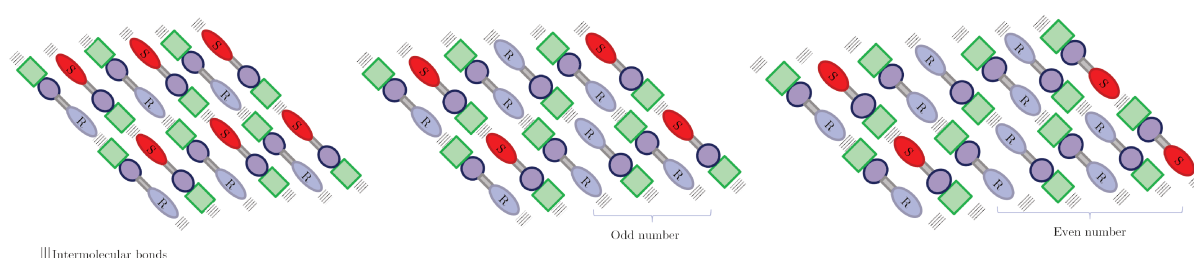


FIGURE I.33 – Schematic representation of the crystal packing in the γ form as a function of the succession of homochiral chains, regular succession (left), odd number of homochiral chains (middle), even number of homochiral chains (right)

3. A polymorphic transition happens and generates the apparition of the δ form.

- If the resulting δ form is made of an alternating sequence of chains of opposite chiralities then the structure is stable (FIGURE I.34).

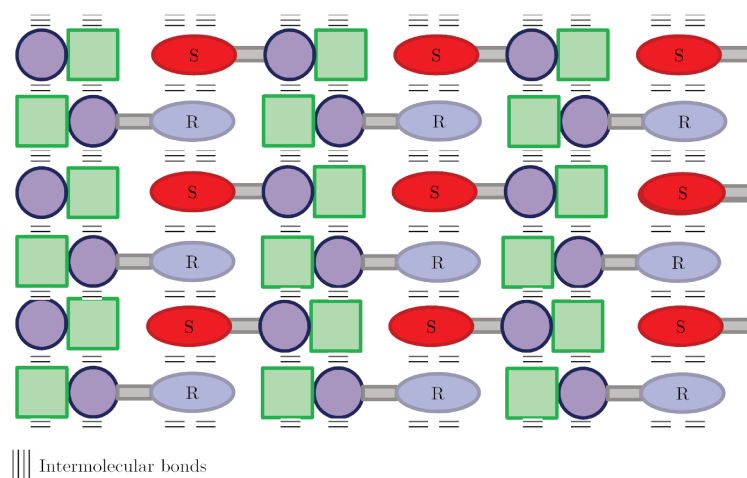


FIGURE I.34 – Schematic representation of the crystal packing in the regular δ form

- If an odd number of 1D homochiral chains occurs successively in the structure, the structure persists (FIGURE I.35).

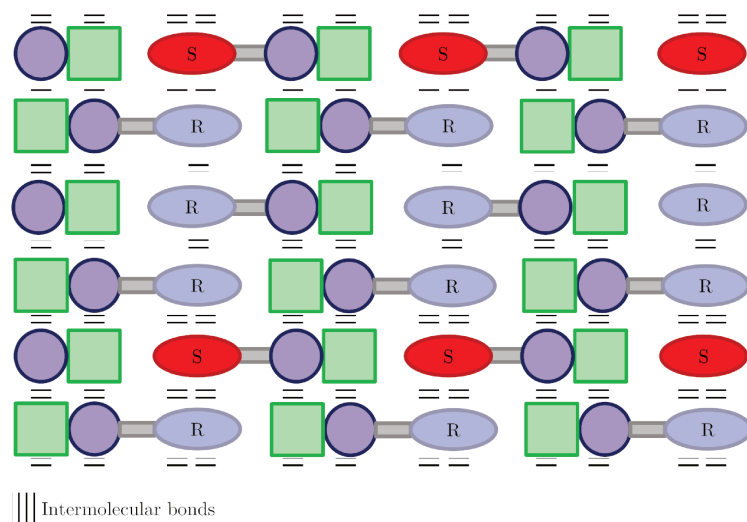


FIGURE I.35 – Schematic representation of the crystal packing in the δ form containing an odd number of homochiral chains

- If an even number of 1D homochiral chains occurs successively in the structure, a *disintegration*^{68,69} happens, and the enantiomer in excess is released inside the solution. This phenomenon is helped by the large solubility of the pure enantiomer (FIGURE I.36). With an odd number of homochiral chains, only one chain has weak interactions, but with an odd number of chains, two chains have weak interactions, consequently destabilizing the structure.

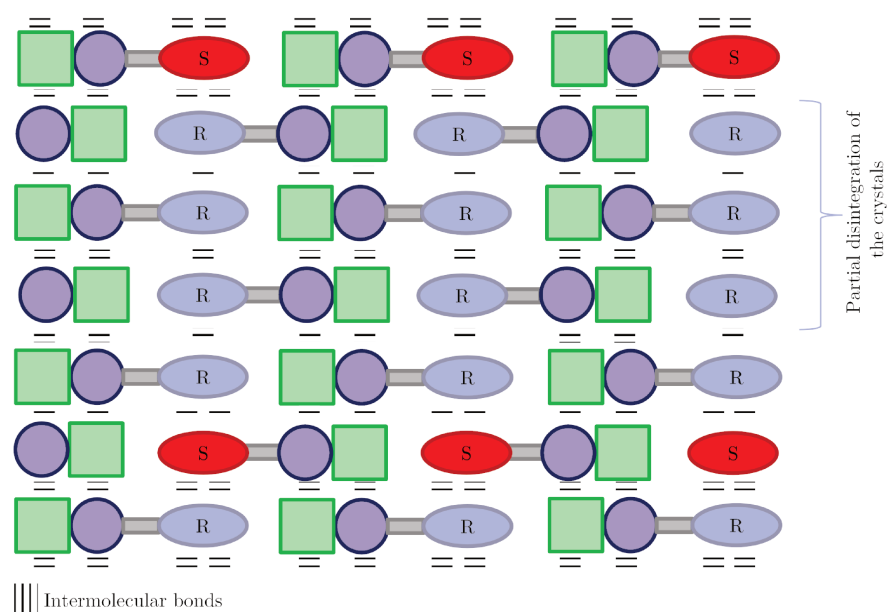


FIGURE I.36 – Schematic representation of the crystal packing in the δ form containing an even number of homochiral chains leading to *disintegration* of the structure

4. The solution is then enriched with the enantiomer which leaves the structure.

Minor enantiomer stays inside the crystal structure into enriched small zones, presenting an odd number of 1D homochiral chains.

6.2.2 Mechanism of 2016 Proposed on the Basis of the First Generation of Compounds and Adapted to the Second Generation of Compounds

A simplified mechanism was proposed in 2016.^{74,75} Two different ways are possible to crystallize the metastable form, either a regular form (alternation of R-S chain) or an irregular form (zones can contain homochiral chains), these zones stem from associations of homochiral chains in solution.

After polymorphic transition, the crystal lattice is composed of stable heterochiral dimers and less stable homochiral dimers, hydrogen bonds are weaker with homochiral dimers (FIGURE I.37).

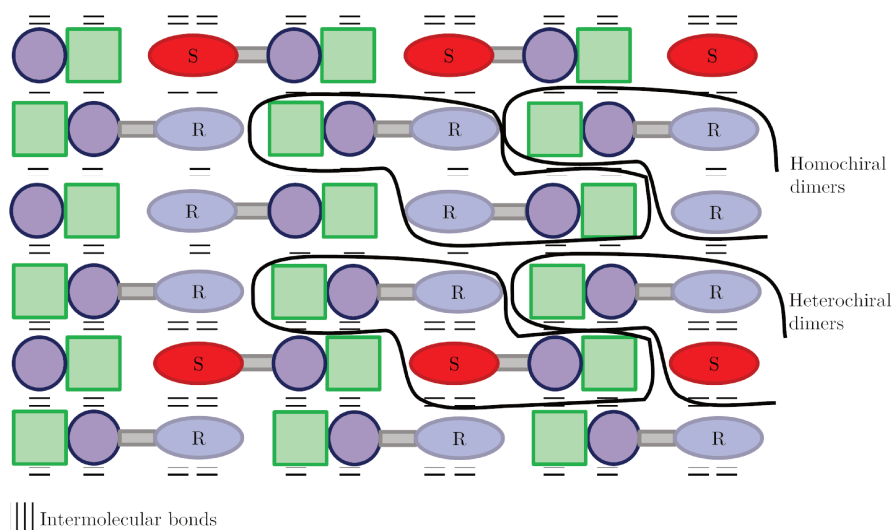


FIGURE I.37 – Schematic representation of the crystal packing in the δ form presenting homochiral and heterochiral dimers

A selective redissolution may occur for the enantiomer in excess forming disordered chains (FIGURE I.38).

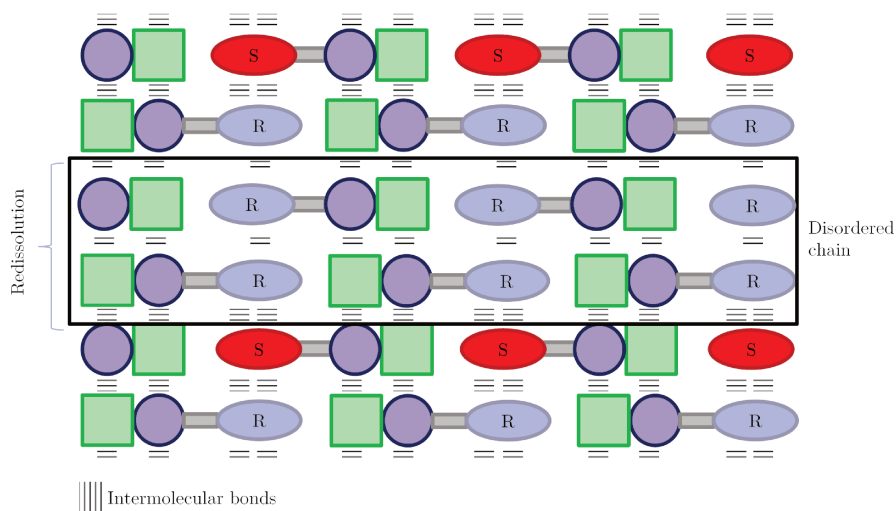


FIGURE I.38 – Schematic representation of the crystal packing for the redissolution of the enantiomer in excess in δ form

In the case of leucine oxalate,⁷² it was discovered that the structure was composed of homochiral bidimensional sheets (FIGURE I.39), these sheets are selectively redissolved into the solution.

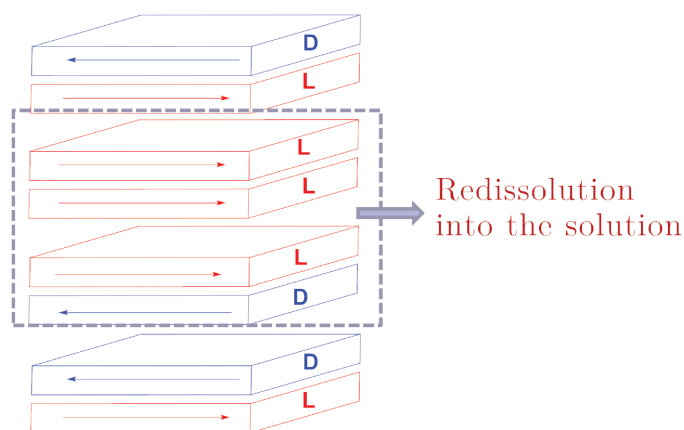


FIGURE I.39 – Illustration of homochiral sheets in the case of leucine oxalate⁷²

6.3 Criteria for the Establishment of Preferential Enrichment

Prof. Tamura *et al.* defined a number of criteria^{22,68} that a system needs to fulfill to achieve PE:

1. solubility of pure enantiomers should be largely greater than the one of the racemic compound (which can contain a solid solution domain), *i.e.* presence of an anti-conglomerate,
2. enantiomers should be associated into 1D homochiral chains at the solvated state,
3. a polymorphic transition should occur during the process,
4. compounds should form heterochiral chains of cyclic dimers and linear homochiral chains in the structure,
5. a selective redissolution of the enantiomer in excess from enriched zones should happen at the beginning of the process,
6. eventual presence^{68,76} of a stable solid solution type form at the racemic composition,
7. at least one polymorph should crystallize in the $P\bar{1}$ space group (not compulsory but happens in 24 cases over 27).

Chapter II

Analytical Methods

1 Introduction

Analysis methods were developed in order to check the impurity profile, and to measure the concentration of enantiomers of arginine fumarate in solution and in the solid phase, the enantiomeric excess, and the concentration of labeled arginine ($^{13}\text{C}_6\text{-L-Arginine}$). For that different HPLC methods were developed using conventional and chiral stationary phases.

2 Method for the Impurity Profile Determination

First of all it is necessary to control the purity of the arginine fumarate salt. Impurities can hinder the crystallization process or interfere with the quantification. This monitoring was conducted using an HPLC-MS method.

In order to develop this method, different objectives were defined: the method should provide a sufficient retention time for the arginine, a great separation between arginine and its impurities (citrulline and ornithine), and the possibility to be coupled with mass spectrometry detection. So the salt additive, if one is needed, should be volatile and used in a concentration compatible with the ESI source.

In the literature different separations were described using various modes of liquid chromatography for the separation of arginine from these impurities.⁷⁷ In our case the method should be suitable to separate arginine from its impurities but also from fumaric acid. Several of these methods were tested (TABLE II.1). The detection for most of the cases was performed with an ELSD (Evaporative Light Scattering Detector) due to the absorbance of additives (at wavelength for the detection of arginine) which were added to the mobile phase in order to fix the pH.

TABLE II.1 – Tests of the method for the determination of impurities of Arginine

Column	Dimmension	Mobile phase	Detection	Results
Thermo C18 Aq	150 mm x 4.6 mm x 3µm	Formic acid solution 0.04%	ELSD	$k_{\text{Arg}} = 0.12$
Zorbax Phenyl	250 mm x 4.6 mm x 5 µm	2/98 ACN/Formic acid solution 0.04%	ELSD	$k_{\text{Arg}} = 0.00$
		2.5/97.5 MeOH/AcOH 100mM pH=5.2	ELSD	$k_{\text{Arg}} = 0.15$
Thermo Hypercarb (Porous Graphitic Carbon)	100 mm x 4.6 mm x 3 µm	2.5/97.5 MeOH/AcOH 100mM pH=5.2	ELSD	$k_{\text{Arg}} = 0.63$
Supelco Ascentis Express (HILIC)	50 mm x 2.1 mm x 2.7 µm	50/50 ACN/50 mM NaH_2PO_4	UV $\lambda=207$ nm	$k_{\text{Arg}} = 0.16$
		50/50 ACN/50 mM AcNH_4	ELSD	$k_{\text{Arg}} = 0.16$
Interchim HIT (HILIC)	150 mm x 4.6 mm x 2.6 µm	60/40 ACN/(2.5/97.5 MeOH/AcOH 100mM pH=5.2)	ELSD	$k_{\text{Arg}} = 2.46, k_{\text{Orn}} = 2.69, k_{\text{Cit}} = 1.08$ C_{additive} too high
		70/30 ACN/100 mM AcOH pH=5.2	ELSD	$k_{\text{Arg}} = 6.79, k_{\text{Orn}} = 8.29, k_{\text{Cit}} = 2.42$ C_{additive} too high
		70/30 ACN/25 mM AcOH pH=5.2	ELSD	$k_{\text{Arg}} = 11.79, k_{\text{Orn}} = 13.58, k_{\text{Cit}} = 2.13$ C_{additive} OK

First of all a classical octadecyl silane stationary phase⁷⁸ was tested, but the retention was too short ($k_{\text{Arg}} = 0.12$), whatever the composition of the mobile phase, due to the high polarity of arginine ($\log P = -3.2$). Then another polarity of reverse stationary phase was tested, a phenyl based stationary phase,⁷⁹ but there was no retention (arginine in the dead time).

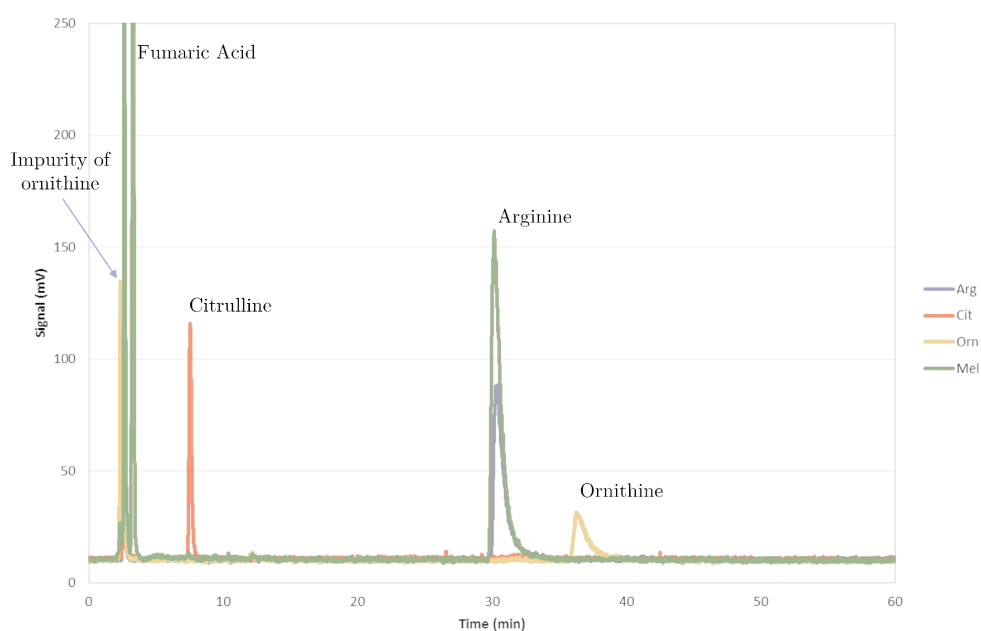
A porous graphitic carbon (PGC) stationary phase was also tested for its polar retention ability, but the retention of arginine was too short ($k_{\text{Arg}} = 0.63$), and it could not be separated from its impurities.

Since the retention in reverse phase is too low, and it gave unsatisfying separation between arginine, its impurities and fumaric acid, another chromatographic mode was tested: HILIC (Hydrophilic Interaction Liquid Chromatography).^{77,80,81} Two different columns were tested: a Supelco Ascentis Express and an Interchim HIT. The second one gave satisfying results (*i.e.* a complete separation of fumaric acid, citrulline, arginine and ornithine (in the order of elution)) after optimization of the mobile phase conditions.

The last method (TABLE II.2) was the only one compatible with mass spectrometry detection and which provided a good separation towards citrulline and ornithine (FIGURE II.1).

TABLE II.2 – HILIC Chromatographic Conditions (**HPLC conditions 1**)

Column	Interchim HIT 150 mm × 4.6 mm × 2.6 μm
Mobile phase	70/30 Acetonitrile/Ammonium acetate pH=5.2 25mM
Flow rate	0.8 mL/min
Detection	ELSD or ESI-MS (ElectroSpray Ionization - Mass Spectrometry)
Temperature	25 °C
Injection volume	20 μL

FIGURE II.1 – HPLC-ELSD chromatograms of arginine, citrulline, ornithine, arginine fumarate (**HPLC conditions 1**)

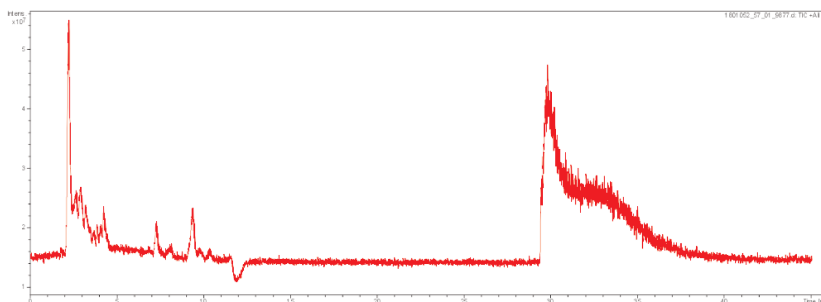
The method is transferred to HPLC-MS with conditions described in TABLE II.4, in order to improve the method sensitivity and to identify impurities (FIGURE II.2). Possible impurities and their m/z ratios are listed in TABLE II.3.

TABLE II.3 – Potential impurities of arginine and their protonated m/z

Compound	[M+H] ⁺ m/z
Arginine	175
Citrulline	176
Ornithine	133
Asymmetric dimethyl arginine	203
Symmetric dimethyl arginine	203
Monomethyl arginine	189

TABLE II.4 – Mass spectrometer conditions (and MS/MS fragmentation conditions) (**MS conditions**)

ESI	positive mode
Nebulizer	45 psi/300 °C
Dry gas	12 L/min
Capillary	3000 V
Skimmer	40 V
CapExit	104.5 V
	0.29
Amplitude fragmentation	(smart frag 30-200%)

FIGURE II.2 – HPLC-MS analysis of the arginine fumarate salt made by simple mix of powders ($tr = 2,5$ min fumaric acid, $tr = 30$ min Arginine) full scan between m/z 50 and 250 (**HPLC conditions 1, MS conditions**)

The poor peak shape in FIGURE II.2 was attributed to an overloading of the stationary phase and of the ESI source. This overloading was necessary in order to observe impurities.

Mass spectrometry allowed us to observe selective m/z even after analysis with extracted ion chromatograms (EIC). Arginine fumarate was analyzed before recrystallization (FIGURE II.3).

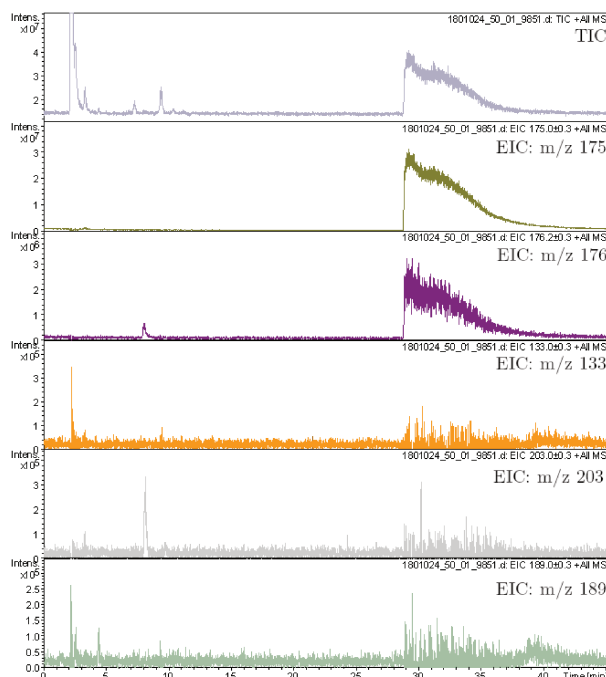


FIGURE II.3 – Total ion current chromatogram (TIC) and EIC of the m/z ratios in TABLE II.3 of the chromatogram presented in FIGURE II.2 (before recrystallization) (the large peak at 30 min for m/z 176 is due to the precision of the mass spectrometer, arginine m/z 175.2)

Before recrystallization different impurities were observed, some of them were identified, citrulline at 8 min, dimethyl-arginine at 8 min, and monomethyl-arginine at 4.5 min. Two peaks at 7.2 and 9.5 min (MS/MS mass spectra in FIGURE II.4) were also detected with m/z ratios of 158 and 217 which can be possibly attributed to arginine without an amine group and a propyl or isopropyl ester of arginine respectively.

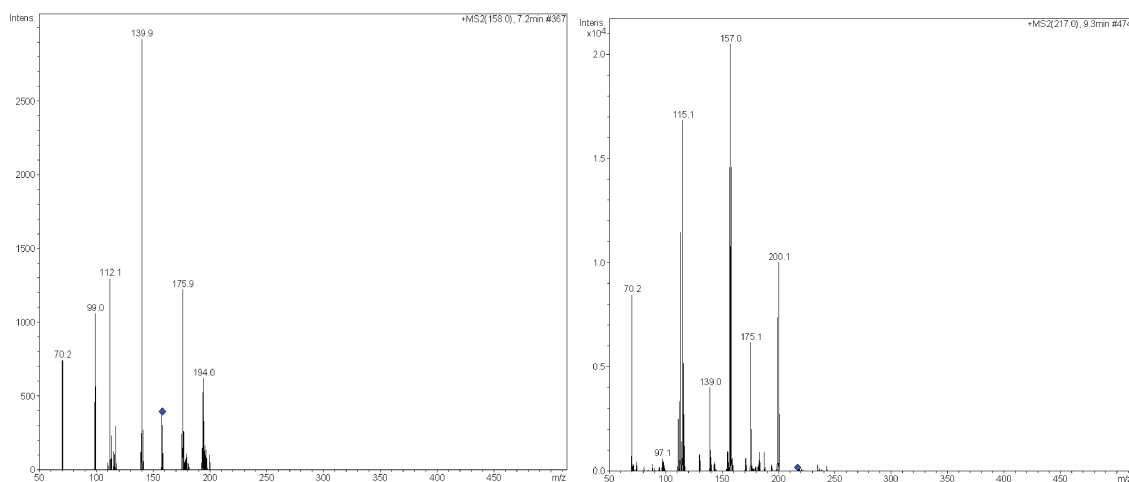


FIGURE II.4 – Mass spectra of MS/MS of the peaks at 7.2 and 9.5 min

A recrystallization method was developed in order to remove impurities of the arginine fumarate salt (Appendix A.2). The solid was analyzed by HPLC-MS (FIGURE II.5).

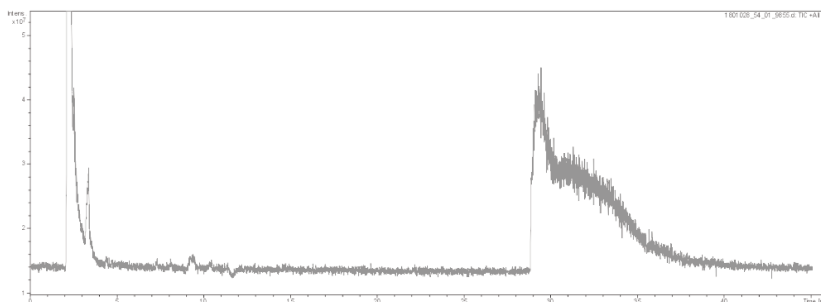


FIGURE II.5 – HPLC-MS analysis of the arginine fumarate salt after recrystallization, full scan between m/z 50 and 250 (**HPLC conditions 1, MS conditions**)

The same EIC were extracted for the HPLC-MS analysis of the recrystallized solid in the same way as before the recrystallization (FIGURE II.3).

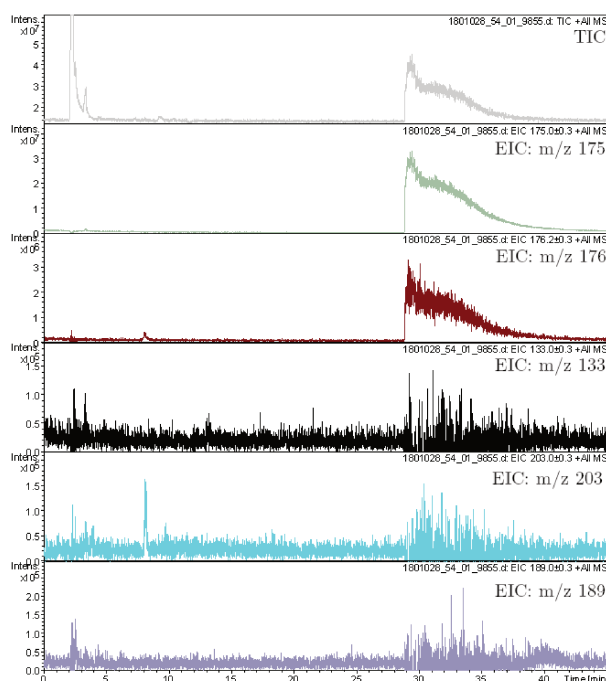


FIGURE II.6 – Total ion current chromatogram (TIC) and EIC of the m/z ratios in TABLE II.3 of the chromatogram presented in FIGURE II.5 (after recrystallization) (the large peak at 30 min for m/z 176 is due to the precision of the mass spectrometer, arginine m/z 175.2)

Most of the impurities were removed. The amount of citrulline and dimethyl-arginine were divided by ten, and no more monomethyl-arginine was observed. One can notice that the first peak is more intense; it can be attributed to fumaric acid. The amount of fumaric acid remained the same but before recrystallization inorganic salts can be present and they could achieve a suppression of the signal in the first part of the chromatogram.

This purified salt was used for all the PE experiments. The obtained salt has the same X-Ray powder diffraction (XRPD) pattern as the calculated one from the single crystal structure parameters²² (FIGURE II.7).

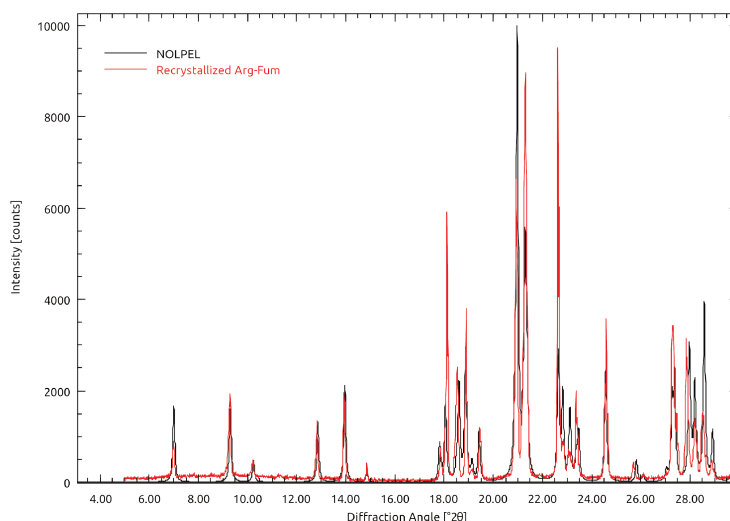


FIGURE II.7 – Comparison of the XRPD of the recrystallized salt and the calculated one from the single crystal structure parameters (ref. code in CSD (Cambridge Structure Database): NOLPEL)

3 Quantification and Determination of Enantiomeric Excess Using HPLC-UV Method

Determination of the precise quantity of each enantiomer in liquid and solid phases is necessary in order to understand mechanisms of the preferential enrichment. A chiral HPLC-UV method was developed in order to quantify both enantiomers.

3.1 Method Development

The first step to develop methods in chiral chromatography is to check the CHIR-BASE.⁸² Results with commercially available columns are shown in TABLE II.5 with the chromatographic resolution (R) when it is available

$$R = 2 \left(\frac{t_{r(A)} - t_{r(B)}}{\omega_{(A)} + \omega_{(B)}} \right) \quad (\text{Eq. II.1})$$

for A and B two compounds, with t_r being the retention time, and ω being the width at the base of the peak.

The main issue of these results is that the arginine was derivatized in each hit. Despite

the strong improvement in signal intensity with derivatized arginine, the derivatization remains a long process, and racemization can occur during the derivatization. Moreover water was used as a solvent for PE experiments with arginine fumarate, and water is often not compatible with derivatization, *i.e.* in order to perform derivatization all samples needed to be dried.

TABLE II.5 – CHIRBASE Hits

Analyte	Phase	Mobile phase	Resolution
N-benzoyl-arginine- β -naphthamide ⁸³		50/50 MeOH/H ₂ O	0.60
Dansyl-arginine ⁸⁴	Astec Cyclobond I	70/30 MeOH/H ₂ O	0.60
AQC-Arginine ⁸⁵		80/20 ACN/MeOH + 0.2% AcOH + 1% Et ₃ N	1.45
FMOC-Arginine ⁸⁶	Merck Chiraldex	20/80 ACN/0.1 M AcNH ₄ pH=4.4	/
	Merck Chiraldex gamma	10/90 ACN/0.1 M AcNH ₄ pH=4.4	/
N-Dabsyl-arginine ⁸⁷	Sumika Sumichiral OA-3100	MeOH + 0.03 M AcNH ₄	/
	Sumika Sumichiral OA-3200		/
N- α -benzoyl-arginine- β -naphthylamine ⁸⁸	Chirobiotic T	54.5/45.5 MeOH/ACN + 0.2% Et ₃ N + 0.2% AcOH	0.80
Dansyl arginine ⁸⁹	Merck Chiraldex	70/30 MeOH/0.1 M AcNH ₄ 0.1% Et ₃ N pH=5.5	/
Dabsyl-arginine ⁸⁹		90/10 MeOH/0.1 M AcNH ₄ 0.1% Et ₃ N pH=5.5	/
PITC-arginine ⁸⁹		/	
NITC-arginine ⁸⁹		40/60 MeOH/0.1 M AcNH ₄	/
DNITC-arginine ⁸⁹		0.1% Et ₃ N pH=6.5	/
DABITC-arginine ⁸⁹		/	
AQC-Arginine ⁸⁹		50/50 MeOH/0.1 M AcNH ₄ 0.1% Et ₃ N pH=6.5	/
N-benzoyl-arginine ⁹⁰			50/50 MeOH/H ₂ O
N-t-butoxycarbonyl- Nw-p-tosyl-arginine ⁹⁰	Chirobiotic R	20/80 MeOH/0.1% AcO-Et ₃ NH pH=7	0.90
		20/80 MeOH/0.1% AcO-Et ₃ NH pH=4.1	0.80
20/80 MeOH/0.1% AcO-Et ₃ NH pH=7		1.56	
20/80 MeOH/0.1% AcO-Et ₃ NH pH=4.1		1.40	
(7-nitro-2,1,3- benzoxadiazol-4-yl)-arginine ⁹¹	Sumika Sumichiral OA-2500S	MeOH	1.12

Nevertheless, three possible enantioselective separations of native arginine were reported in the literature :

- using crown ether stationary phase,²² but the mobile phase, a perchloric acid solution is not compatible with mass spectrometry detection,
- Daicel ZWIX stationary phase, based on quinine, but the mobile phase is not compatible with the UV detection of arginine due to the important concentration of ammonium acetate buffer and the low UV response of arginine,
- using Chirobiotic T stationary phase,^{42,92} the mobile phase is compatible with mass spectrometry and UV detection (MeOH and water with formic acid).

The Chirobiotic T phase is based on a macrocyclic antibiotic, Teicoplanin, naturally produced by the mildew *Actinoplanes teichomyeticus*.⁹³ Teicoplanin is an anti Gram-positive bacteria agent. It is composed of four macrocycles of aromatic ring, amide and ether functions, on which three sugar units were grafted (FIGURE II.8). These different interaction sites form a “basket” shape macrocycle.

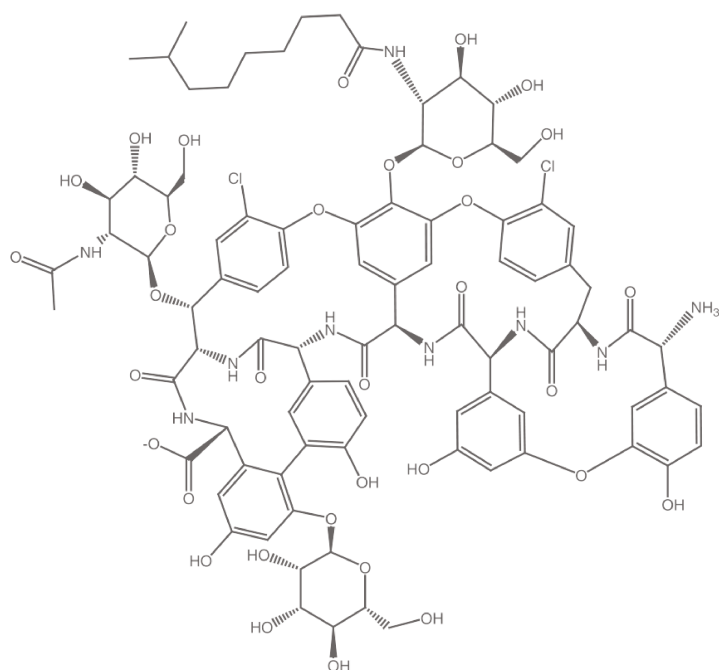


FIGURE II.8 – Structure of Teicoplanin A2-2 used in Chirobiotic T columns⁹⁴

The advantage of the method developed for this work (based on existing methods^{42,92}) (TABLE II.6) was the ability to be coupled to mass spectrometry.

TABLE II.6 – Chromatographic conditions for the chiral separation on an Ultimate 3000 chromatographic apparatus (**HPLC conditions 2**) the same conditions were also used with a Dionex dual chromatographic apparatus (**HPLC conditions 2b**)

Column	Chirobiotic T (Supelco) 150 mm × 2.1 mm × 5 μm
Mobile phase	65/35 Methanol/Formic acid 0.04 % (v/v)
Flow	0.2 mL/min
Detection	UV (λ = 207 nm)
Temperature	25 °C
Injection volume	5 μL

These conditions were optimized in order to achieve a fast separation with a resolution higher than 1.5 (minimum value to avoid overlapping of two peaks of the same size and shape). The retention according to the percentage of organic solvent on a Teicoplanin column differs from reverse phase chromatography. Retention factor (k) values of the two enantiomers are plotted against the percentage of MeOH in the mobile phase with constant formic acid concentration. The minimum k values is for a composition of 60% MeOH.

$$k = \left(\frac{t_r - t_m}{t_m} \right) \quad (\text{Eq. II.2})$$

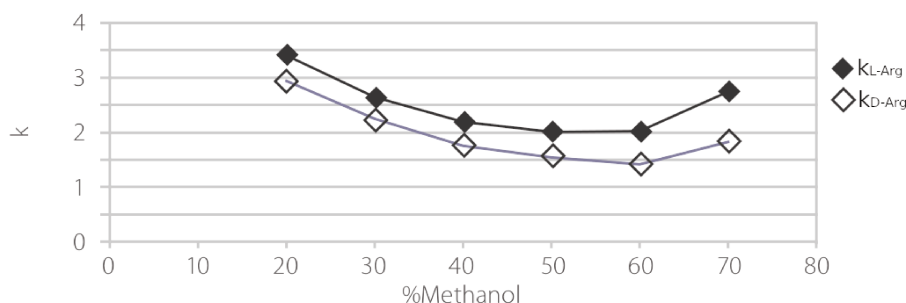


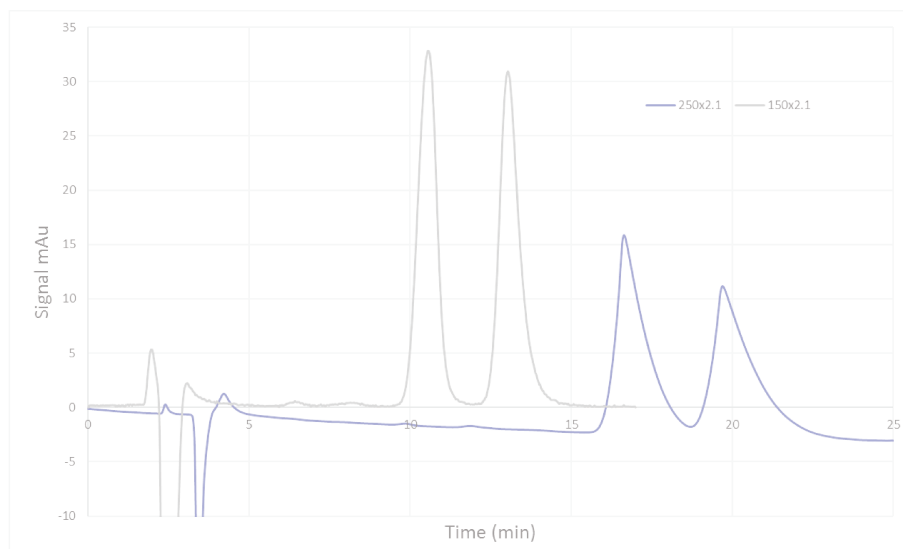
FIGURE II.9 – Variation of retention factors for DL-arginine⁹² versus MeOH percentage (at constant formic acid concentration)

The wavelength is set at 207 nm to optimize the signal-to-noise ratio of the peaks of arginine enantiomers. The maximum absorption of arginine is below 200 nm.

Sometimes batches of Chirobiotic T present more adsorption sites than others leading to tailing peaks (TABLE II.7 and FIGURE II.10).

TABLE II.7 – Comparison of parameters of two new Chirobiotic T columns (**HPLC conditions 2**)

column	k_L	k_D	α	As_L	As_D	N_L	N_D	R
150 mm x 2.1 mm	5.77	7.37	1.28	0.98	1.35	1431	2206	2.24
250 mm x 2.1 mm	5.91	7.18	1.22	1.63	1.86	1801	1487	1.70

FIGURE II.10 – Comparison of chromatograms of two new Chirobiotic T columns (in this case, the 250 x 2.1 column was used with **HPLC conditions 2** and the 150x2.1 column was used with **HPLC conditions 2b**) at 0.500 mg/mL of each enantiomers

The 250 mm one exhibited a lower resolution than the 150 mm one. The peak tailing is probably due to a less efficient end-capping, leading to interactions between free silanol group and arginine enantiomers.

In order to reduce uncertainties of measurement for the quantification, an internal calibration is necessary. Uncertainties can be due to injection or sample preparation. To choose an internal standard some criteria were required :

- have a similar structure as the analyte (here an amino acid),
- have a detection response in the same order of magnitude,
- do not react with the analyte,
- not be present in the sample,
- do not increase the analysis time (if possible).

Amino-acids fulfill most of these criteria. Some enantiomers of amino-acids were tested (TABLE II.8) in mixture with racemic arginine and fumaric acid.

TABLE II.8 – Internal standards

Compound	Separation	Detector response ($\lambda = 207$ nm) at the same level of concentration as Arginine
L-Asparagine	co-eluted with fumaric acid	same as arginine
D-Phenylalanine	eluted between Arg and fumaric acid	higher than arginine
L-Citrulline	co-eluted with fumaric acid	same as arginine
L-Ornithine	co-eluted with arginine	same as arginine
D-Tryptophan	eluted between Arg and fumaric acid	higher than arginine
L-Methionine	co-eluted with fumaric acid	same as arginine
D-Methionine	eluted between Arg and fumaric acid	same as arginine
L-Proline	co-eluted with fumaric acid	same as arginine
L-Cysteine	co-eluted with fumaric acid	same as arginine
L-Lysine	co-eluted with arginine	same as arginine

D-Methionine was chosen as an internal standard because it fulfilled all the conditions (FIGURE II.11).

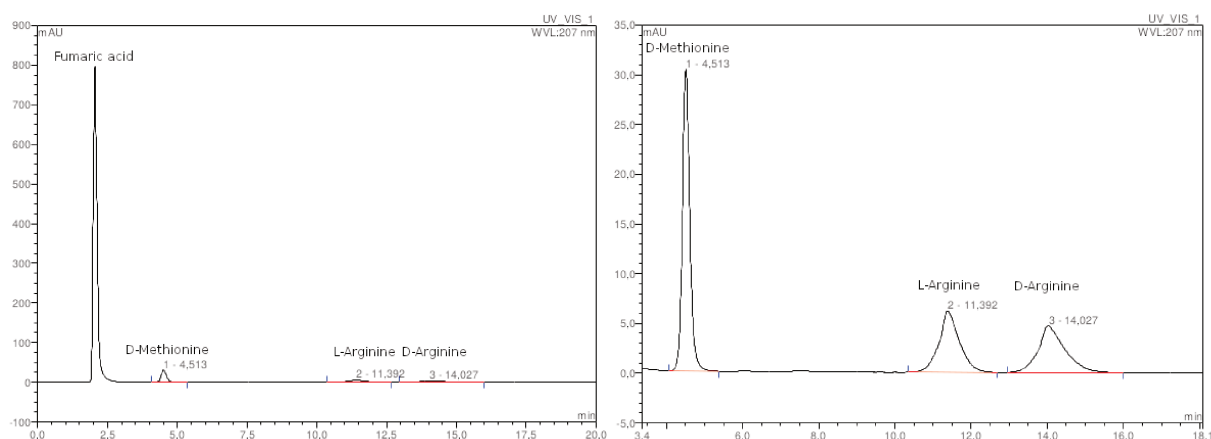


FIGURE II.11 – Chromatogram of arginine fumarate with D-Methionine as internal standard (left: full size, and right: zoom between 3.4 and 18 min)(**HPLC conditions 2**) at 0.300 mg/mL of each enantiomer

3.2 Method Validation

To validate the quantification method of the two enantiomers of the arginine fumarate for the preferential enrichment process, the following performance parameters were evaluated:^{95–98} specificity, linearity, accuracy, precision, limit of detection (LoD), and limit of quantification (LoQ).

3.2.1 Specificity

The interest of specificity is to check if the quantification is performed only on the analyte inside the matrix.

The matrix is composed of 3 known compounds (Fumaric acid, L-Arginine, D-Arginine). An internal standard (D-Methionine) is added before analysis. The four compounds are well separated (FIGURE II.11), and the chromatogram was compared to an injection of the medium of PE experiments: water/ethanol (Appendix C.1). There was no interference either with the peaks of the analytes nor with the internal standard. The method can be considered *specific*.

3.2.2 Linearity

Linearity is the capacity of a method to give a linear relation between the concentration of analyte in the sample and the detector response.

To evaluate linearity, 14 standard solutions were analyzed at concentrations of 0.010, 0.025, 0.050, 0.100, 0.150, 0.200, 0.250, 0.300, 0.350, 0.400, 0.450, 0.500, 0.550, 0.600 mg/mL in each enantiomer of Arginine Fumarate, in three replicates, in order to measure samples with $0 \leq \text{e.e.} \leq 96\%$. After the analyses, a plot was drawn relating the ratio between enantiomer and internal standard peak areas to the ratio between enantiomer and internal standard concentrations. The slope, the y-intercept and the coefficient of determination (R^2) were calculated by linear regression, R^2 must be ≥ 0.999 (TABLES II.9 to II.10). Calibration curves are presented in Appendix C.2.

TABLE II.9 – Linearity tests (average results of triplicate injections)

Name	[LRFA] mg/mL	[LRFA]/[DM]	Area LRFA / Area DM	Area DRFA / Area DM	e.e. %
E1	0.010	0.20	0.06	0.06	1.1
E2	0.025	0.50	0.15	0.15	0.4
E3	0.050	0.99	0.29	0.28	0.7
E4	0.100	1.98	0.56	0.56	0.0
E5	0.150	2.98	0.85	0.85	0.1
E6	0.200	3.97	1.12	1.12	0.1
E7	0.250	4.96	1.42	1.42	-0.1
E8	0.300	5.95	1.68	1.69	0.0
E9	0.350	6.95	1.96	1.95	0.2
E10	0.400	7.94	2.24	2.24	0.1
E11	0.450	8.93	2.52	2.52	0.1
E12	0.500	9.92	2.80	2.79	0.1
E13	0.550	10.92	3.06	3.06	0.0
E14	0.600	11.91	3.38	3.38	0.0

TABLE II.10 – Linearity test compliance

	L-arginine fumarate	D-arginine fumarate
Equation	$A = 0.28147C + 0.00732$	$A = 0.28140C + 0.00559$
$R^2 \geq 0.999$	0.99995	0.99993
Relative slope difference	0.03%	

The two calibration curves were linear ($R^2 \geq 0,999$). The relative slope difference between both curves is negligible (0.03%), only the calibration curve of L-arginine is used for the other parameter evaluations. The method can be considered *linear*.

3.2.3 Precision

Precision of a method expresses the compliance of the results in a series of measures of one sample in identical conditions. Precision can be defined by three factors, repeatability, intermediate precision, and ruggedness.

3.2.3.1 Repeatability

The precision of the measure was evaluated by determining the relative standard deviation (RSD) under repeatability conditions by 6 successive injections of three concentration levels: Low 0.050 mg/mL (E3), Medium 0.300 mg/mL (E8), High 0.600 mg/mL (E14).

The RSD of peak areas must be $\leq 1\%$ for both enantiomers, the internal standard and the ratio between enantiomers and internal standard. E1 and E2 have a $1 \leq \text{RSD} \leq 5\%$ for D enantiomer measurement. Results of repeatability measurements are presented in TABLE II.11 for the Low level. Other levels are presented in Appendix C.3.1.

$$\text{RSD}(\%) = \frac{\text{standard deviation}}{\text{average}} \times 100 \quad (\text{Eq. II.3})$$

TABLE II.11 – Repeatability measurements at Low level (0.050 mg/mL)

	Area DM	Area LR	Area DR	Area LR/ Area DM	Area DR/ Area DM	e.e. (%)
E3	8.46	2.37	2.39	0.280	0.282	-0.3 %
E3	8.43	2.39	2.35	0.283	0.279	0.8 %
E3	8.42	2.35	2.34	0.280	0.278	0.2 %
E3	8.45	2.36	2.38	0.280	0.281	-0.2 %
E3	8.48	2.39	2.40	0.282	0.284	-0.4 %
E3	8.45	2.39	2.39	0.284	0.283	0.1 %
Average	8.45	2.38	2.37	0.281	0.281	0.0 %
RSD %	0.3%	0.7%	1.0%	0.6%	0.8%	N/A

The RSD of each peak area, and the RSD of the ratio of enantiomers peak area and internal standard peak area (TABLES II.11, C.1 and C.2) were less or equal to 1%. The method can be considered *repeatable*.

3.2.3.2 Ruggedness and Intermediate Precision

The ruggedness and the intermediate precision were evaluated by modifying the day of analysis of the 3 precision samples (the 3 levels of concentration used for the repeatability measurements). RSD was calculated with the sample of day 1. RSD must be $\leq 2\%$. The recovery was calculated using equation Eq. II.4 (R must be $98\% < R < 102\%$).

$$R = \frac{C_{\text{ruggedness}}}{C_{\text{repeatability}}} \times 100 \quad (\text{Eq. II.4})$$

The precision measurements were defined as day 1 and the ruggedness measurements were defined as day 2. Calculation are presented here for the Low level of concentration (TABLE II.12 to II.13). Other levels are presented in Appendix C.3.2.

TABLE II.12 – Ruggedness measurements at Low level (0.050 mg/mL)

	Aire DM	Aire LR	Aire DR	Aire LR/ Aire DM	Aire DR/ Aire DM	e.e. (%)
E3	8.46	2.38	2.39	0.282	0.283	-0.2%
E3	8.45	2.37	2.39	0.280	0.283	-0.5%
E3	8.53	2.40	2.39	0.282	0.281	0.2%
E3	8.48	2.37	2.35	0.280	0.277	0.5%
E3	8.46	2.37	2.36	0.280	0.278	0.3%
E3	8.50	2.39	2.40	0.282	0.282	-0.1%
Average	8.48	2.38	2.38	0.281	0.281	0.0%
RSD %	0.40%	0.60%	0.90%	0.30%	0.80%	N/A

TABLE II.13 – Ruggedness calculation at Low level (0.050 mg/mL)

	Aire DM	Aire LR	Aire DR	Aire LR/ Aire DM	Aire DR/ Aire DM	e.e. (%)
Average day 1	8.45	2.38	2.37	0.281	0.281	0.0%
Average day 2	8.48	2.38	2.38	0.281	0.281	0.0%
Average days 1 and 2	8.46	2.38	2.38	0.281	0.281	0.0%
RSD (%) days 1 and 2	0.4%	0.6%	0.9%	0.5%	0.8%	N/A

RSD between day 1 and 2 were less than 2% for each level of concentration. RSD of day 2 are less than 1% for each concentration level. The recovery of averages are included between 98% and 102%. The method can be considered *rugged*.

Results of repeatability and ruggedness respected the specifications described above. The method can be considered *precise*.

3.2.4 Accuracy

The accuracy expresses the closeness between real values and experimental values determined using the linearity equation.

To evaluate accuracy, 14 samples with different enantiomeric excess (0, 1, 2, 3, 5, 10, 35, 50, 65, 90, 94, 95, 96, 100%) were analyzed in triplicate injections with the concentrations shown in TABLE II.14.

TABLE II.14 – Concentrations (mg/mL) in both enantiomers

e.e. %	0	1	2	3	5	10	35	50	65	90	94	95	96	100
$C_{\text{LR-FA}}$	0.225	0.228	0.230	0.232	0.236	0.248	0.304	0.338	0.371	0.428	0.437	0.439	0.442	0.451
$C_{\text{DR-FA}}$	0.225	0.223	0.221	0.218	0.214	0.203	0.146	0.113	0.079	0.023	0.014	0.011	0.009	0.000

The recovery was calculated using equation (Eq. II.5) (with $98\% < R < 102\%$):

$$R = \frac{C_{\text{experimental}}}{C_{\text{theoretical}}} \times 100 \quad (\text{Eq. II.5})$$

The enantiomeric excess was calculated using equation⁶ Eq. II.6:

$$\text{e.e.}(\%) = \frac{C_{\text{LR-FA}} - C_{\text{DR-FA}}}{C_{\text{LR-FA}} + C_{\text{DR-FA}}} \times 100 \quad (\text{Eq. II.6})$$

the absolute error on the measurements of the enantiomeric excess must be less than 0.5% for e.e. < 10% and less than 1% for e.e. \geq 10%.

Average values are reported in TABLE II.15.

TABLE II.15 – Accuracy average results for 3 injections of each solution

calculated e.e.	experimental e.e.	error e.e.	recovery L	recovery D
0.0%	0.1%	0.1%	101.2%	101.0%
1.0%	1.4%	0.4%	101.9%	101.1%
2.0%	2.3%	0.3%	102.0%	101.3%
3.0%	3.3%	0.3%	102.4%	101.8%
5.0%	5.4%	0.4%	100.4%	99.5%
10.0%	10.7%	0.7%	100.5%	99.0%
35.0%	35.6%	0.6%	101.3%	99.5%
50.0%	50.3%	0.3%	98.5%	97.0%
65.0%	65.8%	0.8%	100.3%	96.3%
90.0%	90.6%	0.6%	102.0%	90.0%
94.0%	94.7%	0.7%	100.7%	79.3%
94.9%	95.3%	0.4%	101.9%	82.4%
95.9%	96.4%	0.4%	98.0%	73.2%
100.0%	100.0%	0.0%	101.6%	N/A

Errors on enantiomeric excess were less than 0.5% for $0 \leq \text{e.e.} < 10\%$ and less than 1% for $10 \leq \text{e.e.} \leq 100\%$. By expressing recovery values it is possible to estimate measurement error of the mass according to the enantiomeric excess (TABLE II.16).

TABLE II.16 – Error on mass measurements

	e.e.	Error on mass in L-arginine	Error on mass in D-arginine
Excess of L	$0 \leq \text{e.e.} \leq +35\%$	2.5%	2.5%
	$+35 \leq \text{e.e.} \leq +90\%$	2.5%	10.0%
	$+90 \leq \text{e.e.} \leq +95\%$	2.5%	20.0%
	$+95 \leq \text{e.e.} \leq +96\%$	2.5%	25.0%
Excess of D	$0 \geq \text{e.e.} \geq -35\%$	2.5%	2.5%
	$-35 \geq \text{e.e.} \geq -90\%$	10.0%	2.5%
	$-90 \geq \text{e.e.} \geq -95\%$	20.0%	2.5%
	$-95 \geq \text{e.e.} \geq -96\%$	25.0%	2.5%

These values (TABLE II.16) were used as precision for the results on each experiment.

3.2.5 Limit of Detection and Limit of Quantification

LoD is the lowest amount of analyte which can be detected. Based on signal-to-noise LoD was defined as the concentration when the signal-to-noise ratio equal 3.

LoQ is the lowest amount of analyte which can be quantitatively determined. Based on signal-to-noise LoQ was defined as the concentration when the signal-to-noise ratio equal 10.

Signal-to-noise ratio was calculated by the Chromeleon 6.80 software according to *American Society for Testing and Materials* (ASTM) method E 685-93(2013).⁹⁹ Values of the lowest measured concentrations are reported in TABLE II.17.

TABLE II.17 – Lowest measured concentrations

$C_{\text{LR-FA}}$ (mg/mL)	$S/N_{\text{LR-FA}}$	$S/N_{\text{DR-FA}}$
0.005	9.9	6.9
0.008	33.9	26.4

The LoD and LoQ concentrations are lower than the lowest measured concentrations and lower than the concentration linearity standards. LoQ had a concentration between 0.005 and 0.008 mg/mL, and LoD had a concentration lower than 0.005 mg/mL.

3.2.6 Conclusion of the validation

Considering results on the different parameters, the HPLC-UV method for the determination of concentrations and enantiomeric excess of the Arginine Fumarate salt is validated. The absolute error on enantiomeric measurement is less than 0.5% for e.e. < 10% and 1% for e.e. \geq 10%, error on mass can also been determined (TABLE II.16).

Quantification of samples was performed with the calibration curve, precision of the method was checked periodically (every 5 samples) with the injection of three standards (E3, E8 and E14).

4 Quantification Method of the $^{13}\text{C}_6\text{L-Arginine}$: HPLC-MS/MS

For the study of the mechanism of preferential enrichment, additions of labeled-L-arginine was implemented (Chapter III Section 4.1). In order to quantify $^{13}\text{C}_6\text{-L-Arginine}$ at μg level, a HPLC method coupled with mass spectrometry was developed on an Agilent 1200 HPLC coupled with a Bruker HCT.

4.1 Method Development

4.1.1 Analytical Conditions

The chiral HPLC-UV method was transposed directly to HPLC-MS. Parameters of the mass spectrometer were optimized using an automated method on m/z 175.2 (protonated arginine) in mobile phase solvent conditions. Conditions were the same as the ones presented in TABLE II.4. D-Methionine was used as an internal standard.

4.1.2 Fragmentation

Selected reaction monitoring is one of the methods of choice for the quantification of traces and to have a good selectivity of the signal. In an ion trap the fragmentation is done inside the trap. Fragmentation tests were performed in order to determine the best transitions in terms of specificity and intensity (TABLE II.18 and FIGURE II.12).

TABLE II.18 – Fragmentations for non labeled and labeled arginine

	Non labeled	Labeled	Lost fragment
Mass $[\text{M}+\text{H}]^+$	m/z 175	m/z 181	/
Fragments	m/z 158	m/z 164	NH_3
	m/z 157	m/z 163	H_2O
	m/z 116	m/z 121	Guanidine
	m/z 60	m/z 61	Norvaline

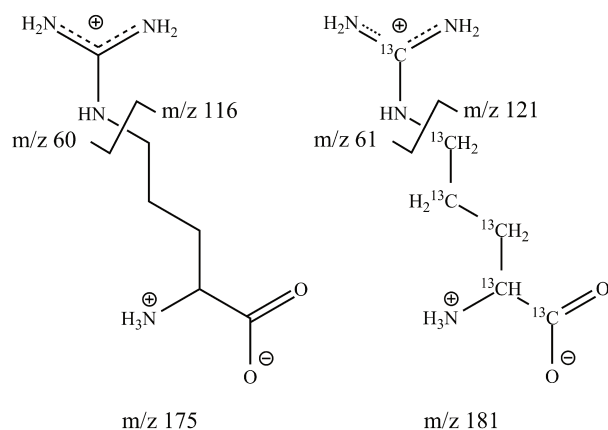
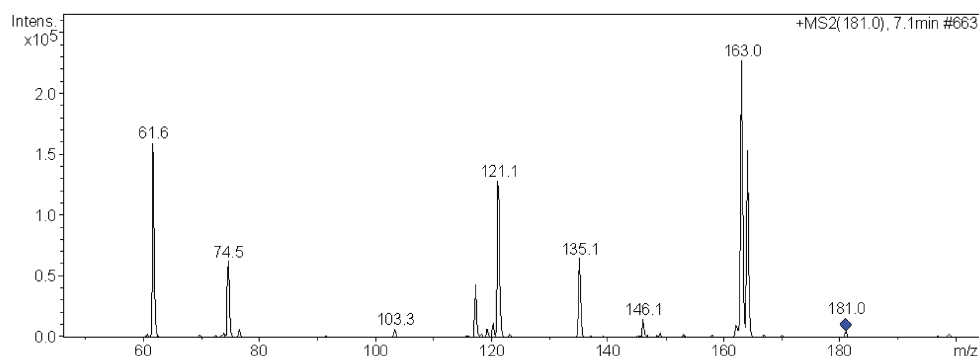


FIGURE II.12 – Fragmentation of guanidinium from non-labeled and labeled arginine

The two most intense fragmentations correspond to the loss of water and guanidine (mass spectrum in FIGURE II.13). To realize selective quantification of labeled arginine these two transitions (m/z 181 \rightarrow 163, m/z 181 \rightarrow 121) were used.

FIGURE II.13 – Mass spectrum of the fragmentation of labeled arginine m/z 181 (**MS conditions**)

The method for the mass spectrometer sequence during a chromatogram consisted in following two ion fragmentations one on m/z 181 (argininium) and one for the internal standard m/z 150 (D-methionine, mass spectrum in FIGURE II.15) then the obtained fragments were scanned from m/z 50 to 200. The obtained chromatogram is represented in FIGURE II.14.

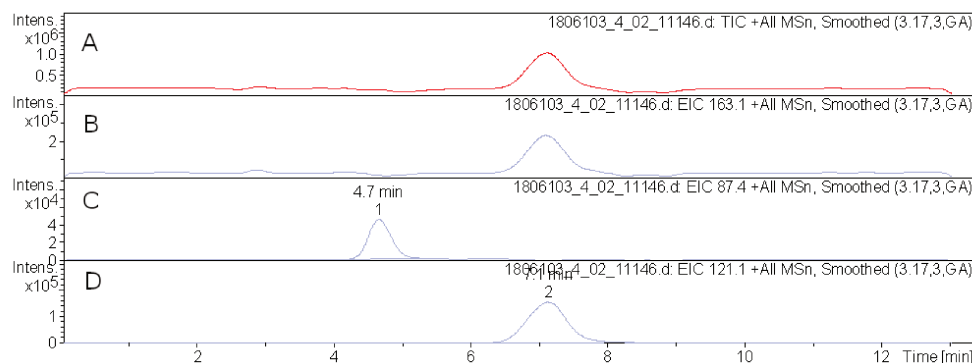


FIGURE II.14 – Chromatograms of a sample containing labeled arginine (**MS conditions**), A full HPLC-MS chromatogram, B Extracted ion chromatogram (EIC) of m/z 163, C EIC of m/z 87 (D-Methionine) and D EIC of m/z 121

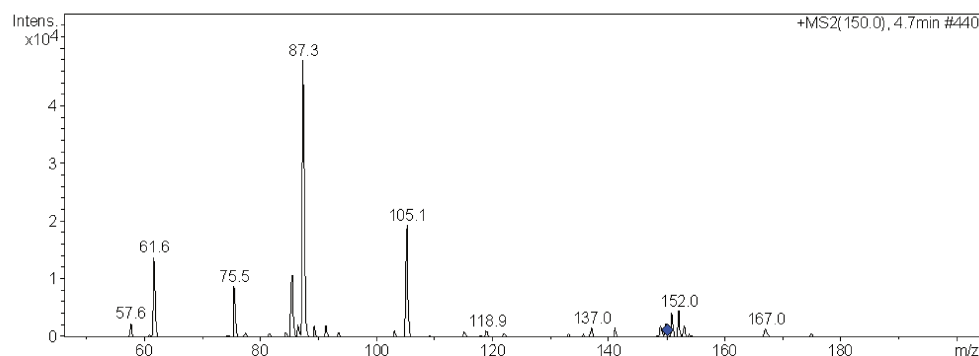


FIGURE II.15 – Mass spectrum of the fragmentation of methioninium m/z 150 (**MS conditions**)

4.2 Quantification

The response ratio of labeled arginine and non-labeled arginine was estimated equal to 0.9 (due to isotopic effect) with injection of samples with known arginine and $^{13}\text{C}_6$ -L-Arginine concentrations. Before each HPLC-MS/MS sequence, two external calibrations were performed with non-labeled arginine from 0.025 to 0.62 $\mu\text{g}/\text{mL}$ (FIGURE II.16) and from 0.62 to 6.2 $\mu\text{g}/\text{mL}$ (FIGURE II.17), injections were done in triplicate with the presence of an internal standard (D-Methionine).

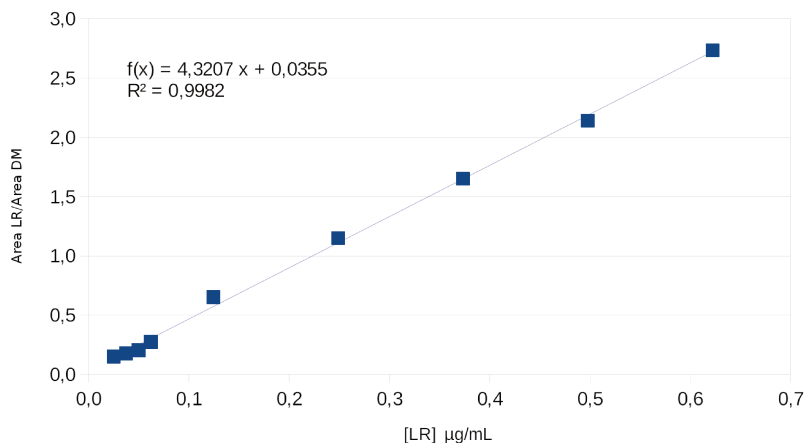


FIGURE II.16 – Calibration curve in L-Arginine from 0.025 to 0.62 µg/mL for the m/z 175→116 transition (**HPLC conditions 2, MS conditions**)

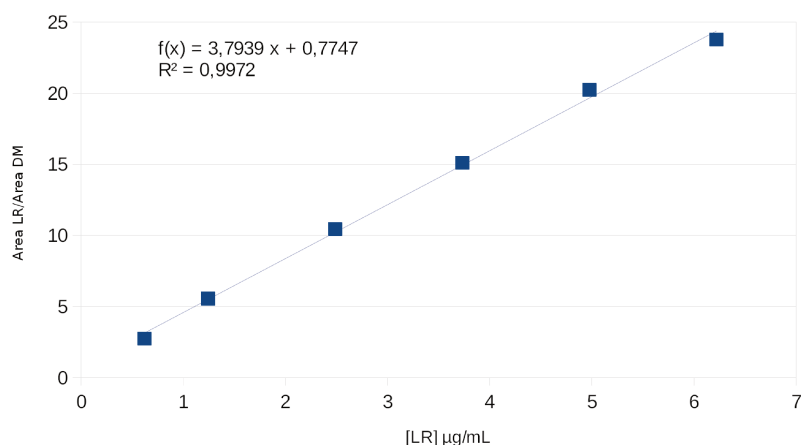


FIGURE II.17 – Calibration curve in L-Arginine from 0.62 to 6.2 µg/mL for the m/z 175→116 transition (**HPLC conditions 2, MS conditions**)

A control was made for each calibration in order to monitor deviations at the extreme values of the range. Concentrations were recalculated with the equation of the calibration curve. Then an error percentage was calculated with the following equation for each point of the range.

$$\%error = \left(1 - \frac{\text{experimental concentration}}{\text{theoretical concentration}} \right) \times 100 \quad (\text{Eq. II.7})$$

With these values, it is possible to determine the uncertainty values of results given by the two calibration curves. For the two calibration curves presented in FIGURE II.16 and II.17 uncertainties were 10 and 7% respectively.

5 Conclusion

The purification step of the arginine fumarate salt was controlled by HPLC-MS using HILIC mode chromatography. A good improvement of the purity was observed after recrystallization.

It was possible to measure mass balance of solid and liquid phases during the PE process, with a validated method in terms of linearity, precision and accuracy. Incertitudes for matter balance were evaluated in TABLE II.16 and thus enantiomeric excesses were determined with uncertainties of 0.5% for e.e. < 10% and 1% for e.e. \geq 10%.

Moreover the HPLC-MS/MS method allows for a specific quantification of labeled arginine, added at 1‰ ratio in experiments, in the solid and liquid phases with uncertainties of 10%.

Chapter III

Mechanism of Preferential Enrichment for Second Generation Compounds – Case Study of Arginine Fumarate

1 Introduction

The main objective of this PhD was to reconsider the mechanisms proposed by Prof. Tamura by a thorough reinvestigation of the PE process of a second generation compound, arginine fumarate (Arg-Fum), reported to exhibit PE by the Prof. Tamura group in 2014.²² The second objective was to verify and establish new criteria for PE.

The following parameters and their incidence on PE were given major attention in the course of this study: presence of solid solutions, supersaturation, hydrodynamics of the solution (*i.e.* stagnant, rocked and stirred), occurrence of polymorphic transitions and initial e.e.

2 Presentation of the Preferential Enrichment Process of Arginine Fumarate and Effects of its Parameters

2.1 The Arginine Fumarate System

Arg-Fum is a salt composed of a chiral amino acid and a dicarboxylic acid, both can be produced naturally. Arginine is an essential amino acid for birds and young mammals, it is also involved in the urea cycle.¹⁰⁰ Racemic Arg-Fum decompose upon melting (around 230 °C), which limits the possibility to draw the binary phase diagram.

Racemic Arg-Fum salt crystallizes in a $P\bar{1}$ space group, the asymmetric unit is composed of one disordered molecule of Arginine, an half of protonated fumaric acid, and an half of fully deprotonated fumarate anion (FIGURE III.1).

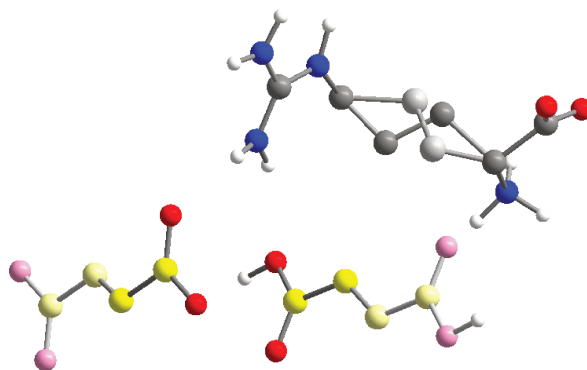


FIGURE III.1 – Asymmetric unit of arginine fumarate, the parts of the fumaric and fumarate entities are displayed in hollow color for the symmetrically generated atoms. The disorder on the arginine entity is displayed in light (37.1%) *vs* standard gray (62.9%) for the carbon atoms

The arginine entities establish strong hydrogen bonds, and give rise to a double layer in *ab* (FIGURES III.2 to III.4). These layers are connected along *c*, by means of hydrogen bonds established with the fumaric entities (the protonated and the deprotonated ones) (FIGURES III.5 to III.8). The cohesion of the packing is ensured by hydrogen bonds formed within each layer of segregated molecules.

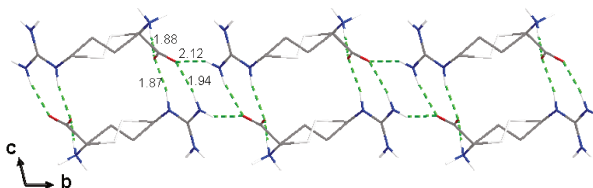


FIGURE III.2 – Projection along *a*, of a double layer of hydrogen bonded (dashed green lines) arginine molecules

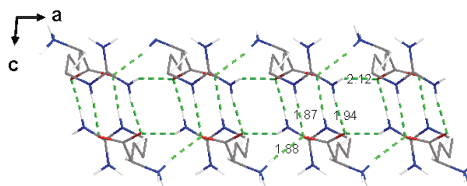


FIGURE III.3 – Projection along *b*, of a double layer of hydrogen bonded (dashed green lines) arginine molecules

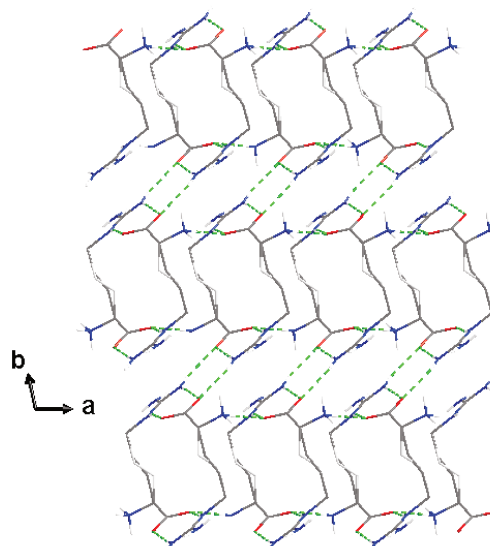


FIGURE III.4 – Projection along c , of a double layer of hydrogen bonded (dashed green lines) arginine molecules

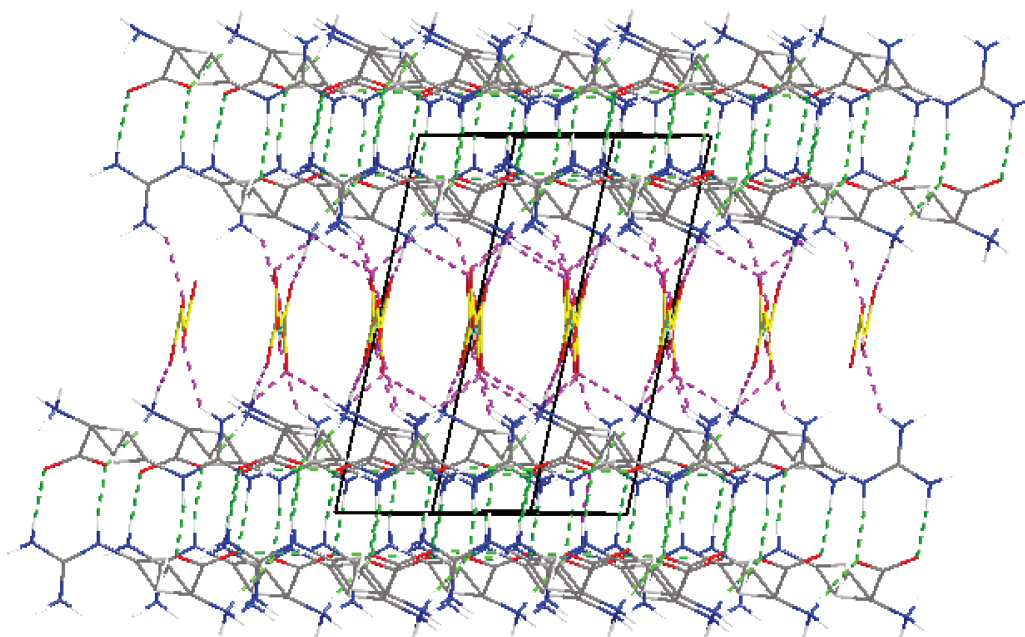


FIGURE III.5 – Aligned fumarate entities are intercalated between two consecutive double layers of arginine molecules, leading to two different type of slices, composed of segregated entities; these slices of different molecules establish hydrogen bonds (dashed pink lines)

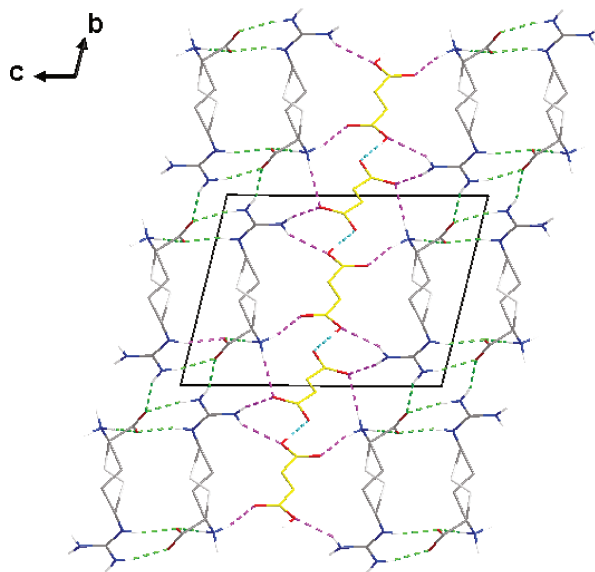


FIGURE III.6 – Projection along a , of connected slices of fumarate and arginine entities

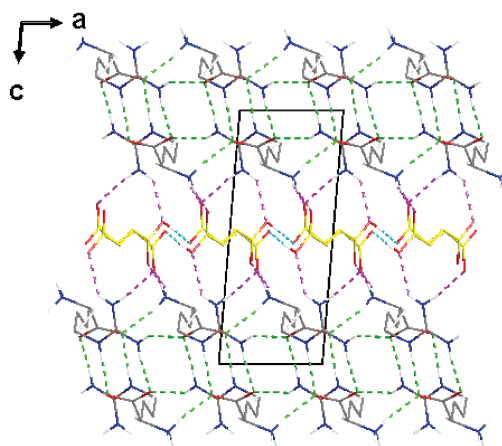


FIGURE III.7 – Projection along b , of connected slices of fumarate and arginine entities

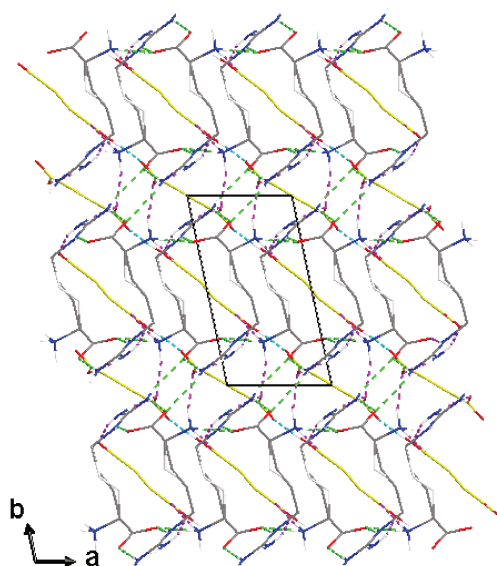


FIGURE III.8 – Projection along c , of connected slices of fumarate and arginine entities

It is possible to calculate the X-Ray Powder Diffraction (XRPD) pattern from the single crystal structure (FIGURE III.9).

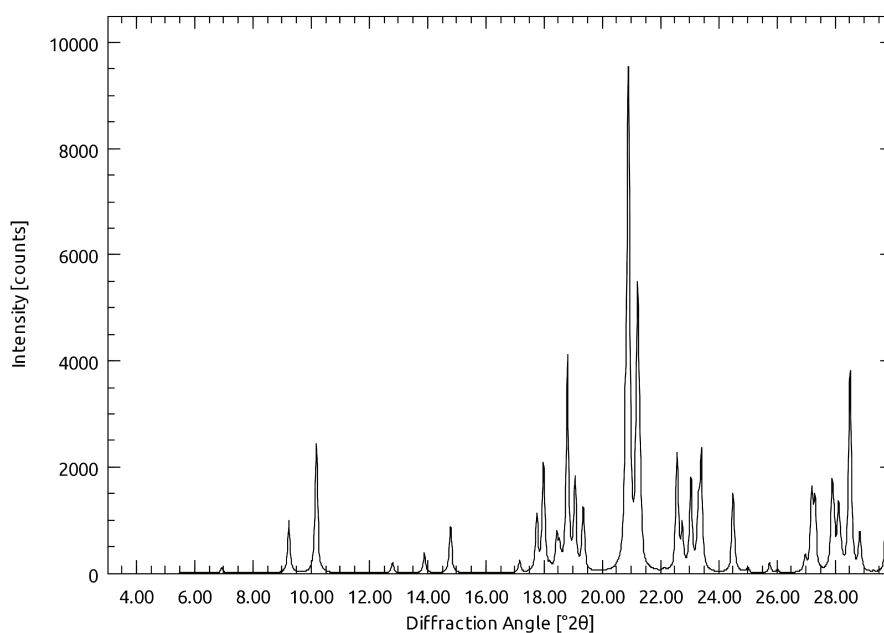
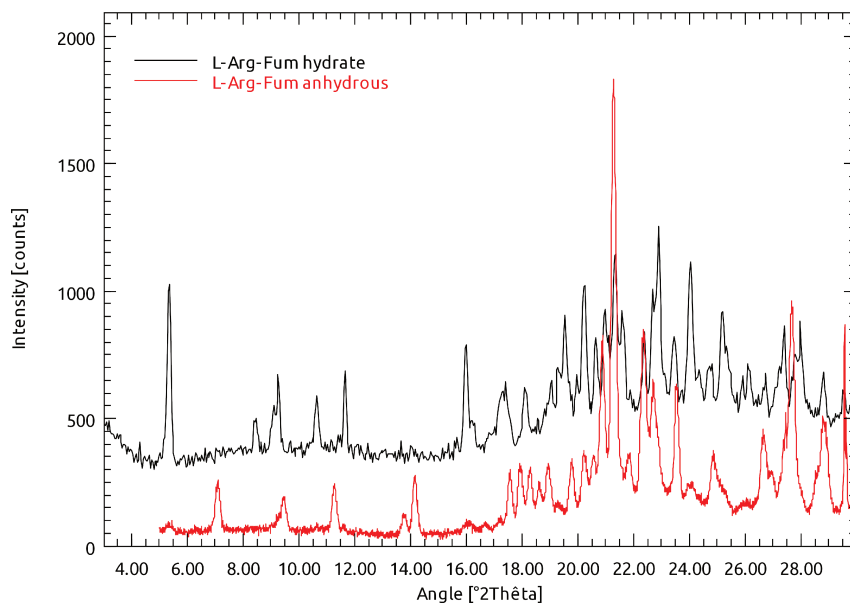


FIGURE III.9 – Calculated XRPD pattern of NOLPEL structure from 3 to 30° (2θ)

At the end of each experiment, XRPD pattern of the solid phase obtained was compared to the calculated one.

By crystallizing from water enantiopure Arg-Fum always gives an hydrate. It is possible after dehydration at 150 °C to obtain an anhydrous form of the L-Arg-Fum. The anhydrous form decompose upon melting around 165 °C. XRPD of anhydrous and hydrate form were represented in FIGURE III.10.

FIGURE III.10 – XRPD patterns of anhydrous and hydrate L-Arg-Fum from 3 to 30° (2θ)

2.2 Presentation of the Preferential Enrichment Process of Arginine Fumarate

All PE experiments were performed with the *standard protocol* detailed in Appendix A.3. Typical results of an experiment are detailed in TABLE III.1.

TABLE III.1 – Results of Arg-Fum PE performed with the *standard protocol*

Initial		Liquid				Solid			
m^a (mg)	e.e. ^b (%)	m_L^c (mg)	m_D^d (mg)	m_{total}^e (mg)	e.e. ^f (%)	m_L^c (mg)	m_D^d (mg)	m_{total}^e (mg)	e.e. ^f (%)
850	5	63 ± 2	1.0 ± 0.1	64 ± 2	96 ± 1	353 ± 9	380 ± 10	733 ± 19	-3.7 ± 0.5

^amass at time = 0; ^be.e. at time = 0; ^cfinal mass of L-Arg-Fum in liquid or solid; ^dfinal mass of D-Arg-Fum in liquid or solid; ^e $m_{total} = m_L + m_D$; ^ffinal e.e. in liquid or solid

Final masses for a PE experiment performed with the *standard protocol* are around 65 mg of quasi enantiopure Arg-Fum in the mother liquor and 750 mg of quasi racemic Arg-Fum in the deposited crystals.

When a system at the composition of the standard protocol was stirred to reach equilibrium state enantiomeric excesses were 0% for the solid phase and 77% for the liquid phase. PE with $\beta = 8$ is considered successful as long as e.e. > 77% for the mother liquor.

2.3 Statistical study

As a starting point to this work, we evaluated the variability of Arg-Fum PE process by performing a statistical study. This process was performed in stagnant conditions. The variability of enantiomeric excess in the solid and the liquid phases were observed.

A single PE experiment was performed 52 times in the same conditions (*standard protocol*), the e.e. values of the mother liquor and of the crystals were systematically measured in HPLC (Chapter II). Results of this study are given in TABLE III.2, FIGURES III.11 and III.12. Each one of the 52 experiments has shown PE (e.e. of the mother liquor $> 77\%$). It is of note that the crystals deposited during PE are strongly inhomogeneous in term of e.e. (with some crystals with opposite e.e. inside the same solid). Therefore an accurate quantification of the solid phase e.e. requires dissolution of the whole solid fraction: each time the whole solid was dissolved before analysis.

TABLE III.2 – Statistics on the 52 experiments of 6 days

	Mean e.e. _{solid}	e.e. _{liquid}
Average	3.3%	93.0%
Median	3.4%	94.0%
RSD	33.8%	4.7%
Minimum	0.8%	80.0%
Maximum	5.9%	98.0%
3 rd quartile	4.0%	96.0%
1 st quartile	2.7%	90.9%
9 th decile	4.7%	97.0%
1 st decile	1.7%	87.2%

1st quartile is defined as the middle value between the minimum and the median (25%).

3rd quartile is defined as the middle value between the maximum and the median (75%).

1st and 9th decile are defined with the same principle but at 10 and 90%.

In FIGURES III.11 and III.12 the axis steps used to count results were chosen according to the absolute error on enantiomeric measurements described in Chapter II, *i.e.* 0,5% for $|e.e.| < 10\%$ (solid phase) and 1% for $|e.e.| \geq 10\%$ (liquid phase).

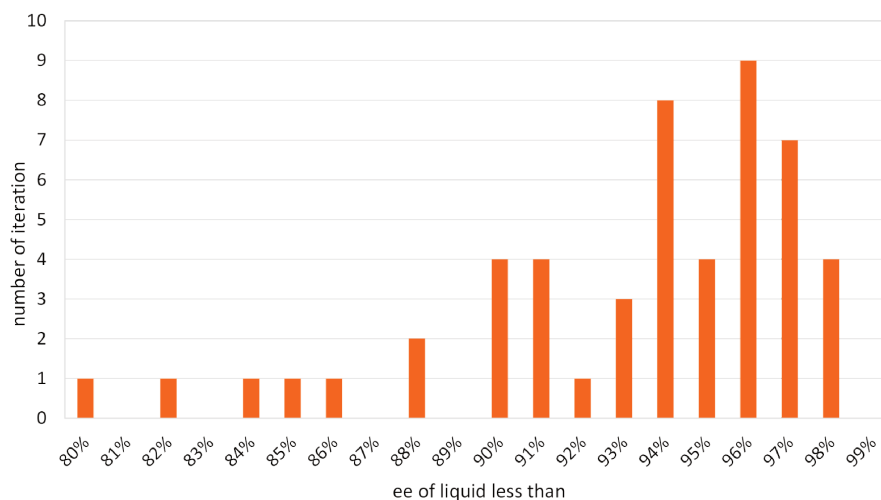


FIGURE III.11 – Number of iterations per unit of e.e. for the liquid phase

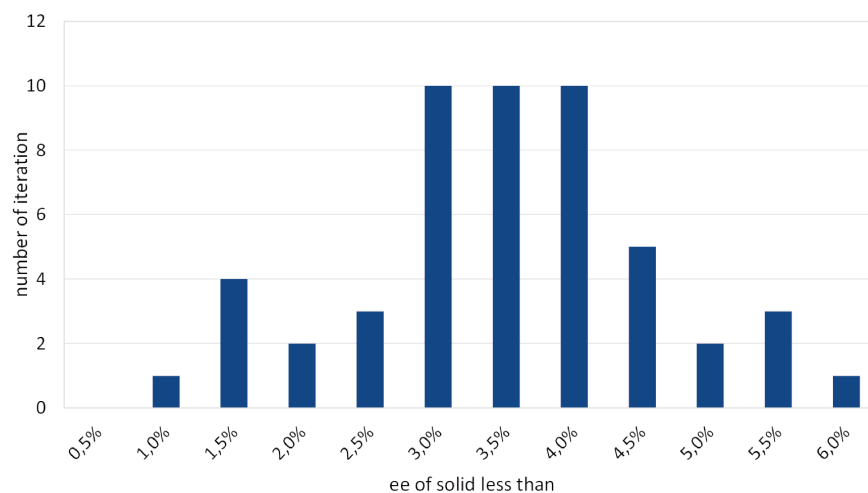


FIGURE III.12 – Number of iterations per half unit of e.e. for the solid phase

Iterations per half unit of e.e. in FIGURE III.12 show a Gaussian like distribution.

All enantiomeric excess were measured from 0.8% to 5.9% for the solid phase and from 80% to 98% for the liquid phase. RSD are 33.8% for the solid phase and 4.7% for the liquid phase. Half of the experiments have an excess between 2.7% and 4.0% for the solid and between 91% and 96% for the liquid.

The statistical study gives us the range of dispersion for a PE experiment with the *standard protocol* used in this study. This kind of dispersion is expected with an experiment performed with a supersaturation $\beta = 8$, and in stagnant conditions.

2.4 Effect of the Parameters

2.4.1 Overall Composition Effect

Knowledge of the overall composition (Ω), and of the tie lines should give the composition of the liquid and the solid for a crystallization process. Here experimental conditions have been adapted so that the Ω point evolves either along the S-R axis (variation of the starting enantiomeric excess) or along the Racemic composition-Solvent isoplethal section (variation of the starting supersaturation).

2.4.1.1 Effect of Starting Enantiomeric Excess

Six different initial e.e. were tested, 0, 1, 5, 10, 15, 20%; the e.e. of liquids and solids at the end of PE are reported in FIGURE III.13.

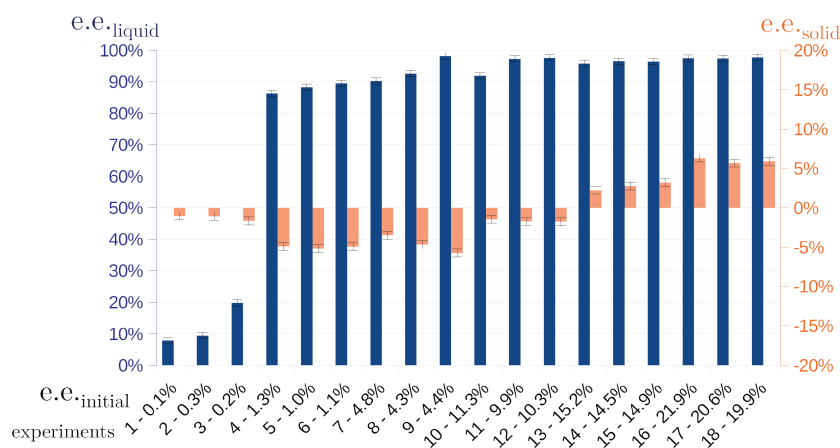


FIGURE III.13 – Enantiomeric excess of solid and liquid phases at the end of the process as function of initial e.e.

The e.e. of final liquids were similar, and close to 95% for $e.e. \geq 1\%$. For an initial e.e. of 0% the process is very slow: after 6 days the final e.e. of the liquids was still around 10 to 20%. Nevertheless, in the solid phase the e.e. shifts according to the initial e.e. If $0 \leq$ starting e.e. $\leq 11.3\%$, the deposited crystals have negative e.e. (*i.e.* opposite e.e.). If $14.5 \leq$ starting e.e. $\leq 21.9\%$ and onwards, the deposited crystals have positive e.e. There is thus a threshold above which the crystals are not enriched in the minor enantiomer.

This phenomenon can be represented with a ternary phase diagram (FIGURE III.14), to show the unexpected “tie-line” evolution.

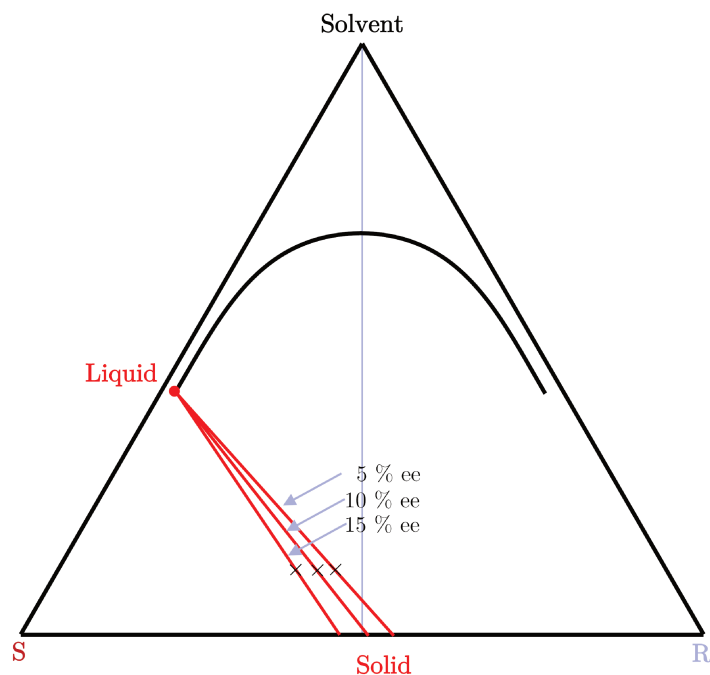


FIGURE III.14 – Theoretical diagram representing different final solid e.e. compositions as function of initial e.e.

In the PE process the composition of the solid phase seems to be directed by the line connecting the final liquid and the overall composition, and not by the composition of the solid and the overall composition.

2.4.1.2 Effect of starting supersaturation

Changing the supersaturation (β), change the overall composition Ω along the racemic (or quasi racemic) composition – solvent isoplethal section. To observe the impact of supersaturation and to determine the lower β threshold for successful PE, several PE experiments were performed at different β ratios. The results are given in TABLE III.3.

TABLE III.3 – Results of supersaturation tests

Experiments	Supersaturation	e.e. _{solid}	e.e. _{liquid}
19	8	-1.6	93
20	8	-2.3	90
21	6	-1.7	89
22	6	-2.1	90
23	4	-2.0	85
24	4	-2.5	90
25	2	1.8	66

With the decrease of β , a slight decrease of enantiomeric excess can be observed in the solid and liquid phases, down to $\beta = 2$ for which PE is considered unsuccessful. This slight decrease is significant and can be explained with the theoretical ternary phase diagram (FIGURE III.15). Indeed considering Ω_6 (schematically representing a $\beta = 6$) in FIGURE III.15, one can see that increasing the e.e. of the mother liquor up to 95% (as expected in an experiment with a higher β , for instance represented with Ω_8) would result in too high e.e. in the solid state that would bring the structure to collapse. In addition a lower β also reduces the capability of the system to evolve out of equilibrium. Actually, our results (TABLE III.3) at $\beta = 2$ are compatible with a regular crystallization (FIGURE I.26 left, p. 33).

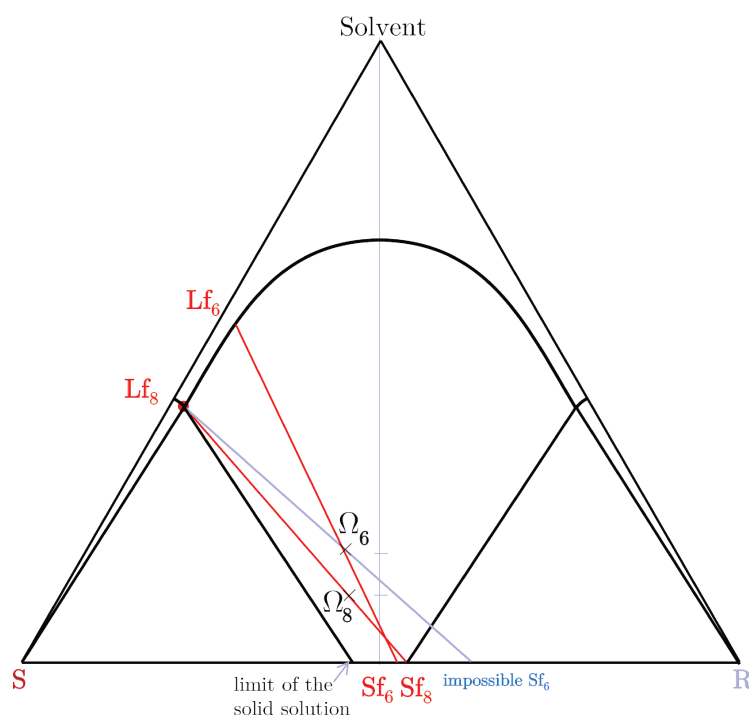


FIGURE III.15 – Theoretical diagram representing different final compositions as a function of initial supersaturation

2.4.2 Equilibrium state

It is established that PE is an *out of equilibrium* process which necessitates to be operated under stagnant conditions. It is also a slow process (more than 1 day). An early objective was to perform experiments with a very slow agitation apparatus in order to increase the speed of the process. Indeed, the use of regular magnetic stirring completely jeopardizes PE. A second objective was to perform long experiments in order to observe the *stability* of the system during a very long period with opposite enantiomeric excesses in the liquid and solid phases.

2.4.2.1 Influence of Agitation: Use of a Rocking plate

The apparatus used to perform agitation is a rocking plate (scheme in FIGURE III.16). The rocking plate can generate very mild agitation from 5 to 100 rpm (a rpm is a complete cycle).

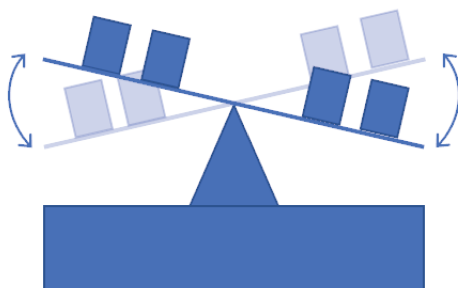


FIGURE III.16 – Schematic representation of a rocking plate

Two different speeds, 6 and 30 rpm, were tested, and compared with the same experiment performed under stagnant conditions (TABLE III.4 and FIGURE III.17).

TABLE III.4 – Results of PE performed with different agitation mode

Experiment	Agitation speed (rpm)	Time (h)	e.e.solid	e.e.liquid
26	0	144	-2.7	90
27	0	144	-3.9	94
28	0	77	-1.3	97
29	6	144	-1.3	90
30	6	144	-2.0	95
31	6	77	-2.7	97
32	6	24	-1.5	94
33	30	144	0.0	77
34	30	144	0.0	77
35	30	77	-1.2	95
36	30	24	-1.5	90
37	30	24	-1.7	97

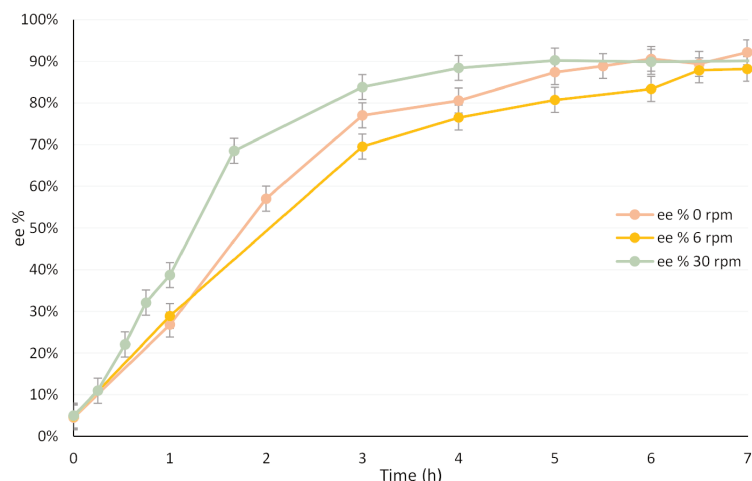


FIGURE III.17 – Variation of the e.e. of the liquid versus time as function of agitation speed (rpm)

The rocking plate accelerates the increase of e.e. of the solution. Nevertheless continuing agitation leads the system to equilibrium (experiments 33 and 34). In 6 days (144 h) at 30 rpm the system has an enantiomeric excess in the liquid of 77% and in the solid of 0%. At 6 rpm the same trend was observed but the return to an equilibrium state was longer (more than 6 days).

2.4.2.2 Evolution of a System after PE

Longer experiments were performed and compared to standard ones (TABLE III.5). The system can remain for at least 1 year with opposite enantiomeric excess with a slight trend to return to equilibrium.

TABLE III.5 – Results of stability tests compared with standard PE experiments at 5 °C

Experiment	Time (h)	e.e. _{solid}	e.e. _{liquid}
26	144	-2.7	90
27	144	-3.9	94
38	2 months	-3.0	95
39	1 year	-1.6	80

3 Monitoring of the Preferential Enrichment Process of Arginine Fumarate

3.1 Monitoring of Preferential Enrichment *versus* Time

Beside the statistical analysis and the multiparameter analyses presented in the previous section, a time-based monitoring of the PE process is central to gain knowledge on its mechanism.

To this end, monitoring of the enantiomeric composition of the mother liquor was performed during a single PE experiment (performed with the *standard protocol*), by sampling aliquots of the mother liquor. As mentioned previously, monitoring by sampling the e.e. of the crystal is not possible in this case due to the crystal inhomogeneities (monitoring the e.e. of the deposited crystals requires to run the same process several times and to stop it at different times to analyze the crystal composition).

For the first six hours of PE, a sampling was made every hour, afterwards the sampling was made every day for 6 days. For each sampling, 5 μL of the mother liquor are taken from the mother liquor (the volume cannot be greater in order to limit interferences on the system by modification of its total volume). A plot showing e.e. of the liquid phase *versus* time is shown in (FIGURE III.18). Nevertheless, imprecisions were important due to the possibility to pick-up particles with the liquid sample (despite much care during sampling), and the inhomogeneity of the liquid due to low diffusion in stagnant conditions.

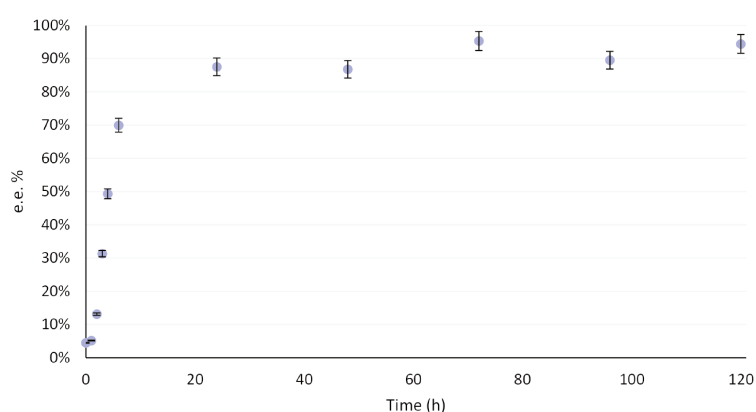


FIGURE III.18 – Monitoring of the liquid phase of a Preferential Enrichment experiment

To gain accuracy during monitoring and to have information about the solid phase

during PE the following procedure was adapted: for each value of time, two or three manipulations were done with the standard protocol. Experiments performed in the same conditions were stopped at 11 different times: 0.25, 0.50, 0.75, 1, 1.5, 2.5, 6, 12, 24, 72, and 144 h, to monitor the quantity of each enantiomer. Working in this way also served to analyze the solid phase.

Enantiomeric excesses of the 11 experiments were plotted in FIGURE III.19 and zooms are presented in FIGURE III.20.

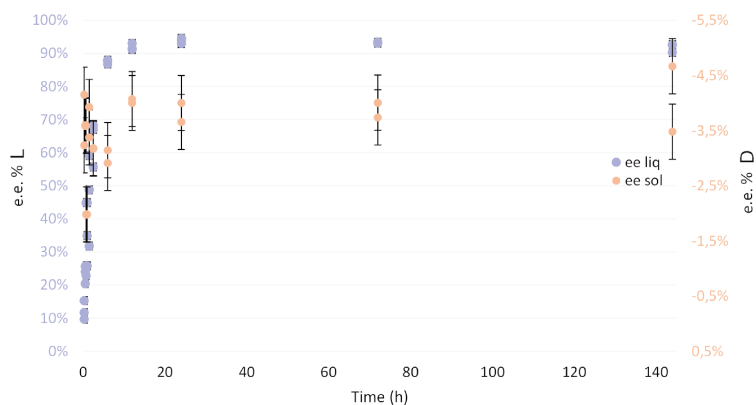


FIGURE III.19 – Monitoring of the enantiomeric excess measured in the solid and liquid phases during PE experiments

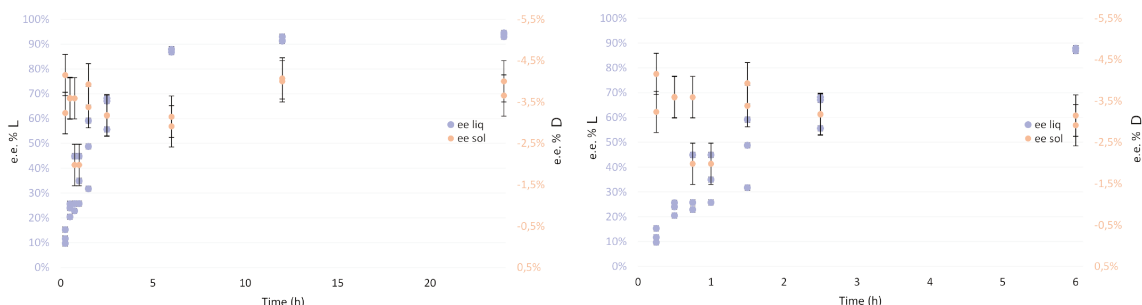


FIGURE III.20 – Zooms of the FIGURE III.19

The e.e. of the liquid reached 95% in 24 hours. At 15 min the enantiomeric excess measured in the solid phase was already similar to the e.e. measured after 6 days. It can be noticed that after 5 min, in the first 50 milligrams of solid, the e.e. of the D-rich solid was 1.2%. The PE process starts to enrich the deposited crystals with the counter enantiomer at the beginning of the process.

In FIGURE III.21, profiles of increasing solid masses and profiles of decreasing liquid concentrations are shown. Knowing the mass of each enantiomer, an histogram can be drawn with the percentage of the total crystallized mass (FIGURE III.22).

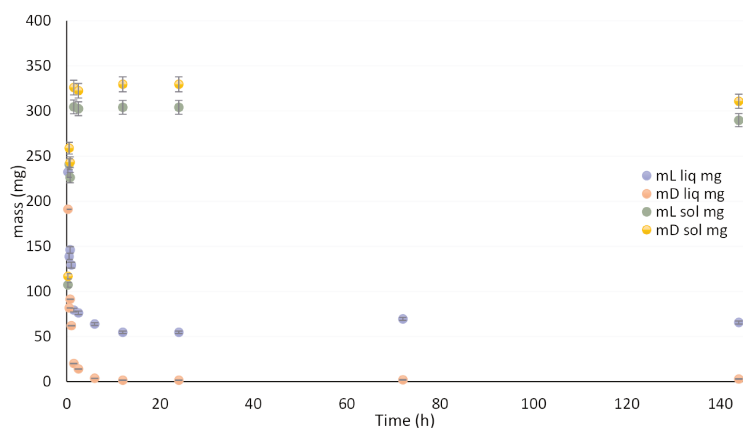


FIGURE III.21 – Monitoring of the mass of each enantiomer in the solid and liquid phases at different times of the PE process

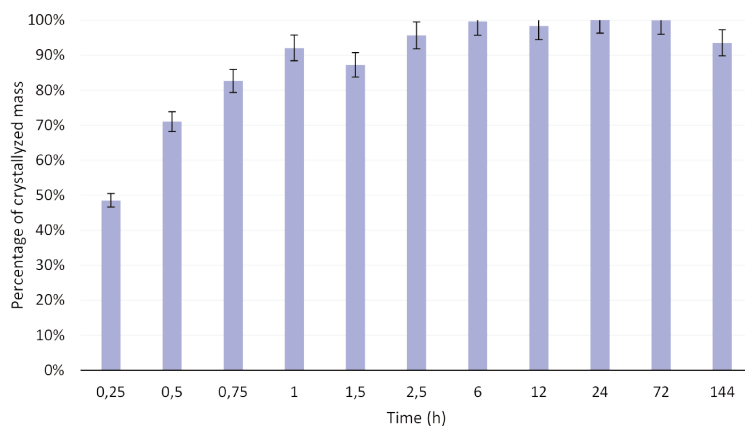


FIGURE III.22 – Percentage of crystallized mass

Due to the high supersaturation ($\beta = 8$) at the beginning of the process, about 50% of the mass was crystallized after 15 min. After 6 h, the entire mass was crystallized; the subsequent mass variation was quite stable until the end of the process, as expected.

Regarding these results it can be concluded that *Preferential Enrichment is a continuous one step process*, which starts as soon as the first crystals are deposited. Moreover, there are no longer measurable increase of e.e. and variation of mass after 1 day of PE, both in the solid and liquid phases.

3.2 Successive Dissolution of the Solid Phase

This procedure was designed to peel back sequentially the different layers of the crystal to analyze them and to reconstruct the crystallization history. This procedure is of course limited by the fact that the crystals exhibit inhomogeneities in size and in their e.e. composition. This is however a backdoor option to monitor the PE process indirectly.

Different protocols were used in the course of this study, the one presented here is optimized for the dissolution of 100% of the crystal, and is shown for the sake of clarity.

3.2.1 Protocol

Protocol for the dissolution of 100% of the crystals for a 850 mg scale experiment:

1. After stopping a PE process at a given time, the system was filtered at 5 °C;
2. 2×5 mL (EtOH/H₂O) 90:10 v:v at 5 °C: direct filtration (removal of remaining solvent $\approx 10 - 15$ mg, with e.e. $> 90\%$), supposed to simply wash off the solid particles from the remaining mother liquor;
3. 9×5 mL (EtOH/H₂O) 50:50 v:v at 5 °C $\approx 15\%$ of the mass;
4. 9×5 mL (H₂O) at 45 °C $\approx 85\%$ of the mass

For steps 3 and 4 the solvent and crystals were left 30 s on a rocking plate at 15 rpm, then the suspension was filtered during 15 s. Fractions collected were stored for further analyses. The solutions obtained with the step 2 have an e.e. higher than 90%, these two washings were composed of mother liquor.

3.2.2 Results of Successive Dissolution of Solid Phase

Plots of enantiomeric excess of the partial successive dissolutions are presented in FIGURES III.23 to III.26 for experiments stopped at 2.5, 6, 24 and 144 h.

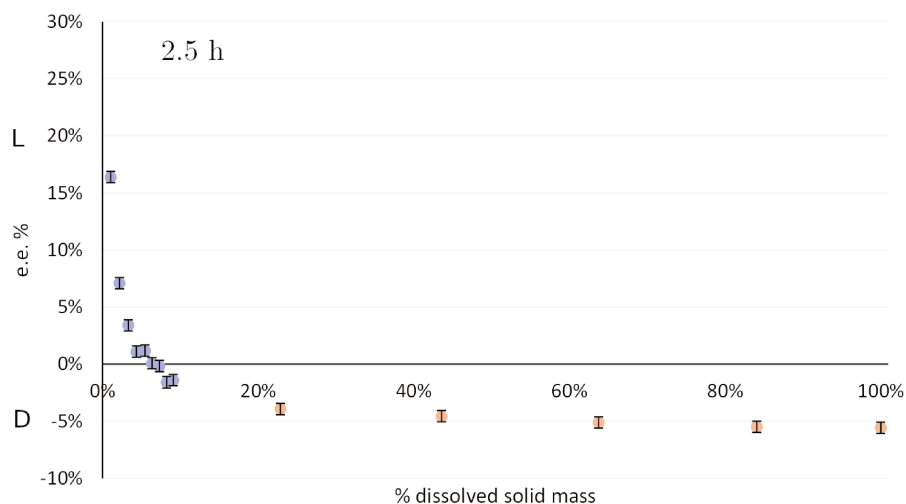


FIGURE III.23 – Successive dissolution of solid phases at 2.5 h (the solutions represented in blue were obtained with step 3, and the ones represented in orange were obtained with step 4 of the protocol)

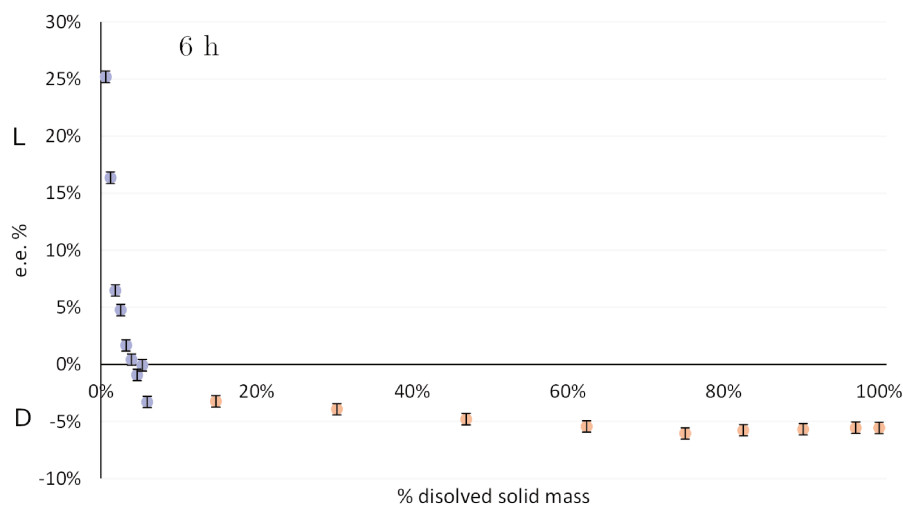


FIGURE III.24 – Successive dissolution of solid phase at 6 h (the solutions represented in blue were obtained with step 3, and the ones represented in orange were obtained with step 4 of the protocol)

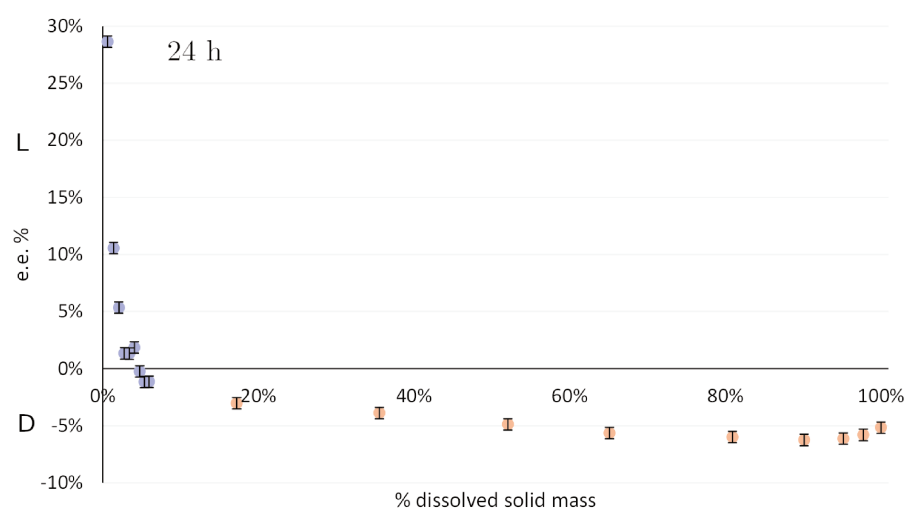


FIGURE III.25 – Successive dissolution of solid phase at 24 h (the solutions represented in blue were obtained with step 3, and the ones represented in orange were obtained with step 4 of the protocol)

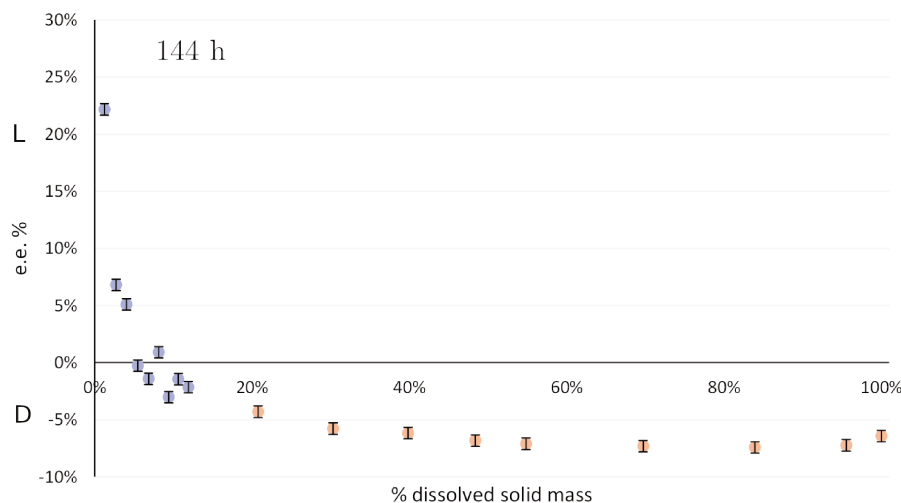


FIGURE III.26 – Successive dissolution of solid phase at 144 h (the solutions represented in blue were obtained with step 3, and the ones represented in orange were obtained with step 4 of the protocol)

The same profile is observed for the four different filtration times, this is a supplementary evidence that the PE process is continuous and starts proceeding at the early stages. The first 10% of the mass of dissolved solid present an enantiomeric excess of the same sign as the mother liquor. This *layer* can contain trapped mother liquor (FIGURE III.27). Trapped mother liquor can have a faster increase of e.e. than free mother liquor due to confinement, and impossibility to exchange with free mother liquor. By dissolving the external layer of the crystals, the trapped mother liquor is released into the solvent of dissolution, which explains the opposite e.e. of the first layers.

It is shown in TABLE III.2 that for PE performed using the *standard protocol*, the average e.e. of the crystals at the end of the process is of $|3.3\%|$ e.e. Although solvent trapping also occurred during our statistical analysis, this result might seem contradictory to our successive redissolution experiments since some washed fractions exhibit e.e. as low as -5% e.e. (especially the deepest layers).

One should however keep in mind that this value is counterbalanced by the higher e.e. value of the shallowest layer of the solid phase giving an overall e.e. composition close to our e.e. value found in our statistical analysis.

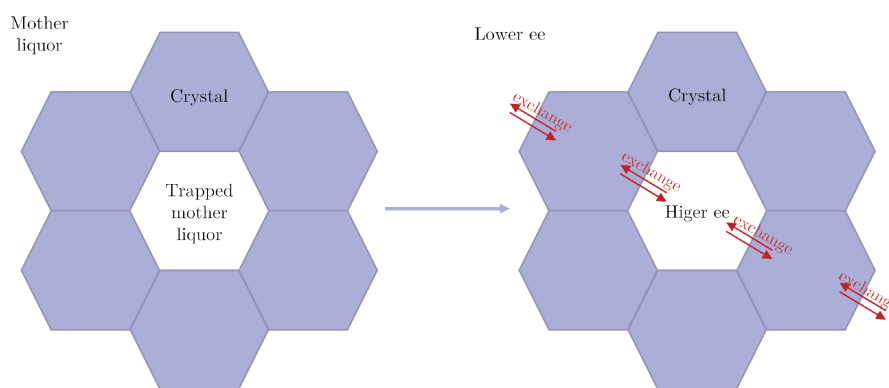


FIGURE III.27 – Representation of trapped solvent inside crystalline aggregates

It is thus possible to analyze the solid into *layers*, albeit the first 10% contain also trapped solvent. An important conclusion of this work is that the first deposited solid fractions already have e.e. as low as -5% e.e.

4 Study of the Mechanism of Arginine Fumarate Preferential Enrichment

4.1 Addition of Labeled Arginine

In order to monitor matter flow from the solution, a setup of experiments was designed. This setup consists of an addition of a minute amount of $^{13}\text{C}_6$ -L-Arginine representing 0.1 wt% of the total mass of Arginine fumarate. This addition was made at different times, during PE, (2.5, 6 h or 6 days). After the addition, the system was left for 6 days at 5 °C before filtration. The quantity ratio of $^{13}\text{C}_6$ -L-Arginine to L-Arginine in the mother liquor immediately after the addition of $^{13}\text{C}_6$ -L-Arg at a different time (2.5, 6, or 144 h) is presented in TABLE III.6 and the experimental results after the subsequent standing for additional 6 days at 5 °C followed by filtration are discussed in TABLES III.7 to III.11 and FIGURES III.28 to III.32.

TABLE III.6 – Comparison of the quantity ratios of $^{13}\text{C}_6$ -L-Arginine to L-Arginine in the mother liquor immediately after addition of $^{13}\text{C}_6$ -L-Arginine at different time

Time	Initial e.e. D ^a			Initial e.e. L ^b		
	m_L^c (mg)	m_D^d (mg)	ratio $m_{L\text{ labeled}}/m_L^e$	m_L^c (mg)	m_D^d (mg)	ratio $m_{L\text{ labeled}}/m_L^e$
2.5 h	10	46	7.4%	46	10	1.7%
6 h	3.2	1.6	25%		N/A	
144 h	0.9	39.6	48%	43	1.6	2.2%

^aexperiment with an initial excess in D; ^bexperiment with an initial excess in L; ^cquantity of non labeled L enantiomer dissolved in the mother liquor at different times; ^dquantity of D enantiomer dissolved in the mother liquor at different times; ^eratio = $m_{\text{added labeled-L-arginine}}/m_{L\text{-enantiomer}}$ at the given time

The objective was to check if L-arginine can enter inside the crystal structure after the beginning of PE experiments starting with an initial enantiomeric excess of D, and whether or not it can enter the crystal structure after the beginning of PE experiments starting with an initial enantiomeric excess of L.

If the labeled enantiomer (which is minor in solution) is retrieved in the solid, it means either that it has crystallized on the deposited crystals or that it has been exchanged with the counter enantiomer from the solid. In order to discriminate between those 2 possibilities, the successive dissolution presented in Section 3.2 was used: if the labeled enantiomer is exchanged, it should be retrieved deeply inside the crystal structure.

4.1.1 Addition during PE experiments starting with an initial e.e. of D

For each experiment the dissolution protocol (described in Section 3.2.1 page 83) was used in order to determine where the labeled arginine has set. Results of addition of labeled L-arginine are reported in TABLES III.7 to III.9, and FIGURES III.28 to III.30.

4.1.1.1 Addition after 2.5 h of PE

FIGURE III.28 shows that the labeled L-Arginine added after 2.5 h of PE is distributed within the different layers of the crystals. TABLE III.7 indicates that 95% of the added L-Arginine is inserted in the solid. It highlights that labeled L-Arginine diffused deeply in the crystals since it is still detected even after dissolving 50% of the deposited crystal mass, although 95% of the solid expected during the PE has already crystallized at this time (*i.e.* the process is almost over – FIGURE III.22). The profiles were found identical in all 3 experiments (number 40-42).

TABLE III.6 shows that the ratio $m_{L\text{ labeled}}/m_L$ immediately after addition of $^{13}\text{C}_6$ -L-Arg was of 7.4%. FIGURES III.23 (Section 3.2) indicates that a fraction of the dissolved minor

L-Arg enters into the solid by 2.5 h. This fraction can be calculated^a and corresponds to 10.2 mg of L-Arginine. Assuming no discrimination between labeled and non labeled Arginine,^b the ratio of 7.4% is constant. Thus the fraction of labeled L-Arginine which should remain at the end of PE is 40 μg . TABLE III.7 shows that at the end of the experiment, 56 mg of dissolved enantiomers are still present in the mother liquor with an e.e. of -97% (this corresponds to 0.7 mg of L-enantiomer). Surprisingly, 23 μg of labeled L-Arginine were detected in the liquid phase. Thus the ratio $m_{\text{L labeled}}/m_{\text{L}}$ was 3.2%.

TABLE III.7 – Incorporation of additional Labeled-L-Arginine into the solid phase at 2.5 h after the beginning of the PE experiment of D-rich Arg (bold experiment represented in FIGURE III.28)

Experiment number	e.e.Initial ^a (%)	$m_{\text{Liquid}}^{\text{b}}$ (mg)	e.e.Liquid ^c (%)	$m_{\text{Solid}}^{\text{d}}$ (mg)	e.e.Solid ^e (%)	$m_{\text{Total}}^{\text{f}}$ (mg)	
Global	40	-5.8	56 ± 14	-91 ± 1	547 ± 82	3.9 ± 0.5	609 ± 96
mass	41	-6.0	56 ± 14	-97 ± 1	668 ± 101	2.9 ± 0.5	726 ± 115
balance	42	-4.4	56 ± 14	-97 ± 1	623 ± 93	2.8 ± 0.5	679 ± 107
Experiment number	$m_{\text{Initial}}^{\text{g}}$ (μg)	$m_{\text{Liquid}}^{\text{h}}$ (μg)	$\%_{\text{Liquid}}^{\text{i}}$	$m_{\text{Solid}}^{\text{j}}$ (μg)	$\%_{\text{Solid}}^{\text{k}}$	$m_{\text{Total}}^{\text{l}}$ (μg)	
Labeled	40	835	34 ± 3	5	697 ± 146	95	731 ± 149
Arginine	41	892	32 ± 3	5	647 ± 193	95	674 ± 196
mass balance	42	837	23 ± 2	3	715 ± 215	97	739 ± 217

Each experiment was performed according to Appendix A.3 under eight-fold supersaturation using D-rich Arg (5% ee 850 mg) in the mixed solvent (3.4 mL) of H_2O and EtOH (1:1 v/v), followed by addition of $^{13}\text{C}_6\text{-L-Arg}$ (850 μg) after 2.5 h and standing for additional 6 days at 5 °C before filtration. ^ae.e. at time = 0; ^bfinal mass of Arg-Fum in solution; ^cfinal e.e. in solution; ^dfinal mass of Arg-Fum in solid; ^efinal e.e. in solid; ^f $m_{\text{Total}} = m_{\text{Liquid}} + m_{\text{Solid}}$; ^gmass of labeled-L-Arginine added in solution; ^hfinal mass of labeled-L-Arginine in solution; ⁱpercentage of the mass in solution; ^jfinal mass of labeled-L-Arginine in solid; ^kpercentage of the mass in solid; ^l $m_{\text{Total}} = m_{\text{Liquid}} + m_{\text{Solid}}$

a. $m_{\text{L } 2.5 \text{ h}} - m_{\text{L } 6 \text{ days}}$ calculated with data of Section 3.1

b. To the best of our knowledge, isotopic discrimination has little impact on the crystallization phenomenon.

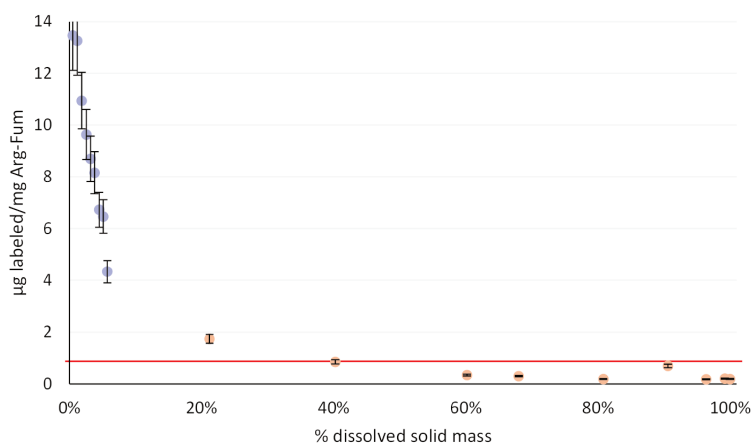


FIGURE III.28 – Repartition profile of labeled Arginine inside Arg-Fum solid phase after an addition at 2.5 h of experiment 42 (the red line represents the 1 ‰ ratio; the solutions represented in blue were obtained with step 3, and the ones represented in orange were obtained with step 4 of the protocol)

4.1.1.2 Addition after 6 h of PE

After 6 hours, almost 100% of the expected solid phase is crystallized (FIGURE III.22 page 82). TABLE III.8 shows that 93% of the labeled L-Arginine is inserted in the solid. The repartition profile observed in experiment 43 and 45 (FIGURE III.29) is similar to that found when adding labeled L-Arginine at 2.5 h.

As described in Section 4.1.1.1, the initial ratio of labeled L-Arginine over L-Arginine in the liquid phase was 25% (TABLE III.6), and at the end of the PE experiment, it was 3.6% (representing 30 µg of labeled L-Arginine), while theoretically the quantity should be 190 µg (25% ratio). Thus the added quantity of labeled arginine should be less inserted inside the solid.

TABLE III.8 – Incorporation of additional Labeled-L-Arginine into the solid phase at 6 h after the beginning of the PE experiment of D-rich Arg (bold experiment represented in FIGURE III.29)

Experiment number	e.e.Initial ^a (%)	m _{Liquid} ^b (mg)	e.e.Liquid ^c (%)	m _{Solid} ^d (mg)	e.e.Solid ^e (%)	m _{Total} ^f (mg)
Global 43	-5.4	63 ±15	-94 ±1	614 ±93	3.2 ±0.5	677 ±108
mass balance 44	-5.6	75 ±18	-94 ±1	595 ±89	3.3 ±0.5	670 ±108
Experiment number	m _{Initial} ^g (µg)	m _{Liquid} ^h (µg)	% _{Liquid} ⁱ	m _{Solid} ^j (µg)	% _{Solid} ^k	m _{Total} ^l (µg)
Labeled Arginine 43	839	39 ±4	7	537 ±161	93	576 ±165
mass balance 44	831	34 ±3	6	575 ±173	94	609 ±176

Each experiment was performed according to Appendix A.3 under eight-fold supersaturation using D-rich Arg (5% ee 850 mg) in the mixed solvent (3.4 mL) of H₂O and EtOH (1:1 v/v), followed by addition of ¹³C₆-L-Arg (850 µg) after 2.5 h and standing for additional 6 days at 5 °C before filtration. ^ae.e. at time = 0; ^bfinal mass of Arg-Fum in solution; ^cfinal e.e. in solution; ^dfinal mass of Arg-Fum in solid; ^efinal e.e. in solid; ^fm_{Total} = m_{Liquid} + m_{Solid}; ^gmass of labeled-L-Arginine added in solution; ^hfinal mass of labeled-L-Arginine in solution; ⁱpercentage of the mass in solution; ^jfinal mass of labeled-L-Arginine in solid; ^kpercentage of the mass in solid; ^lm_{Total} = m_{Liquid} + m_{Solid}

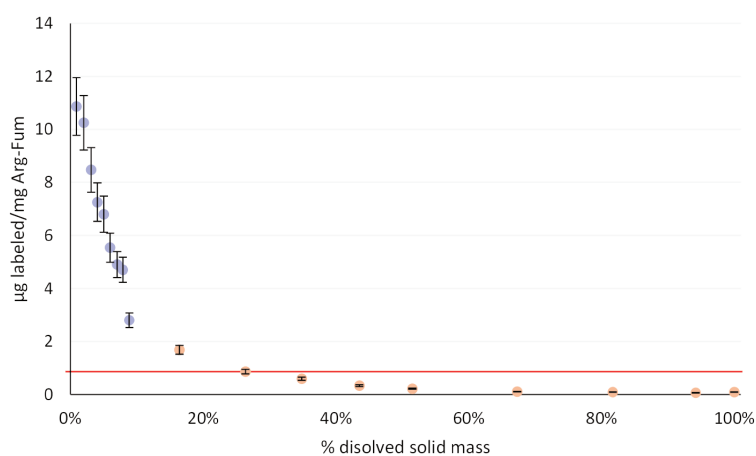


FIGURE III.29 – Repartition profile of labeled Arginine inside Arg-Fum solid phase after an addition at 6 h of experiment 44 (the red line represents the 1 ‰ ratio; the solutions represented in blue were obtained with step 3, and the ones represented in orange were obtained with step 4 of the protocol)

4.1.1.3 Addition after 6 days of PE

After 6 days the PE process should be finished, nevertheless 75% of the labeled arginine were inserted in the solid, and the profile was comparable to the profiles at 2.5 and 6 h. TABLE III.9 shows that 75% of the labeled L-Arginine is inserted in the solid although after 6 days the PE process is finished. The repartition profile observed in experiment 6

and 7 (FIGURE III.30) is similar to those found when adding labeled L-Arginine at 2.5 h and 6 h.

As described in Section 4.1.1.1, the initial ratio of labeled L-Arginine over L-Arginine in the liquid phase was 48% (TABLE III.6), at the end of the PE experiment, it was 23% (representing 190 μg of labeled L-Arginine), while theoretically the quantity should be 410 μg (48% ratio).

TABLE III.9 – Incorporation of additional Labeled-L-Arginine into the solid phase at 6 days after the beginning of the PE experiment of D-rich Arg (bold experiment represented in FIGURE III.30)

Experiment number	e.e.Initial ^a (%)	m _{Liquid} ^b (mg)	e.e.Liquid ^c (%)	m _{Solid} ^d (mg)	e.e.Solid ^e (%)	m _{Total} ^f (mg)
Global	45	-5.0	68 ± 17	-94 ± 1	575 ± 86	4.0 ± 0.5
mass balance	46	-5.0	66 ± 16	-94 ± 1	631 ± 89	3.0 ± 0.5
Experiment number	m _{Initial} ^g (μg)	m _{Liquid} ^h (μg)	% _{Liquid} ⁱ	m _{Solid} ^j (μg)	% _{Solid} ^k	m _{Total} ^l (μg)
Labeled Arginine	45	832	185 ± 18	26	520 ± 156	74
mass balance	46	841	174 ± 17	23	600 ± 180	77

Each experiment was performed according to Appendix A.3 under eight-fold supersaturation using D-rich Arg (5% ee 850 mg) in the mixed solvent (3.4 mL) of H₂O and EtOH (1:1 v/v), followed by addition of ¹³C₆-L-Arg (850 μg) after 2.5 h and standing for additional 6 days at 5 °C before filtration. ^ae.e. at time = 0; ^bfinal mass of Arg-Fum in solution; ^cfinal e.e. in solution; ^dfinal mass of Arg-Fum in solid; ^efinal e.e. in solid; ^fm_{Total} = m_{Liquid} + m_{Solid}; ^gmass of labeled-L-Arginine added in solution; ^hfinal mass of labeled-L-Arginine in solution; ⁱpercentage of the mass in solution; ^jfinal mass of labeled-L-Arginine in solid; ^kpercentage of the mass in solid; ^lm_{Total} = m_{Liquid} + m_{Solid}

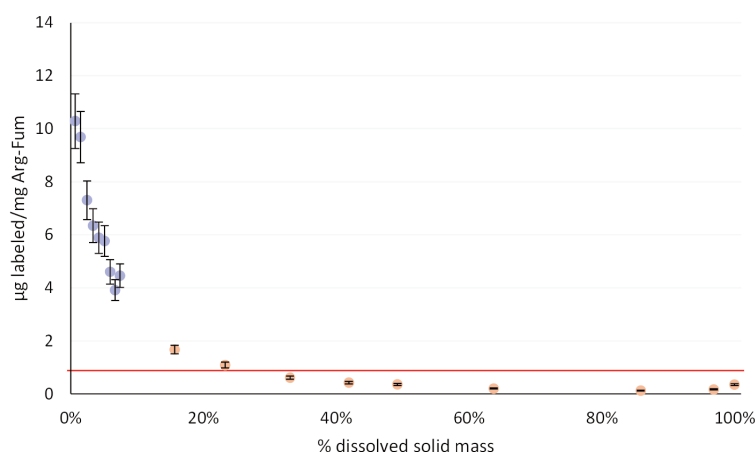


FIGURE III.30 – Repartition profile of labeled Arginine inside Arg-Fum solid phase after an addition at 6 days of experiment 45 (the red line represents the 1% ratio; the solutions represented in blue were obtained with step 3, and the ones represented in orange were obtained with step 4 of the protocol)

In every experiment, the results show that: 1) the amount of labeled L-Arginine in the liquid phase is lower than expected, 2) labeled L-Arginine has therefore entered the crystal structure in spite of the absence of supersaturation, 3) labeled L-Arginine is retrieved rather deeply in the crystals since dissolving 50% of the crystal mass still resulted in detection of labeled L-Arginine .

4.1.2 Addition during PE experiments starting with an initial e.e. of L

When PE starts with a slightly D rich solution in the liquid phase, the enrichment in the mother liquor systematically proceeds in this direction and L-Arginine is retrieved in the solid. Conversely, starting PE with a slightly L rich solution results in the opposite situation. As a consequence, addition of labeled L-Arginine should not enter the solid.

Two experiments have been designed to verify this; PE was performed using the *standard protocol* with an L rich sample of 5% ee. In the first experiment labeled L-Arginine was added after 2.5 h. In the second experiment labeled L-Arginine was added after 6 days. For the second experiment, the repartition profile was established. Results are reported in TABLES III.10 to III.11, and in FIGURE III.31.

4.1.2.1 Addition after 2.5 h of PE

TABLE III.10 shows that 50% of the labeled L-Arginine was inserted in the solid. This 50% of insertion represents the diffusion and corresponds to the crystallization of the last 5% of the solid.

As described in Section 4.1.1.1, the initial ratio of labeled L-Arginine over L-Arginine in the liquid phase was 1.7% (TABLE III.6), at the end of the PE experiment, it was 1.1% (representing 420 μg of labeled L-Arginine), while with the initial ratio (1.7%) the L-labeled-Arginine quantity in the mother liquor should be 670 μg .

TABLE III.10 – Incorporation of additional Labeled-L-Arginine into the solid phase at 2.5 h after the beginning of the PE experiment of L-rich Arg

Experiment number	e.e.Initial ^a (%)	m _{Liquid} ^b (mg)	e.e.Liquid ^c (%)	m _{Solid} ^d (mg)	e.e.Solid ^e (%)	m _{Total} ^f (mg)
Global	47	68 ±2	80 ±1	743 ±19	-3.4 ±0.5	811 ±21
mass balance	48	71 ±3	96 ±1	739 ±19	-3.6 ±0.5	811 ±22
Experiment number	m _{Initial} ^g (µg)	m _{Liquid} ^h (µg)	% _{Liquid} ⁱ	m _{Solid} ^j (µg)	% _{Solid} ^k	m _{Total} ^l (µg)
Labeled Arginine	47	371 ±37	44	476 ±48	56	847 ±85
mass balance	48	453 ±45	50	447 ±45	50	901 ±90

Each experiment was performed according to Appendix A.3 under eight-fold supersaturation using D-rich Arg (5% ee 850 mg) in the mixed solvent (3.4 mL) of H₂O and EtOH (1:1 v/v), followed by addition of ¹³C₆-L-Arg (850 µg) after 2.5 h and standing for additional 6 days at 5 °C before filtration.

^ae.e. at time = 0; ^bfinal mass of Arg-Fum in solution; ^cfinal e.e. in solution; ^dfinal mass of Arg-Fum in solid; ^efinal e.e. in solid; ^fm_{Total} = m_{Liquid} + m_{Solid}; ^gmass of labeled-L-Arginine added in solution; ^hfinal mass of labeled-L-Arginine in solution; ⁱpercentage of the mass in solution; ^jfinal mass of labeled-L-Arginine in solid; ^kpercentage of the mass in solid; ^lm_{Total} = m_{Liquid} + m_{Solid}

4.1.2.2 Addition after 6 days of PE

TABLE III.11 shows that 12% of the labeled L-Arginine was inserted in the solid. The repartition profile (FIGURE III.31) indicates that the labeled L-Arginine was mainly located in the first crystal layers.

Concerning the liquid, as described in Section 4.1.1.1, the initial ratio of labeled L-Arginine over L-Arginine in the liquid phase was 2.2% (TABLE III.6), at the end of the PE experiment, it was 1.9% (690 µg), theoretically the quantity of L-labeled-Arginine in the mother liquor should be 780 µg with the initial ratio of 2.2%. The ratio between theory and experiment was closer to 1, there was less exchange for the enantiomer in excess in the liquid phase.

TABLE III.11 – Incorporation of additional Labeled-L-Arginine into the solid phase at 6 days after the beginning of the PE experiment of L-rich Arg (bold experiment represented in FIGURE III.31)

Experiment number	e.e.Initial ^a (%)	m _{Liquid} ^b (mg)	e.e.Liquid ^c (%)	m _{Solid} ^d (mg)	e.e.Solid ^e (%)	m _{Total} ^f (mg)	
Global	49	4.5	65 ± 2	96 ± 1	663 ± 100	-4.4 ± 0.5	728 ± 103
mass	50	4.3	60 ± 2	92 ± 1	663 ± 100	-4.0 ± 0.5	724 ± 102
balance	51	4.6	63 ± 2	92 ± 1	674 ± 101	-5.0 ± 0.5	736 ± 103
Experiment number	m _{Initial} ^g (µg)	m _{Liquid} ^h (µg)	% _{Liquid} ⁱ	m _{Solid} ^j (µg)	% _{Solid} ^k	m _{Total} ^l (µg)	
Labeled	49	898	572 ± 40	84	110 ± 33	16	682 ± 77
Arginine	50	883	791 ± 79	93	61 ± 18	7	852 ± 97
mass balance	51	824	567 ± 57	81	130 ± 39	19	698 ± 96

Each experiment was performed according to Appendix A.3 under eight-fold supersaturation using D-rich Arg (5% ee 850 mg) in the mixed solvent (3.4 mL) of H₂O and EtOH (1:1 v/v), followed by addition of ¹³C₆-L-Arg (850 µg) after 2.5 h and standing for additional 6 days at 5 °C before filtration. ^ae.e. at time = 0; ^bfinal mass of Arg-Fum in solution; ^cfinal e.e. in solution; ^dfinal mass of Arg-Fum in solid; ^efinal e.e. in solid; ^fm_{Total} = m_{Liquid} + m_{Solid}; ^gmass of labeled-L-Arginine added in solution; ^hfinal mass of labeled-L-Arginine in solution; ⁱpercentage of the mass in solution; ^jfinal mass of labeled-L-Arginine in solid; ^kpercentage of the mass in solid; ^lm_{Total} = m_{Liquid} + m_{Solid}

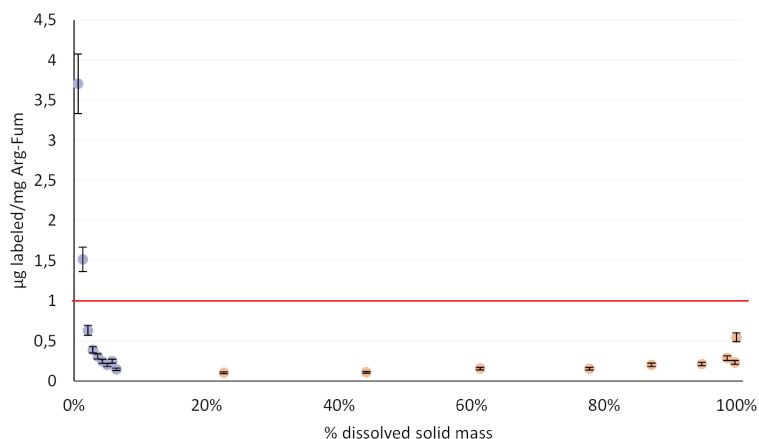


FIGURE III.31 – Repartition profile of labeled Arginine inside Arg-Fum solid phase after an addition at 6 days of experiment 50 (the red line represents the 1 ‰ ratio; the solutions represented in blue were obtained with step 3, and the ones represented in orange were obtained with step 4 of the protocol)

4.1.3 Comparison between addition during PE experiments starting with an initial e.e. of D and starting with an initial e.e. of L

In order to compare the time of addition and the effect of adding L-labeled arginine on experiments starting with a slightly L or D rich sample, a plot was drawn (FIGURE III.32) with the curve of FIGURES III.28 to III.31.

The profiles were similar for experiments starting with slightly D rich samples, with minor influence of the time of addition. However when starting with slightly L rich samples the inserted labeled arginine was only distributed inside the first dissolved layers (besides the small quantity inserted).

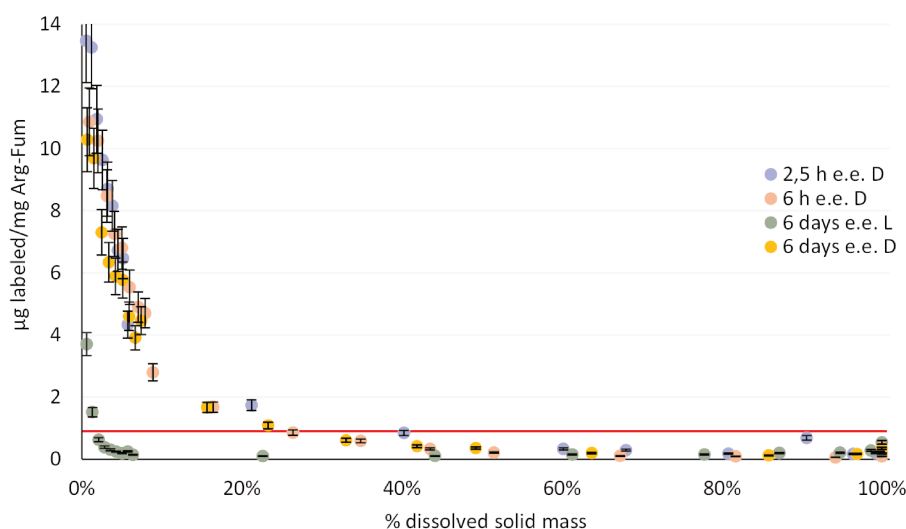


FIGURE III.32 – Comparison of repartition profiles of labeled arginine inside Arginine fumarate solid phases (the red line represents the 1 ‰ ratio)

In experiments starting with a slight initial e.e. of D (-5% e.e.), addition of labeled L-Arginine always resulted in the integration of the labeled molecule inside the solid. The ratio of labeled L-Arginine between solid and liquid varies with the time of addition, 95:5 at 2.5 h, 93:7 at 6 h and 75:25 at 6 days (*i.e.* the latter the addition, the less L-Arginine enters the solid which is a consequence of the decreasing supersaturation). Moreover, an important observation of this experiment is that the labeled L-Arginine was found even after the dissolution of the outer 50% of the mass of the deposited crystals.

Conversely, in experiments starting with slightly L rich samples, followed by an addition of labeled-L-arginine at 2.5 h after the beginning of the PE experiment, the amount of labeled L-Arginine was divided in two halves between solid and liquid, and an analogous experiment by addition of labeled-L-arginine at 6 days the ratio between labeled L-Arginine in the solid and the liquid decreased until 15:85 with the major part distributed in the outer 10% in mass of the deposited crystals. However our successive dissolution experiment did not show any labeled L-Arginine within the deposited crystals even in the

superficial layers

For each experiment, the experimental inserted quantity was lower than the theoretical one, but for experiments starting with a slightly D rich sample, the ratio between experiment and theory was strictly lower than for experiments starting with a slightly L rich sample. There was exchange between enantiomers in the liquid and the solid, the exchanged quantity and the ratio of exchange were higher for opposite enantiomer (*i.e.* exchange of opposite enantiomers is needed for PE).

We can conclude that there is an *exchange* of opposite enantiomers between the solid and the liquid.

4.2 About the Occurrence of Phase Transitions during PE of Arg-Fum

It was demonstrated in 2017⁷⁵ that the occurrence of a polymorphic transition is a central element for the mechanism of PE for the first generation compounds.

In this work, a deeper focus was dedicated to this factor through the use of microscopy and XRPD performed in-situ, by using an in-house technology, In-SituX,¹⁰¹ in order to investigate the occurrence of phase transitions during PE.

4.2.1 Observation of the Deposited Crystals during PE Process by Microscopy

Experiments were performed with an adaptation of the *standard protocol* in 1 mm × 1 cm × 5 cm cells in order to observe crystal growth during the early stage of PE under optical microscopy (OM) (FIGURE III.33).

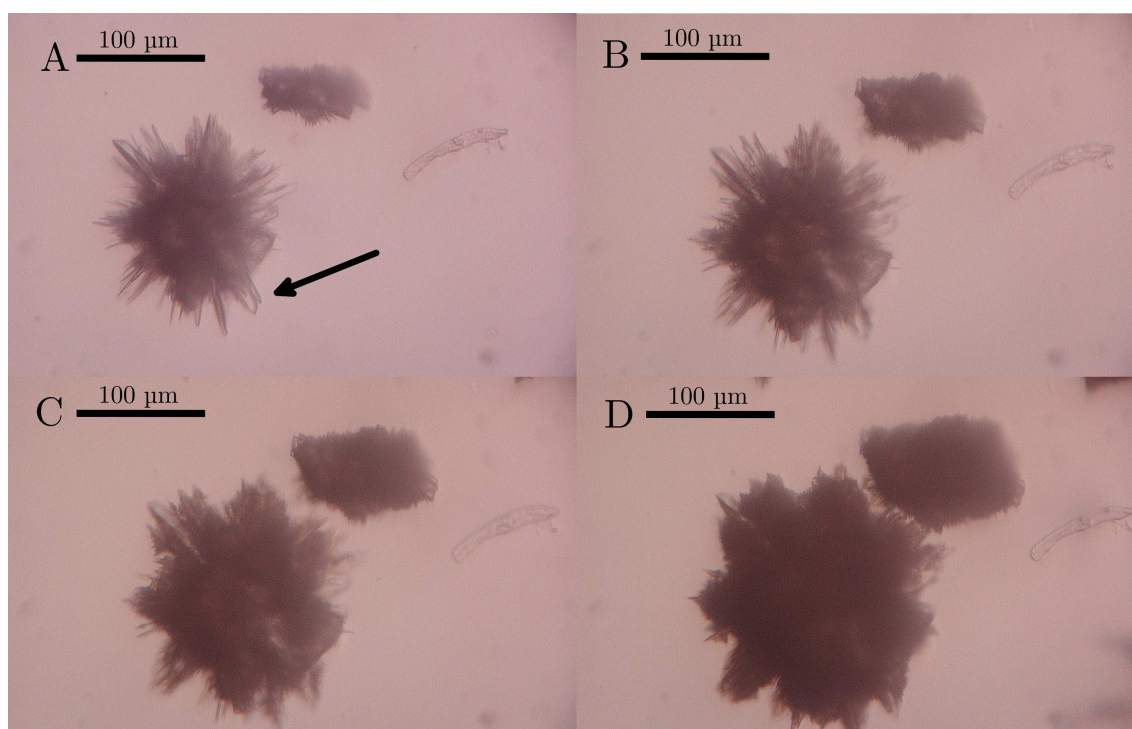


FIGURE III.33 – OM pictures (Hirox KH7700) showing the growth of Arg-Fum salts at 5 °C, after 1 min, 1.5 min, 1.8 min and 2.7 min in PE conditions

In spite of the systematic urchin shape of the deposited crystals during PE it can be seen from FIGURE III.33 that two types of crystals appear: a transparent one, with seemingly plate-like habits (arrow in FIGURE III.33 A) and a darker one (FIGURE III.33 D). From FIGURE III.33 A to D it can be seen that the darker phase grows as well as the transparent one. It is however not clear if the transparent one nucleates first and gets transformed in the latter stage or if the two phases appear concomitantly.

The urchin shape of the dark phase is comparable to the crystal morphology of the phase collected after PE as can be seen from the scanning electron microscopy (SEM), in FIGURE III.34.

Due to the poorly shaped crystals, OM hardly serves conclusion about polymorphic transitions during PE experiments of Arg-Fum: this is the reason why In-SituX experiments were performed.



FIGURE III.34 – SEM analysis of the final solid of a PE experiment

4.2.2 In-situ X-Ray Powder Diffraction: In-SituX

The In-SituX technology (further described in Appendix A.5.5), with its reverse geometry, offers the opportunity to monitor crystallization from solution, and is therefore able to monitor the solid phases deposited during PE. PE experiments were performed using the *standard protocol* inside the In-SituX cell at $-18\text{ }^{\circ}\text{C}$, instead of $5\text{ }^{\circ}\text{C}$, for the observation of possible polymorphic transitions of the solid phase during the PE process.

The experimental conditions are presented in TABLE III.12 and the results are given in FIGURES III.35 to III.37.

TABLE III.12 – Conditions for experiments 52 to 54 in InSituX apparatus

Mass	1.1 g
e.e.	5% in L
Solvent	4.4 mL of EtOH/H ₂ O
Time	50 h
Temperature	$-18\text{ }^{\circ}\text{C}$

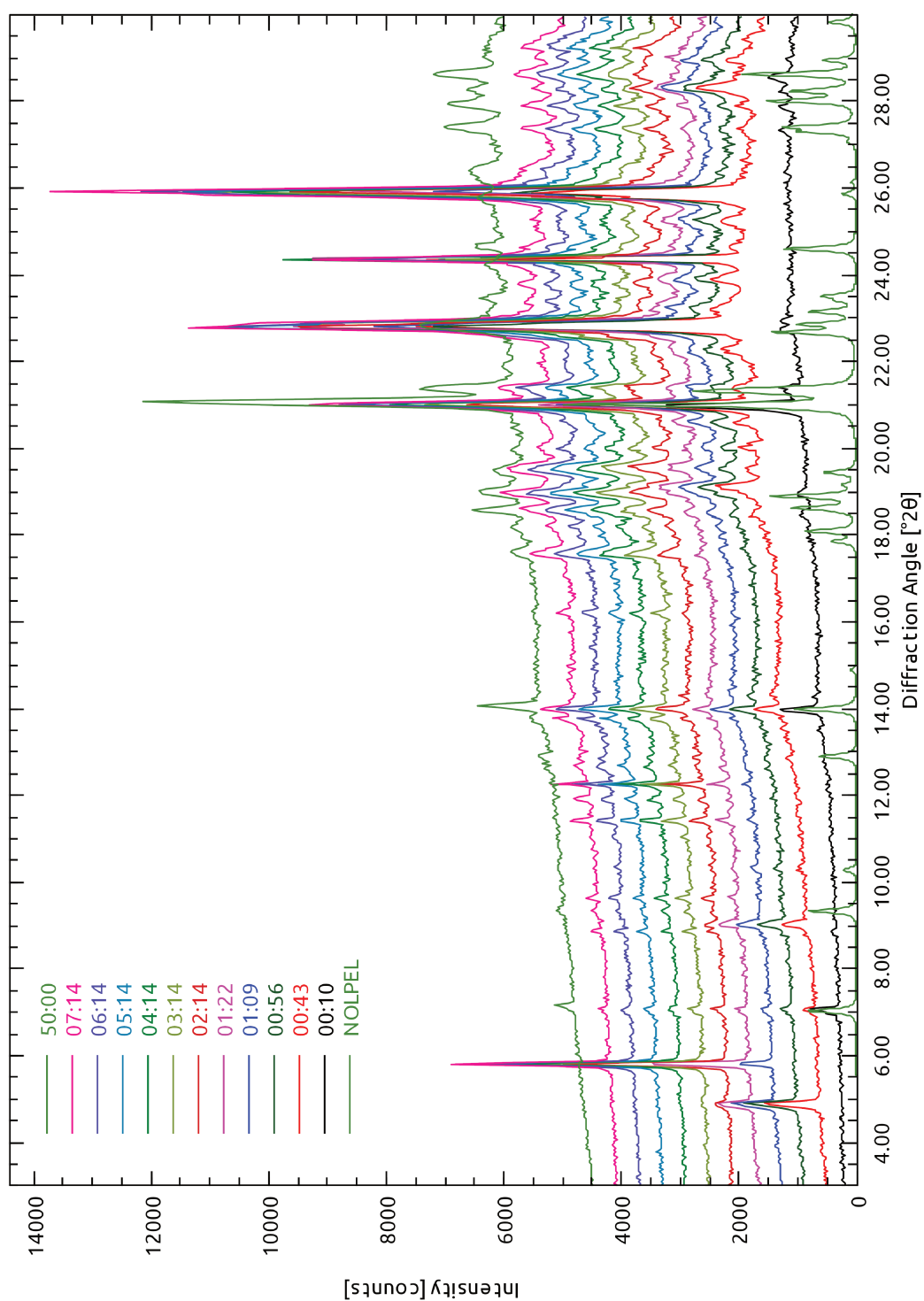


FIGURE III.35 – In-SituX XRPD patterns of experiment 52, $e.e._{solid}=-2.0\%$ $e.e._{liquid}=60\%$ (times are presented in hours:minutes since the start of the experiment)

In experiment 52, three different solid phases can be observed, the stable one first (10 min) with a characteristic peak at 7° (2θ), then a mixture of the stable phase and a first metastable phase with a notable peak at 5° (2θ). After 1 h, a second metastable phase with

a characteristic peak at 6° (2θ) appears concomitantly with the disappearance of the first metastable form (complete disappearance after 3 h). The crystallization of metastable phases after the crystallization of the stable phase was due to the high supersaturation.¹⁰²

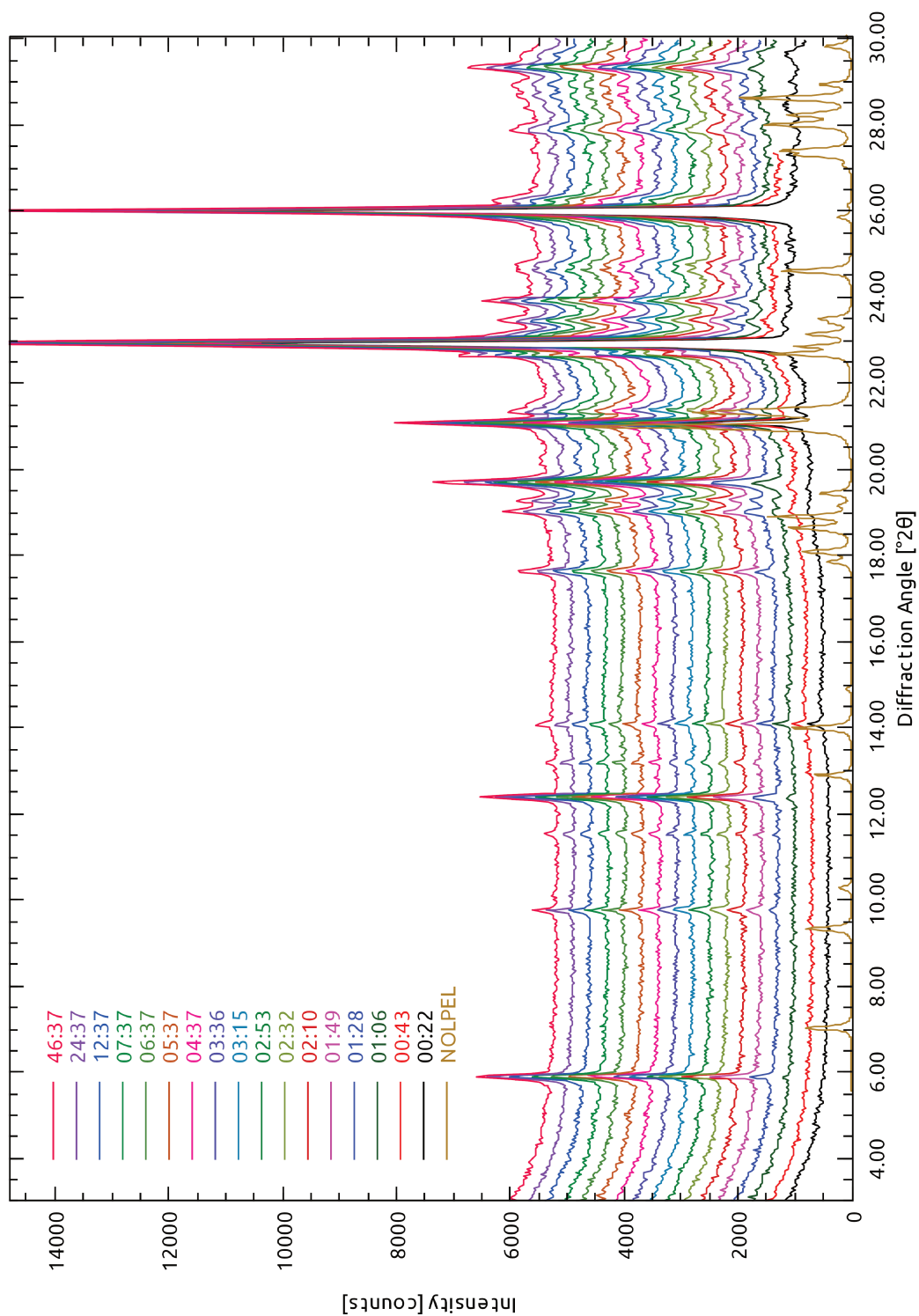


FIGURE III.36 – In-Situ XRPD patterns of experiment 53, $e.e._{solid} = -1.0\%$ $e.e._{liquid} = 71\%$ (times are presented in hours:minutes since the start of the experiment)

In experiment 53, only the second metastable phase with a peak at 6° (2θ) was detected from the beginning to the end of the process.

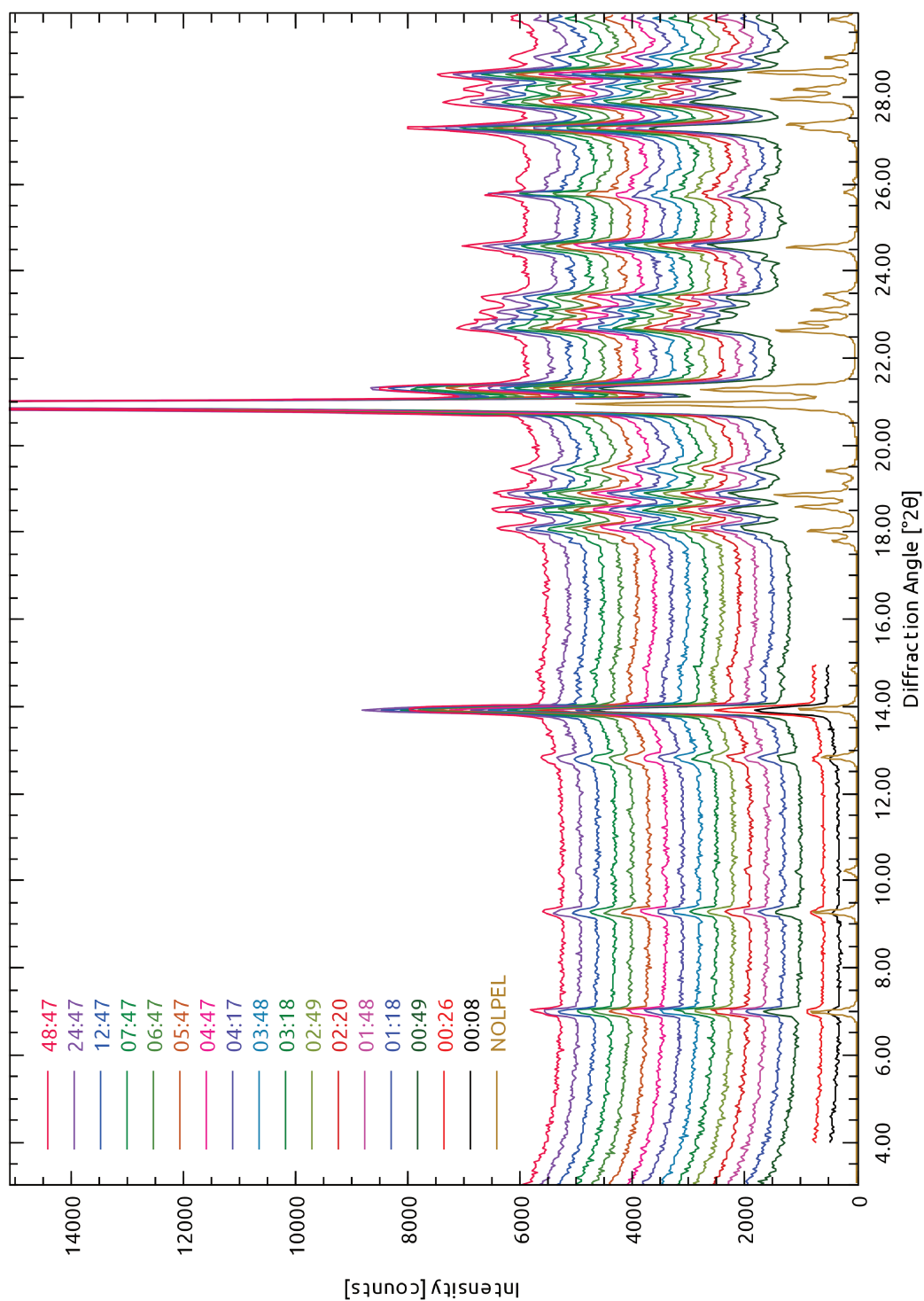


FIGURE III.37 – In-SituX XRPD patterns of experiment 54, $e.e._{solid}=-2.0\%$ $e.e._{liquid}=46\%$ (times are presented in hours:minutes since the start of the experiment)

In experiment 54, only the stable phase with a peak at 7° (2θ) was detected from the

begin to the end of the process.

In-SituX analyses allowed us to observe that *with or without polymorphic transitions* PE can occur. The time of the polymorphic transition detected in experiment 52 (*i.e.* 1 h after the beginning of the experiment, at this point solid phase has almost reached its final composition) is also not compatible with the possible polymorphic transition observed in OM (few minutes).

Therefore we conclude that the occurrence of a polymorphic transition does not seem to be required for PE. Polymorphic transitions during PE experiment were probably due only to the initial supersaturation, without any help to the process.

4.3 Molecular modeling of the solid solution

An extension of our work also consisted in evaluating the importance of chiral discrimination associated to the solid phase. Indeed, using simple molecular mechanics procedure, it is possible to simulate the formation of a solid solution by replacing one enantiomer by its counterpart. The energy difference between the two structures gives a rough assessment about the energetic cost of this substitution and evaluates the stability of the solid solution. This procedure is similar to that adopted by Brandel *et al.*¹⁰³ and Gervais *et al.*¹⁰⁴

If the solid solution is energetically viable this is consistent with a solid solution (in the solid state, the minor enantiomer and its counterpart are almost not discriminated by the lattice).

The same calculations were also applied to several compounds known to exhibit PE and to systems that satisfied all the required criteria but which do not exhibit PE.

Molecular modeling at the semi-empirical level was performed using Material Studio 8 (Accelrys, Appendix A.6).

4.3.1 Modeling Solid Solution from Arginine Fumarate Structure

As indicated in Section 2.1, Arg-Fum stable form crystallizes in the $P\bar{1}$ space group, with Arginine showing a conformational disorder. Only the major conformer was treated in the modeling.

A supercell of $3 \times 3 \times 3$ cells, containing 54 arginine fumarate salts, was constructed. Geometry optimization of the supercell was performed and the energy was computed ($E_{\text{reference}}$). The lattice energy ($U_{\text{reference lattice}}$) was calculated with the following procedure: one arginine was removed from the lattice then the energy of the resulting lattice

was calculated ($E_{\text{host reference}}$). The energy of the isolated arginine was also calculated ($E_{\text{guest reference}}$). $U_{\text{reference lattice}}$ was obtained by the following equation.

$$U_{\text{reference lattice}} = E_{\text{reference}} - (E_{\text{host reference}} + E_{\text{guest reference}}) \quad (\text{Eq. III.1})$$

Then, one enantiomer of arginine in the supercell was substituted by its counter-enantiomer, thus generating a solid solution with 3.7% e.e. Geometry optimization of the solid solution was performed, and its energy was computed ($E_{\text{solid solution}}$). With the same procedure as that used for the reference lattice, $U_{\text{solid solution lattice}}$, $E_{\text{host solid solution}}$, and $E_{\text{guest solid solution}}$ were calculated.

Energetic cost of the enantiomeric substitution ΔU can be calculated with Eq. III.2 and is given in TABLE III.13.

$$\Delta U = U_{\text{solid solution lattice}} - U_{\text{reference lattice}} \quad (\text{Eq. III.2})$$

This difference represents the variation of energy of the structure due to the substitution of an enantiomer of the crystal structure by the counter one.

Further to this, 2 additional permutations were performed sequentially and the same calculation were performed (TABLE III.13).

TABLE III.13 – Computed energy (kcal/mol) from reference structure and modeled solid solutions with 1, 2, and 3 substitutions

Structure	Reference Structure			Solid Solution		
	1	2	3	1	2	3
Number of permutations						
E_{lattice}		-27163.97		-27163.14	-27151.21	-27144.18
E_{guest}	-237.12	-474.25	-711.37	-238.33	-473.22	-708.56
E_{host}	-26780.16	-26400.62	-26025.35	-26774.77	-26391.39	-26003.91
U_{lattice}	-146.69	-289.11	-427.25	-150.04	-286.59	-431.71
ΔU		N/A		-3.35	2.51	-4.46

4.3.2 Modeling Solid Solution for DL-Tryptophan Ethyl Ester Hydrochloride

Appendix D reports our attempts to realize PE with DL-Tryptophan ethyl ester hydrochloride (DLWE) that remained unsuccessful. One possible explanation to this can be associated to the high chiral discrimination of the crystallographic sites of DLWE.

To test this hypothesis, the same modeling procedure was applied to the crystal structure of DLWE. The result of these calculations are given in TABLE III.14.

TABLE III.14 – Computed energy (kcal/mol) from reference structure and modeled solid solutions with 1, 2, and 3 substitutions for DLWE system

Number of permutations	Reference Structure			Solid Solution		
	1	2	3	1	2	3
E_{lattice}		-3650.78		-3604.92	-3576.89	-3557.20
E_{guest}	99.10	198.19	297.29	106.30	207.97	309.51
E_{host}	-3570.34	-3477.55	-3372.42	-3567.60	-3459.46	-3345.24
U_{lattice}	-179.54	-371.42	-575.65	-143.61	-325.39	-521.46
ΔU		N/A		35.93	46.03	54.19

On an energetic point of view, the difference in lattice energy between the reference structure and the modeled solid solution of Arg-Fum is of -3.3 kcal/mol. When these results are compared with computations with DLWE the difference of ΔU is of 35 kcal/mol. Thus the energetic cost for enantiomeric substitution is much higher for DLWE.

The obtained structures for these two models were represented in FIGURE III.38.

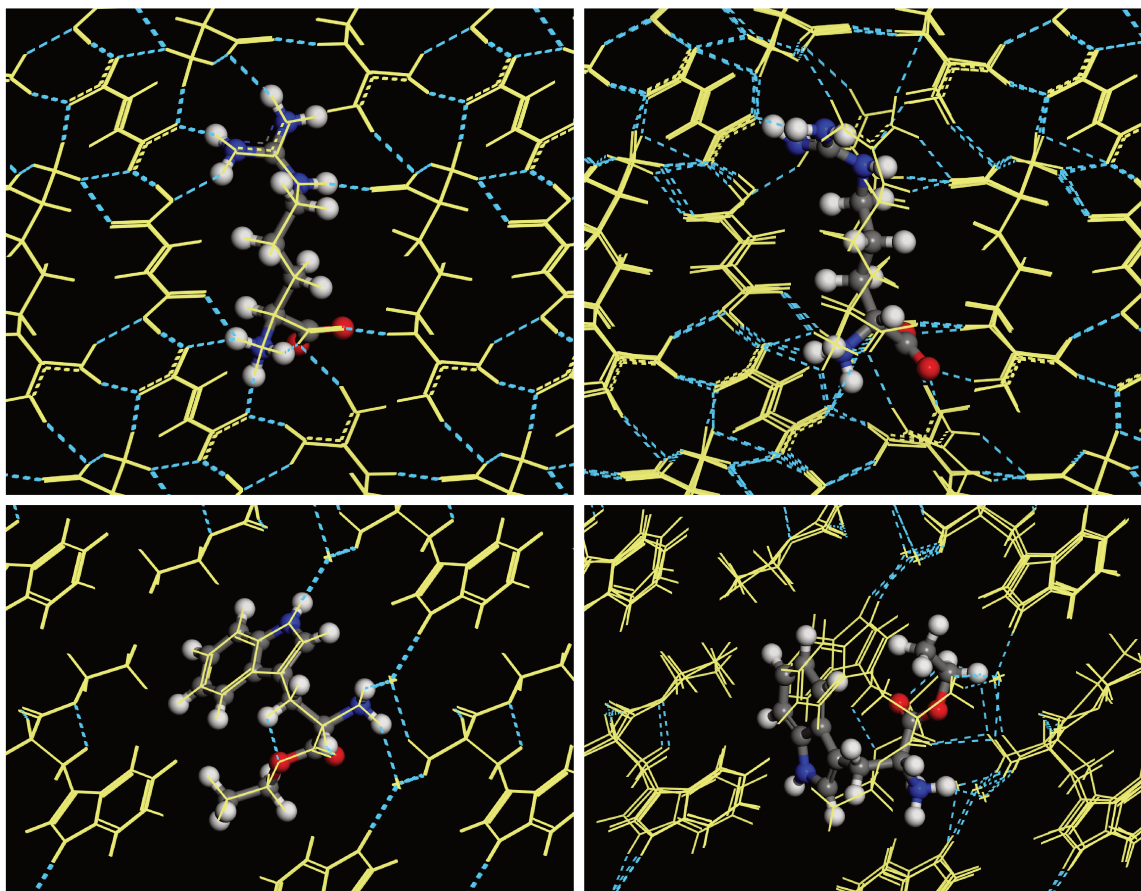


FIGURE III.38 – Representation of structures of Arginine fumarate (top left), arginine fumarate after substitution with conformation 1 (top right), DLWE (bottom left) and DLWE after substitution (bottom right)

For the original structure of racemic arginine fumarate one asymmetric unit contain 11 non-covalent bonds (4 for the amine, 3 for the acid and 4 for guanidinium), after substitution there is one non-covalent bond less (4 for the amine, 3 for the acid and 3 for the guanidinium).

For the original structure of racemic DLWE, one tryptophan make 4 non covalent bonds from the amine to the chloride, with the substitution, there are only 2 ionic bonds.

These results support the hypothesis that PE works for Arg-Fum because of a solid solution type behavior of the crystals which is not retrieved in DLWE. Further computations with other compounds showing PE are needed to validate the hypothesis.

4.3.3 Modeling Solid Solution for Other Compounds of First and Second Generations

Examples from first and second generation were added to the comparison (TABLE III.15). The same computation was performed for one permutation each time with the same protocol as described before (TABLE III.16).

TABLE III.15 – Name and structure of compound used for computation of their ΔU

Name	Structure
NNMe ₃ (FIGURE I.24 p. 32) ⁶⁸	UHAWAB
NBMe ₃ (FIGURE I.24 p. 32) ⁶⁸	XUQYAJ
Arginine fumarate ²²	NOLPEL
Ketoprofen ⁷³	KEMRUP
Leucine oxalate ⁷²	WIPQQE
Tryptophan ethyl ester hydrochloride	DLTRPE

TABLE III.16 – Computed energy (kcal/mol) from reference structure and modeled solid solutions of crystal structures presented in TABLE III.15

Structure	First generation				Second generation						Not performing PE	
	UHAWAB		XUQYAJ		NOLPEL		KEMRUP		WIPQQE		DLTRPE	
	Ref	Solid sol	Ref	Solid sol	Ref	Solid sol	Ref	Solid sol	Ref	Solid sol	Ref	Solid sol
E_{lattice}	-7079.54	-7051.58	-8143.94	-8178.86	-27163.97	-27163.14	-2810.8	-2789.71	-7729.11	-7728.22	-3650.78	-3604.92
E_{guest}	5.96	15.05	1.27	12.98	-237.12	-238.33	-17.29	-15.23	-2.29	-3.53	99.10	106.30
E_{host}	-6890.17	-6885.55	-7961.01	-7997.22	-26780.16	-26774.77	-2724.02	-2717.95	-7560.35	-7559.97	-3570.34	-3567.61
U_{lattice}	-195.34	-181.08	-184.21	-194.62	-146.69	-150.04	-69.49	-56.54	-166.46	-164.72	-179.54	-143.61
ΔU		14.26		-10.42		-3.36		12.94		1.74		35.93

A comparison of the ΔU values shows that the same trend is obtained for all compounds showing PE. ΔU values are rather low which is in agreement with the occurrence of a

solid solution type behavior incompatible with the structure of DLWE.

4.4 Further Preferential Enrichment after the End of the Process

An important conclusion of our work concerning addition of labeled L-Arginine is that even at the end of PE (*i.e.* the absence of supersaturation), the system can still integrate 1‰ of labeled opposite enantiomer in the solid (TABLE III.9 and FIGURE III.30 page 91).

This result prompted us to imagine a derived process of PE that would not require supersaturation.

In agreement with the exchange theory, a first experiment consisting in reducing the e.e. of the mother liquor after PE was designed in order to evaluate the ability of the liquid phase to drive the minor enantiomer inside the deposited crystals.

Firstly, a quantity of a racemic solution was added to the mother liquor after 6 days of a standard PE experiment. The added solution was composed of 12.5 mg of Arg-Fum dissolved in 100 μ L of water (composition corresponding to saturation at 5°C). The system was left for 6 additional days before filtration (TABLE III.17).

TABLE III.17 – Final results (12 days) of PE experiments after the addition of racemic solution at 6 days

Experiment	$m_{\text{initial}}^{\text{a}}$ (mg)	e.e. $_{\text{initial}}^{\text{b}}$ (%)	e.e. $_{\text{liquid 6 d}}^{\text{c}}$ (%)	e.e. $_{\text{after add}}^{\text{d}}$ (%)	$m_{\text{liquid 12 d}}^{\text{e}}$ (mg)	e.e. $_{\text{liquid 12 d}}^{\text{f}}$ (%)	$m_{\text{solid}}^{\text{g}}$ (mg)	e.e. $_{\text{solid}}^{\text{h}}$ (%)
55	850	5.0	92 \pm 2	88 \pm 2	66 \pm 2	95 \pm 1	640 \pm 16	-5.1 \pm 0.5
56	850	5.0	98 \pm 2	74 \pm 2	64 \pm 2	97 \pm 1	693 \pm 17	-4.5 \pm 0.5
57	850	5.0	98 \pm 2	78 \pm 2	67 \pm 2	96 \pm 1	706 \pm 18	-5.3 \pm 0.5

^atotal mass of Arg-Fum at time = 0; ^be.e. at time = 0; ^ce.e. of solution after 6 days; ^de.e. of solution after addition of racemic solution; ^efinal mass of Arg-Fum in solution; ^ffinal e.e. in solution; ^gfinal mass of solid; ^hfinal e.e. of solid

This experiment shows that even if the system is perturbed by manual addition of racemic mother liquor, it spontaneously evolves back to e.e. > 95% as if the system had a memory of chiral discrimination. Further experiments were conducted without any supersaturation they are presented in Appendix E.

5 Conclusion

Results obtained with the monitoring of the preferential enrichment process (*i.e.* final e.e. in the solid phase after less than 15 min after the start of the process) has demonstrated that PE is a continuous process.

The position of the overall composition point is important mainly for the composition of the solid phase. At the same supersaturation, variation of the e.e. can change the sign of the final solid. The low limit of supersaturation for PE is between 2 and 4.

Final composition in the equilibrium state is a racemic solid and a liquid with 75-80% e.e.; after 1 year in stagnant conditions this equilibrium was not reached.

The addition of labeled arginine during the process at different time, with slightly L or D rich samples, demonstrated that there is an exchange between the minor enantiomer in the liquid and the minor enantiomer in the solid.

With or without polymorphic transition, PE can be achieved.

Molecular modeling seems to indicate that for PE success there is a need for low energetic impact of the substitution of enantiomers near the racemic composition. By contrast when there is a high energetic penalty associated with the substitution no PE can be observed (see tryptophan ethyl ester hydrochloride in Appendix D).

It is possible to add a racemic solution to the mother liquor obtained at the end of PE and to observe a return to high e.e. in the solution *i.e.* 95% e.e.

General Conclusion: About the Mechanism of Preferential Enrichment and Revision of the Required Criteria

Summary of the main results

During this work different parameters of the mechanisms proposed by Tamura (described in Chapter I Section 6.2) have been investigated, using an Arg-Fum salt as a model compound.

- First of all, by monitoring the PE process from 15 min to 6 days we observed that the slightly enriched enantiomer in the solid phase was always opposed to the excess enantiomer in the initial solution and in the mother liquor after 6 days; the ee in the mother liquor was continuously increasing up to 95%. This observation allows us to conclude that PE phenomenon observed for Arg-Fum salt does proceed by a continuous process and does not include a two-step process consisting of a first crystallization and the subsequent polymorphic transition followed by a selective redissolution of one enantiomer into the mother liquor, which was commonly observed for the first generation compounds showing an excellent PE phenomenon.
- This first consideration is further supported by our in-situ X-ray diffraction experiments: various phases and polymorphic transitions were observed during several PE experiments while they exhibited the same e.e. evolution for both the solid and the liquid phases. This also highlights that the occurrence of polymorphic transitions is not linked to the mechanism of PE: it is rather a consequence of the high supersaturation of the system.
- Stagnant conditions are required for this *out of equilibrium* process to be achieved.
- Our molecular modeling results suggest that compounds classified into a solid solution with a specific crystal structure are likely to show a PE phenomenon.
- The distribution of L-labeled-Arginine added in the course of a PE experiment proves that there are exchanges between enantiomers from the mother liquor and from the deposited crystals.

In the next section, these main results will be considered to propose a revised version of the PE mechanism.

Mechanism of Preferential Enrichment for Second Generation Compounds

For an easier understanding Arg-Fum salt is schematically represented (FIGURE 1).

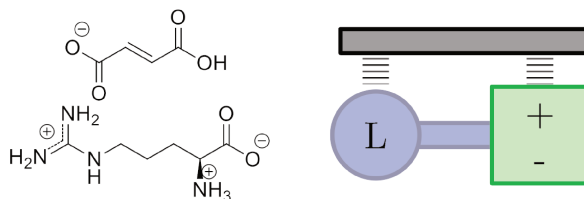


FIGURE 1 – Schematic representation of Arg-Fum salt

From this schematic representation a bidimensional ribbon of the crystal structure (Chapter III Section 2.1) can be derived and is shown in FIGURE 2.

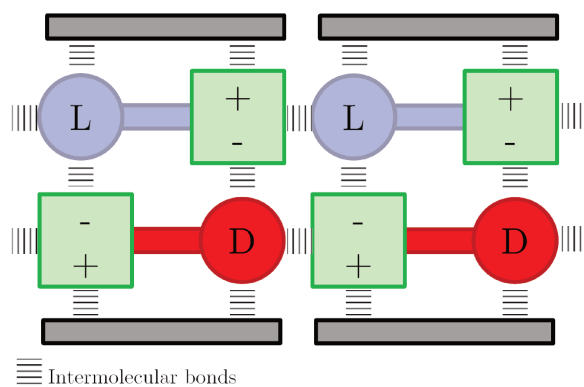


FIGURE 2 – Schematic representation of the crystal packing of Arg-Fum

Analysis of the molecular interactions indicates that H-Bonds linking two arginine entities of opposite chirality (*i.e.* heterochiral dimers ($d_{\text{donnor/acceptor}} = 2.877 \text{ \AA}$)) are stronger than H-Bonds linking arginine entities of the same chiralities (*i.e.* homochiral chains ($d_{\text{donnor/acceptor}} = 2.919 \text{ \AA}$)). Nevertheless by analyzing supersaturated solutions of Arg-Fum by infrared spectroscopy the results obtained by Iwama *et al.* suggest that Arg-Fum is rather preassociated as homochiral sheets in supersaturated sheets in supersaturated aqueous solutions.

As there is no tool to discriminate between these two hypothesis, we propose two variants of the PE mechanism of Arg-Fum.

Hypothesis of heterochiral dimeric preassociations in solution

After complete dissolution, it can therefore be supposed that enantiomers are organized into heterochiral dimers rather than homochiral chains while the system is cooled down to the temperature of the process (FIGURE 3) in stagnant conditions.

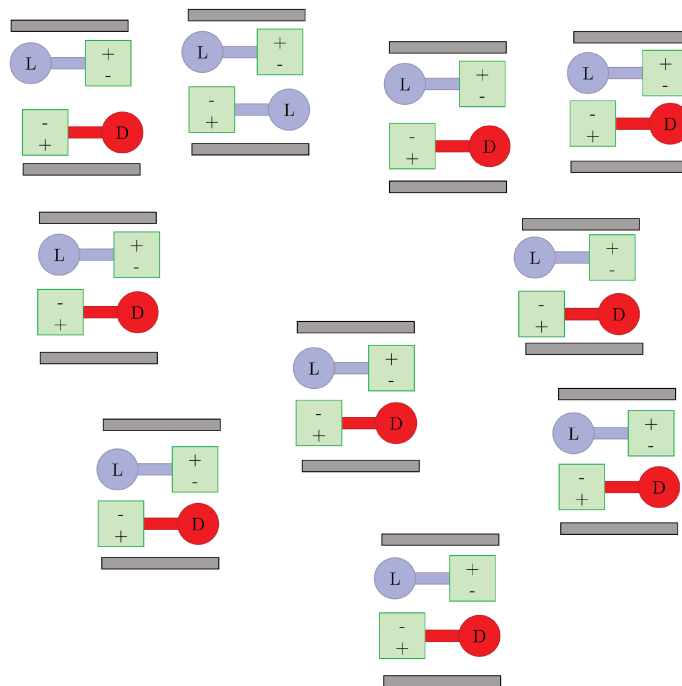


FIGURE 3 – Schematic representation of the putative heterochiral organization in solution of Arg-Fum dimers before crystallization

In order to decrease the high supersaturation ($\beta = 8$ in the case of Arg-Fum), the system kinetically crystallizes these heterochiral dimers (FIGURE 4) due to their lower solubility compared to that of pure enantiomers. Concomitantly, there are exchanges of enantiomers between the mother liquor and the deposited crystals due to the presence of a possible non-stereoselective integration of enantiomers in crystallographic sites (*i.e.* solid solution). The exchanges between the minor enantiomer in the mother liquor and its counter enantiomer in the deposited crystals are favored due to the higher decrease of the supersaturation with the increase of the enantiomeric excess. The exchanges do not occur only at the surface of the crystals: labeled-counter-enantiomer can be found even after dissolving the outer 50% of the mass of deposited crystals although it has been introduced after process completion.

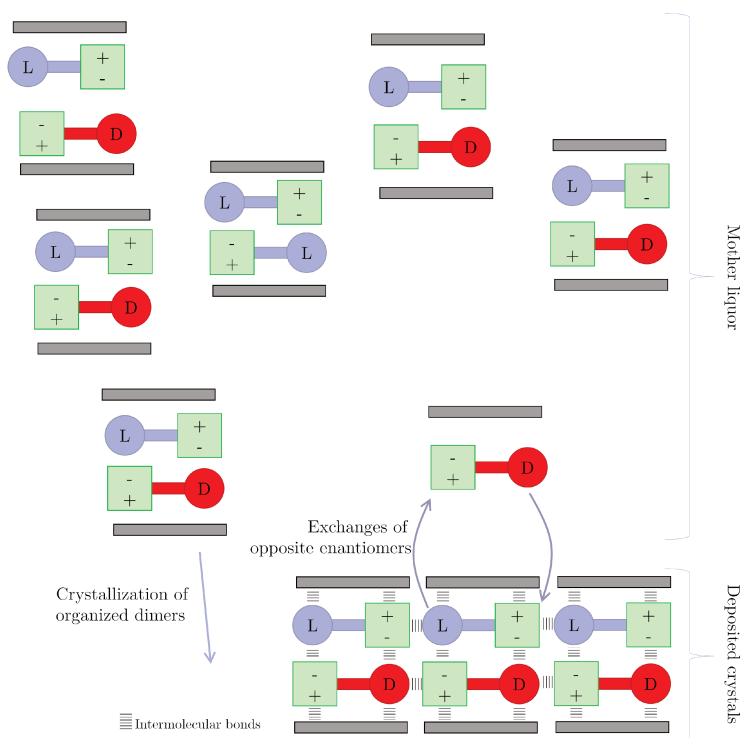


FIGURE 4 – Schematic representation of the crystallization of Arg-Fum dimers occurring concomitantly with exchanges of enantiomers between mother liquor and deposited crystals

The system continues to exchange enantiomers and to increase the e.e. in the mother liquor even after the time where the mass variation of the deposited crystals is no more measurable (*e.g.* 6 h in the Arg-Fum case). At the end of the process, the mother liquor is almost enantiopure and the deposited crystals are slightly enriched with the opposite enantiomer (FIGURE 5). The composition of the mother liquor corresponds to the invariant liquid (doubly saturated^c) (FIGURE 6).

^c. In this case: the invariant point where the solution is saturated in the racemic mixture and in the enantiopure¹⁰⁵

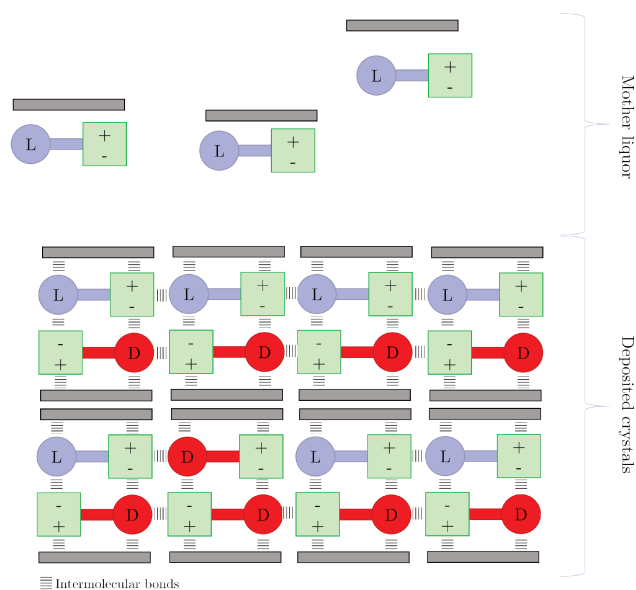


FIGURE 5 – Schematic representation of the final state of the system with almost racemic crystals and a quasi enantiopure mother liquor

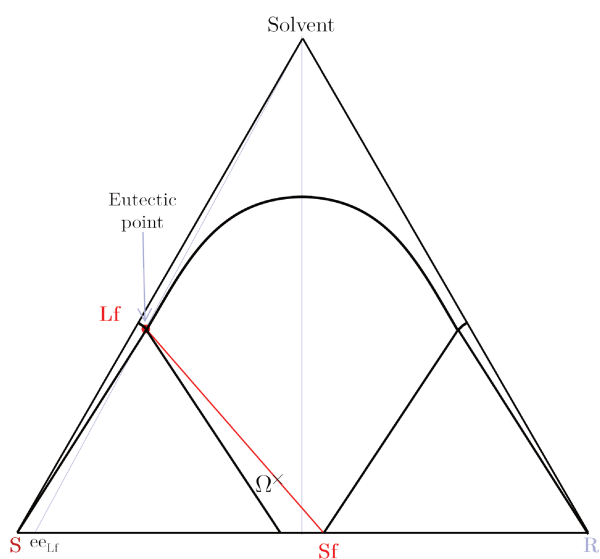


FIGURE 6 – Representation of a theoretical phase diagram of an anticonglomerate system showing PE. The composition of the liquid is limited by the invariant liquid (doubly saturated)

Hypothesis of 2D homochiral preassociations in solution

After complete dissolution, the preassociated Arg-Fum are arranged as homochiral 2D sheets (FIGURE 7) while the system is cooled down to the temperature of the process in stagnant conditions. These sheets stack in an antiparallel fashion, regardless of chirality in a structure that is close to that adopted in the crystalline state (Fig 7b).

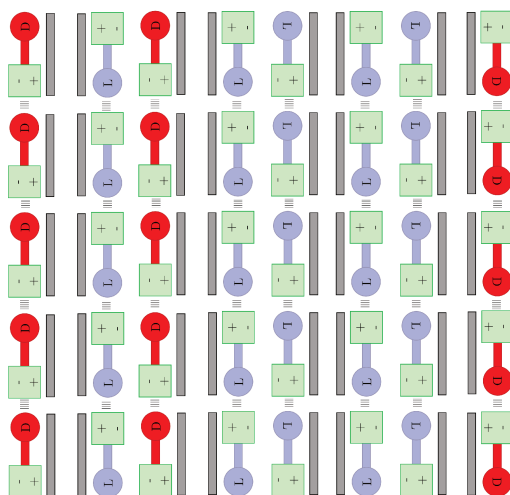


FIGURE 7 – Schematic representation of the putative homochiral organization in solution of Arg-Fum sheets before crystallization

In order to decrease the supersaturation, the system crystallizes these homochiral sheets. Concomitantly there are exchanges of “blocks” of homochiral 2D sheets, these exchanges are non selective. However exchanges between homochiral zone inside the deposited crystals of the global major enantiomer and almost racemic group of sheets from the mother liquor are favored (FIGURE 8).

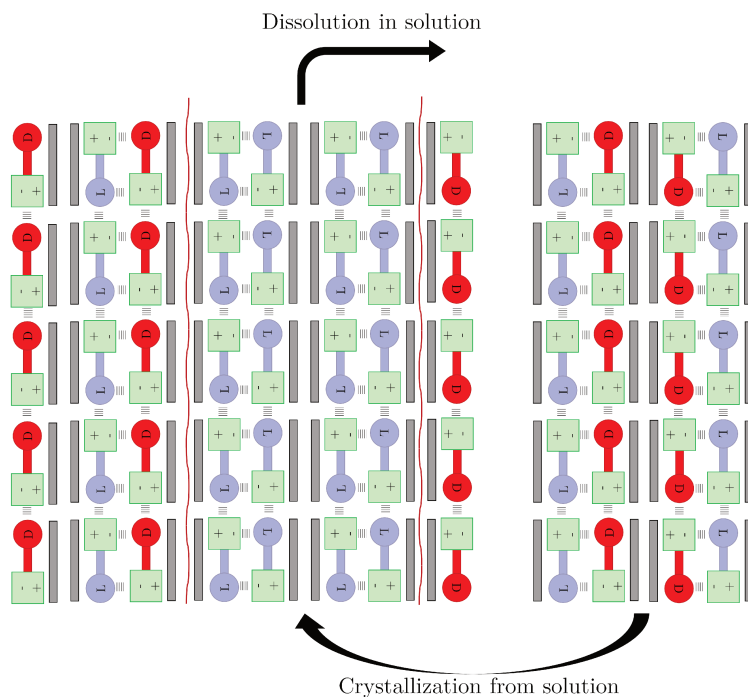


FIGURE 8 – Schematic representation of the replacement of enantiopure sheets from the deposited crystals by a nearly racemic “block” of Arg-Fum giving rise to an exchange of matter between the mother liquor and the deposited crystals

Similarly to the first hypothesis this exchange continues until the mother liquor reaches the doubly saturated invariant (FIGURE 6).

Final state of the system

Yet, the final state of the system (FIGURE 5) has a “certain kind of stability”, it can remain like this during at least 1 year, and after the destabilization of the composition of the liquid phase by reducing its e.e. the system goes back to its “*kind of equilibrium*” in stagnant conditions (*i.e.* e.e._{liquid} = 95%) (FIGURE 9).

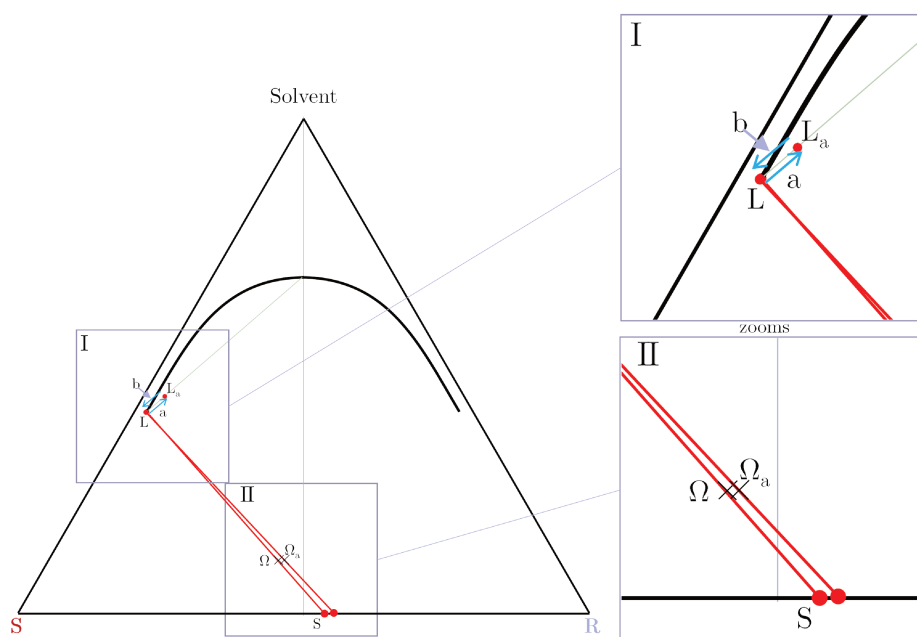


FIGURE 9 – Representation of a simplified theoretical phase diagram of an anticonglomerate system showing PE. The addition of a racemic liquor to the mother liquor creates a slight supersaturation

Indeed, with the addition of a saturated racemic solution, the composition of the mother liquor evolves along the green line (process “a”), and goes back to its initial point (process “b”) at the invariant liquid (doubly saturated). The slight supersaturation induced by the addition is compensated by the deposition of crystals slightly enriched with the same minor enantiomer. The final solid is a bit more enriched.

The most surprising feature of this phenomenon is that the composition of the deposited crystals is driven by the mother liquor and not the reverse: the liquid phase is constantly trying to reach the invariant liquid (doubly saturated), any perturbation (*e.g.* manual addition of opposite enantiomer or racemic mixture) results in the liquid driving the minor enantiomer into the crystals, as if the energy of the system is minimized when this liquid composition is reached. Of course the maximum e.e. of the deposited crystals is

also energetically limited by the boundaries of the solid solution (5 to 6% e.e. in the case of Arg-Fum).

Revised Required Criteria for Preferential Enrichment

Thus, as a consequence of this work, updated requirements for PE can be defined:

1. The solubility of pure enantiomers must be largely higher than the solubility of the racemic composition; more case studies are required to give a definitive ratio of solubility;
2. The deposited crystals need to incorporate the minor enantiomer into the solid phase (*i.e.* solid solution type behavior);
3. The system has to stay in stagnant conditions, because stirring the system jeopardizes PE;
4. The overall composition (Ω) of the system should be in a zone of the ternary phase diagram which allows PE, (*e.g.* for the Arg-Fum system; an initial e.e. < 12% and a $\beta = 4$) are required (FIGURE 10).

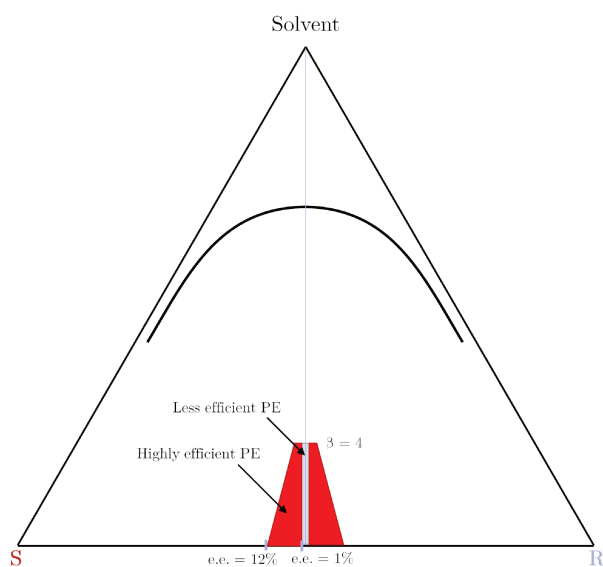


FIGURE 10 – Representation of a simplified theoretical phase diagram of an anticonglomerate system showing PE. The red zone delineates the domain in which PE is optimum; the blue strip corresponds to a zone where PE is observed but with lower performances

In FIGURE 10, the two red zones represent the initial compositions (Ω) for which PE is highly efficient (*i.e.* where $80\% \leq \text{e.e.}_{\text{mother liquor}} \leq 95\%$ at the end of the process). The blue zone represents the initial compositions for which PE is less efficient (*i.e.* $\text{e.e.}_{\text{mother liquor}} < 80\%$ at the end of the process).

Perspectives

Thus, this work opens new perspectives and it is possible to consider new experiments to be conducted to gain an even deeper understanding of PE.

1. Addition of a labeled compound would be useful to prove the enantiomer exchange between the liquid and solid phases for other examples of molecules knowingly performing PE, too.
2. The semi-empirical molecular modeling calculations used during this work can be useful as a new preliminary step to screen for compounds which would perform PE.
3. The work based on Preferential Enrichment after the end of the process (Chapter III Section 4.4) can be pursued to further confirm our mechanism (actually, preliminary works are presented in Appendix E in this regard: a solution at 80% e.e. on a racemic solid which never performed PE seems to go back to the invariant liquid (doubly saturated) at 95% e.e. even with no apparent supersaturation).

It might also be possible to adapt this enrichment without any initial supersaturation and with a solid phase which never performed PE in a continuous flow process for enriching a solution with an e.e. limited to 80%. An enantio-enriched solution would circulate on an immobilized quantity of racemic Arg-Fum, and be enriched up to 95%.

Bibliography

- (1) Lord Kelvin, *Baltimore Lectures on Molecular Dynamics and the Wave Theory of Light*; CUP: 1884.
- (2) Mislow, K. In *Topics in Stereochemistry*; Wiley-Blackwell: 1999, pp 1–82.
- (3) Cahn, R. S.; Ingold, C.; Prelog, V. Specification of Molecular Chirality. *Angewandte Chemie International Edition in English* **1966**, *5*, 385–415.
- (4) Gal, J. In *Differentiation of Enantiomers I*, Schurig, V., Ed.; Topics in Current Chemistry 340; Springer International Publishing: 2013, pp 1–20.
- (5) Schurig, V. In *Differentiation of Enantiomers I*, Schurig, V., Ed.; Topics in Current Chemistry 340; Springer International Publishing: 2013, pp 21–40.
- (6) Morrison, J. D.; Mosher Harry, j. a., *Asymmetric organic reactions*; Englewood Cliffs, N.J. : Prentice-Hall: 1971.
- (7) Nguyen, L. A.; He, H.; Pham-Huy, C. Chiral Drugs: An Overview. *International Journal of Biomedical Science : IJBS* **2006**, *2*, 85–100.
- (8) Harmsen, B.; Leyssens, T. Dual-Drug Chiral Resolution: Enantiospecific Cocrystallization of (S)-Ibuprofen Using Levetiracetam. *Crystal Growth & Design* **2018**, *18*, 441–448.
- (9) Mullin, J. W., *Crystallization*, 4th ed.; Mullin, J. W., Ed.; Butterworth-Heinemann: Oxford, 2001.
- (10) Coquerel, G. Crystallization of molecular systems from solution: phase diagrams, supersaturation and other basic concepts. *Chemical Society Reviews* **2014**, *43*, 2286–2300.
- (11) Gebauer, D.; Kellermeier, M.; D. Gale, J.; Bergström, L.; Cölfen, H. Pre-nucleation clusters as solute precursors in crystallisation. *Chemical Society Reviews* **2014**, *43*, 2348–2371.
- (12) Kashchiev, D.; Rosmalen, G. M. v. Review: Nucleation in solutions revisited. *Crystal Research and Technology* **2003**, *38*, 555–574.
- (13) *Nucleation Theory and Applications*, 1 vols.; Schmelzer, J. W. P., Ed.; Wiley-Blackwell: 2005, 470 pp.
- (14) McCabe, W. L.; Smith, J. C.; Harriott, P., *Unit operations of chemical engineering*; McGraw-Hill: Boston, Etats-Unis d'Amérique, 2005; xxv+1140.
- (15) Voorhees, P. W. The theory of Ostwald ripening. *Journal of Statistical Physics* **1985**, *38*, 231–252.
- (16) Jacques, J.; Collet, A.; Wilen, S. H., *Enantiomers, racemates, and resolutions*; Wiley: 1981.

- (17) Bredikhin, A. A.; Bredikhina, Z. A.; Kurenkov, A. V.; Zakharychev, D. V.; Gubaidullin, A. T. Synthesis, phase behavior and absolute configuration of β -adrenoblocker bupranolol and related compounds. *Journal of Molecular Structure* **2018**, *1173*, 157–165.
- (18) Roozeboom, H. Solubility and melting-point as criteria for racemate compounds, pseudoracemic mix-crystals and inactive conglomerates. *Z. Phys. Chem. Stoechiometrie Verwandtschaftslehre* **1899**, *28*, 494–517.
- (19) Coquerel, G. Solubility of chiral species as function of the enantiomeric excess. *Journal of Pharmacy and Pharmacology* **2015**, *67*, 869–878.
- (20) Ricci, J. E., *The phase rule and heterogeneous equilibrium*, Dover publications, New York, 1966.
- (21) Coquerel, G. In *Novel Optical Resolution Technologies*, Sakai, K., Hirayama, N., Tamura, R., Eds.; Topics in Current Chemistry 269; Springer Berlin Heidelberg: 2006, pp 1–51.
- (22) Iwama, S.; Kuyama, K.; Mori, Y.; Manoj, K.; Gonnade, R. G.; Suzuki, K.; Hughes, C. E.; Williams, P. A.; Harris, K. D. M.; Veessler, S.; Takahashi, H.; Tsue, H.; Tamura, R. Highly Efficient Chiral Resolution of dl-Arginine by Cocrystal Formation Followed by Recrystallization under Preferential-Enrichment Conditions. *Chemistry – A European Journal* **2014**, *20*, 10343–10350.
- (23) Burger, A.; Ramberger, R. On the polymorphism of pharmaceuticals and other molecular crystals. II. *Microchimica Acta* **1979**, *72*, 273–316.
- (24) Bond, A. D. In *Pharmaceutical Salts and Co-crystals*, 2011, pp 9–28.
- (25) Wouters, J.; Quéré, L., *Pharmaceutical salts and co-crystals*; Royal Society of Chemistry: 2011.
- (26) Aitipamula, S. et al. Polymorphs, Salts, and Cocrystals: What's in a Name? *Crystal Growth & Design* **2012**, *12*, 2147–2152.
- (27) Grothe, E.; Meeke, H.; Vlieg, E.; ter Horst, J. H.; de Gelder, R. Solvates, Salts, and Cocrystals: A Proposal for a Feasible Classification System. *Crystal Growth & Design* **2016**, *16*, 3237–3243.
- (28) Roger A., S., *Chirotechnology: Industrial Synthesis of Optically Active Compounds*; CRC Press: 1993; 423 pp.
- (29) Klibanov, A. M. Asymmetric transformations catalyzed by enzymes in organic solvents. *Accounts of Chemical Research* **1990**, *23*, 114–120.
- (30) Schaus, S. E.; Brandes, B. D.; Larrow, J. F.; Tokunaga, M.; Hansen, K. B.; Gould, A. E.; Furrow, M. E.; Jacobsen, E. N. Highly Selective Hydrolytic Kinetic Resolution of Terminal Epoxides Catalyzed by Chiral (salen)CoIII Complexes. Practical Synthesis of Enantioenriched Terminal Epoxides and 1,2-Diols. *Journal of the American Chemical Society* **2002**, *124*, 1307–1315.

- (31) Corey, E. J.; Shibata, S.; Bakshi, R. K. An efficient and catalytically enantioselective route to (S)-(-)-phenyloxirane. *The Journal of Organic Chemistry* **1988**, *53*, 2861–2863.
- (32) Ensley, H. E.; Parnell, C. A.; Corey, E. J. Convenient synthesis of a highly efficient and recyclable chiral director for asymmetric induction. *The Journal of Organic Chemistry* **1978**, *43*, 1610–1612.
- (33) Takaya, H.; Mashima, K.; Koyano, K.; Yagi, M.; Kumobayashi, H.; Taketomi, T.; Akutagawa, S.; Noyori, R. Practical synthesis of (R)- or (S)-2,2'-bis(diarylphosphino)-1,1'-binaphthyls (BINAPs). *The Journal of Organic Chemistry* **1986**, *51*, 629–635.
- (34) Berthod, A. In *Chiral Recognition in Separation Methods: Mechanisms and Applications*, Berthod, A., Ed.; Springer Berlin Heidelberg: Berlin, Heidelberg, 2010, pp 1–32.
- (35) Dalgliesh, C. E. 756. The optical resolution of aromatic amino-acids on paper chromatograms. *Journal of the Chemical Society (Resumed)* **1952**, *0*, 3940–3942.
- (36) *Chiral Recognition in Separation Methods*; Berthod, A., Ed.; Springer Berlin Heidelberg: Berlin, Heidelberg, 2010.
- (37) Pettersson, C. Liquid chromatographic separation of enantiomers using chiral additives in the mobile phase. *TrAC Trends in Analytical Chemistry* **1988**, *7*, 209–217.
- (38) Armstrong, D. W.; Zhang, B. Product Review: Chiral Stationary Phases for HPLC. *Analytical Chemistry* **2001**, *73*, 557 A–561 A.
- (39) Beesley, T. E. Review of Chiral Stationary Phase Development and Chiral Applications. *LCGC Europe* **2011**, *24*, 270–276.
- (40) Ciogli, A.; Kotoni, D.; Gasparri, F.; Pierini, M.; Villani, C. In *Differentiation of Enantiomers I*, Schurig, V., Ed.; Topics in Current Chemistry 340; Springer International Publishing: 2013, pp 73–105.
- (41) Ismail, O. H.; Pasti, L.; Ciogli, A.; Villani, C.; Kocergin, J.; Anderson, S.; Gasparri, F.; Cavazzini, A.; Catani, M. Pirkle-type chiral stationary phase on core-shell and fully porous particles: Are superficially porous particles always the better choice toward ultrafast high-performance enantioseparations? *Journal of Chromatography A* **2016**, *1466*, 96–104.
- (42) Berthod, A.; Liu, Y.; Bagwill, C.; Armstrong, D. W. Facile liquid chromatographic enantioresolution of native amino acids and peptides using a teicoplanin chiral stationary phase. *Journal of Chromatography A* **1996**, *731*, 123–137.
- (43) Juza, M.; Mazzotti, M.; Morbidelli, M. Simulated moving-bed chromatography and its application to chirotechnology. *Trends in Biotechnology* **2000**, *18*, 108–118.
- (44) Lesellier, E.; West, C. The many faces of packed column supercritical fluid chromatography – A critical review. *Journal of Chromatography A* **2015**, *1382*, 2–46.

- (45) Speybrouck, D.; Doublet, C.; Cardinael, P.; Fiol-Petit, C.; Corens, D. The effect of high concentration additive on chiral separations in supercritical fluid chromatography. *Journal of Chromatography A* **2017**, *1510*, 89–99.
- (46) Grand-Guillaume Perrenoud, A.; Veuthey, J.-L.; Guillarme, D. Comparison of ultra-high performance supercritical fluid chromatography and ultra-high performance liquid chromatography for the analysis of pharmaceutical compounds. *Journal of Chromatography A* **2012**, *1266*, 158–167.
- (47) Hostettmann, K.; Marston, A.; Hostettmann, M. In *Preparative Chromatography Techniques: Applications in Natural Product Isolation*; Springer Berlin Heidelberg: Berlin, Heidelberg, 1998, pp 128–134.
- (48) Hardt, I.; König, W. A. Preparative enantiomer separation with modified cyclodextrins as chiral stationary phases. *Journal of Chromatography A* **1994**, *666*, 611–615.
- (49) Hostettmann, K.; Marston, A.; Hostettmann, M. In *Preparative Chromatography Techniques: Applications in Natural Product Isolation*; Springer Berlin Heidelberg: Berlin, Heidelberg, 1998, pp 217–229.
- (50) Schurig, V. Separation of enantiomers by gas chromatography. *Journal of Chromatography A* **2001**, *906*, 275–299.
- (51) Levilain, G.; Coquerel, G. Pitfalls and rewards of preferential crystallization. *CrystEngComm* **2010**, *12*, 1983–1992.
- (52) Gernez Séparation des tartrates gauches et des tartrates droits, à l'aide des solutions saturées. *Comptes rendus hebdomadaires des séances de l'Académie des sciences* **1866**, *63*, 843.
- (53) Secor, R. M. Resolution of Optical Isomers by Crystallization Procedures. *Chemical Reviews* **1963**, *63*, 297–309.
- (54) Collet, A.; Brienne, M. J.; Jacques, J. Optical resolution by direct crystallization of enantiomer mixtures. *Chemical Reviews* **1980**, *80*, 215–230.
- (55) (Coquerel, G.; Petit, M.-N.; Bouaziz, R.). Method of Resolution of Two Enantiomers by Crystallization., WO/1995/008522, 1995.
- (56) (Coquerel, G.; Levilain, G.). Process for the Resolution of Enantiomers by Preferential Evaporative Crystallization., WO/2011/073300, 2011.
- (57) Suwannasang, K.; Flood, A. E.; Coquerel, G. A Novel Design Approach To Scale Up the Temperature Cycle Enhanced Deracemization Process: Coupled Mixed-Suspension Vessels. *Crystal Growth & Design* **2016**, *16*, 6461–6467.
- (58) Viedma, C. Chiral Symmetry Breaking During Crystallization: Complete Chiral Purity Induced by Nonlinear Autocatalysis and Recycling. *Physical Review Letters* **2005**, *94*, 065504.

- (59) Kaptein, B.; Noorduin, W. L.; Meekes, H.; van Enkevort, W. J. P.; Kellogg, R. M.; Vlieg, E. Attrition-Enhanced Deracemization of an Amino Acid Derivative That Forms an Epitaxial Racemic Conglomerate. *Angewandte Chemie International Edition* **2008**, *47*, 7226–7229.
- (60) Noorduin, W. L.; Vlieg, E.; Kellogg, R. M.; Kaptein, B. From Ostwald Ripening to Single Chirality. *Angewandte Chemie International Edition* **2009**, *48*, 9600–9606.
- (61) Sögütöglü, L.; Steendam, R. R. E.; Meekes, H.; Vlieg, E.; Rutjes, F. P. J. T. Viedma ripening: a reliable crystallisation method to reach single chirality. *Chemical Society Reviews* **2015**, *44*, 6723–6732.
- (62) Steendam, R. R. E.; Dickhout, J.; van Enkevort, W. J. P.; Meekes, H.; Raap, J.; Rutjes, F. P. J. T.; Vlieg, E. Linear Deracemization Kinetics during Viedma Ripening: Autocatalysis Overruled by Chiral Additives. *Crystal Growth & Design* **2015**, *15*, 1975–1982.
- (63) Noorduin, W. L.; van Enkevort, W. J. P.; Meekes, H.; Kaptein, B.; Kellogg, R. M.; Tully, J. C.; McBride, J. M.; Vlieg, E. The Driving Mechanism Behind Attrition-Enhanced Deracemization. *Angewandte Chemie International Edition* **2010**, *49*, 8435–8438.
- (64) Uwaha, M. A Model for Complete Chiral Crystallization. *Journal of the Physical Society of Japan* **2004**, *73*, 2601–2603.
- (65) Li, W. W.; Spix, L.; de Reus, S. C. A.; Meekes, H.; Kramer, H. J. M.; Vlieg, E.; ter Horst, J. H. Deracemization of a Racemic Compound via Its Conglomerate-Forming Salt Using Temperature Cycling. *Crystal Growth & Design* **2016**, *16*, 5563–5570.
- (66) Tamura, R.; Takahashi, H.; Hirotsu, K.; Nakajima, Y.; Ushio, T.; Toda, F. Unusual Disordered Crystal Structure of a Racemate Exhibiting a Novel Enantiomeric Resolution: Preferential Enrichment. *Angewandte Chemie International Edition* **1998**, *37*, 2876–2878.
- (67) Tamura, R.; Takahashi, H.; Fujimoto, D.; Ushio, T. In *Novel Optical Resolution Technologies*, Sakai, K., Hirayama, N., Tamura, R., Eds.; Topics in Current Chemistry 269, DOI: 10.1007/128_069; Springer Berlin Heidelberg: 2006, pp 53–82.
- (68) Tamura, R.; Iwama, S.; Takahashi, H. Chiral Symmetry Breaking Phenomenon Caused by a Phase Transition. *Symmetry* **2010**, *2*, 112–135.
- (69) Tamura, R.; Fujimoto, D.; Lepp, Z.; Misaki, K.; Miura, H.; Takahashi, H.; Ushio, T.; Nakai, T.; Hirotsu, K. Mechanism of Preferential Enrichment, an Unusual Enantiomeric Resolution Phenomenon Caused by Polymorphic Transition during Crystallization of Mixed Crystals Composed of Two Enantiomers. *Journal of the American Chemical Society* **2002**, *124*, 13139–13153.
- (70) Iwama, S.; Horiguchi, M.; Sato, H.; Uchida, Y.; Takahashi, H.; Tsue, H.; Tamura, R. Observation of the Preferential Enrichment Phenomenon for Essential α -Amino Acids with a Racemic Crystal Structure. *Crystal Growth & Design* **2010**, *10*, 2668–2675.

- (71) Gonnade, R. G.; Iwama, S.; Mori, Y.; Takahashi, H.; Tsue, H.; Tamura, R. Observation of Efficient Preferential Enrichment Phenomenon for a Cocrystal of (dl)-Phenylalanine and Fumaric Acid under Nonequilibrium Crystallization Conditions. *Crystal Growth & Design* **2011**, *11*, 607–615.
- (72) Manoj, K.; Takahashi, H.; Morita, Y.; Gonnade, R. G.; Iwama, S.; Tsue, H.; Tamura, R. Preferential Enrichment of DL-Leucine Using Cocrystal Formation With Oxalic Acid Under Nonequilibrium Crystallization Conditions. *Chirality* **2015**, *27*, 405–410.
- (73) Gonnade, R. G.; Iwama, S.; Sugiwake, R.; Manoj, K.; Takahashi, H.; Tsue, H.; Tamura, R. Occurrence of spontaneous resolution of ketoprofen with a racemic crystal structure by simple crystallization under nonequilibrium preferential enrichment conditions. *Chemical Communications* **2012**, *48*, 2791.
- (74) Uchida, Y.; Iwama, S.; Coquerel, G.; Tamura, R. A Kinetic/Thermodynamic Origin of Regular Chiral Fluctuation or Symmetry Breaking Unique to Preferential Enrichment. *Chemistry – A European Journal* **2016**, *22*, 11660–11666.
- (75) Takahashi, H.; Iwama, S.; Clevers, S.; Veessler, S.; Coquerel, G.; Tsue, H.; Tamura, R. In Situ Observation of Polymorphic Transition during Crystallization of Organic Compounds Showing Preferential Enrichment By Means Of Temperature-Controlled Video-Microscopy and Time-Resolved X-ray Powder Diffraction. *Crystal Growth & Design* **2017**, *17*, 671–676.
- (76) Iwama, S.; Takahashi, H.; Tsue, H.; Tamura, R. Case Study on the Interpretation of Crystal Structures Inducing Preferential Enrichment Based on the Graph Set Analysis of Hydrogen Bond Motifs. *Crystal Growth & Design* **2015**, *15*, 3052–3062.
- (77) Squellerio, I.; Tremoli, E.; Cavalca, V. Quantification of arginine and its metabolites in human erythrocytes using liquid chromatography–tandem mass spectrometry. *Analytical Biochemistry* **2011**, *412*, 108–110.
- (78) Wang, H.-Y.; Hu, P.; Jiang, J. Rapid Determination of Underivatized Arginine, Ornithine, Citrulline and Symmetric/Asymmetric Dimethylarginine in Human Plasma by LC–MS. *Chromatographia* **2010**, *71*, 933–939.
- (79) Wang, Z.; Tang, W. H. W.; Cho, L.; Brennan, D. M.; Hazen, S. L. Targeted Metabolomic Evaluation of Arginine Methylation and Cardiovascular Risks. *Arteriosclerosis, Thrombosis, and Vascular Biology* **2009**.
- (80) Brown, C. M.; Becker, J. O.; Wise, P. M.; Hoofnagle, A. N. Simultaneous Determination of 6 l-Arginine Metabolites in Human and Mouse Plasma by Using Hydrophilic-Interaction Chromatography and Electrospray Tandem Mass Spectrometry. *Clinical Chemistry* **2011**, *57*, 701–709.
- (81) Bh, P.; are; Madhavan, P.; Rao, B. M.; Rao, N. S. Determination of arginine, lysine and histidine in drug substance and drug product without derivatisation by using HILIC column LC technique. *Journal of Chemical and Pharmaceutical Research* **2010**, *2*.

- (82) Koppenhoefer, B.; Graf, R.; Holzschuh, H.; Nothdurft, A.; Trettin, U.; Piras, P.; Roussel, C. CHIRBASE, a molecular database for the separation of enantiomers by chromatography. *Journal of Chromatography A* **1994**, *666*, 557–563.
- (83) Armstrong, D. W.; DeMond, W. Cyclodextrin Bonded Phases For the Liquid Chromatographic Separation of Optical, Geometrical, and Structural Isomers. *Journal of Chromatographic Science* **1984**, *22*, 411–415.
- (84) Hinze, W. L.; Riehl, T. E.; Armstrong, D. W.; DeMond, W.; Alak, A.; Ward, T. Liquid chromatographic separation of enantiomers using a chiral β -cyclodextrin-bonded stationary phase and conventional aqueous-organic mobile phases. *Analytical Chemistry* **1985**, *57*, 237–242.
- (85) Pawlowska, M.; Chen, S.; Armstrong, D. W. Enantiomeric separation of fluorescent, 6-aminoquinolyl-N-hydroxysuccinimidyl carbamate, tagged amino acids. *Journal of Chromatography A* **1993**, *641*, 257–265.
- (86) Automatized precolumn derivatization as a tool for the direct enantioseparation of amino acids., Symposium, Symposium, International Symposium on Chiral Discrimination (3rd), Tübingen, 1992.
- (87) Ôi, N.; Kitahara, H.; Kisu, N. Enantiomer separation of small amounts of amino acids and hydroxy acids by HPLC using chiral stationary phases and achiral derivatizing reagents. *Bunseki Kagaku* **1995**, *44*, 301–305.
- (88) Armstrong, D. W.; Liu, Y.; Ekborgott, K. H. A covalently bonded teicoplanin chiral stationary phase for HPLC enantioseparations. *Chirality* **1995**, *7*, 474–497.
- (89) Rizzi, A. M.; Cladrowa-Runge, S.; Jonsson, H.; Osla, S. Enantiomeric resolution of derivatized dl-amino acids by high-performance liquid chromatography using a β -cyclodextrin chiral stationary phase: A comparison between derivatization labels. *Journal of Chromatography A* **1995**, *710*, 287–295.
- (90) Ekborg-Ott, K. H.; Liu, Y.; Armstrong, D. W. Highly enantioselective HPLC separations using the covalently bonded macrocyclic antibiotic, ristocetin A, chiral stationary phase. *Chirality* **1998**, *10*, 434–483.
- (91) Hamase, K.; Miyoshi, Y.; Ueno, K.; Han, H.; Hirano, J.; Morikawa, A.; Mita, M.; Kaneko, T.; Lindner, W.; Zaitzu, K. Simultaneous determination of hydrophilic amino acid enantiomers in mammalian tissues and physiological fluids applying a fully automated micro-two-dimensional high-performance liquid chromatographic concept. *Journal of Chromatography A* **2010**, *1217*, 1056–1062.
- (92) Claus, J. E. Chiral HPLC Analysis of Underivatized Amino Acid Enantiomers. *Reporter (Sigma)* **2011**, *29.4*, 8–9.
- (93) Hunt, A. H.; Molloy, R. M.; Occolowitz, J. L.; Marconi, G. G.; Debono, M. Structure of the major glycopeptide of the teicoplanin complex. *Journal of the American Chemical Society* **1984**, *106*, 4891–4895.

- (94) Berthod, A.; Qiu, H. X.; Staroverov, S. M.; Kuznestov, M. A.; Armstrong, D. W. In *Chiral Recognition in Separation Methods: Mechanisms and Applications*, Berthod, A., Ed.; Springer Berlin Heidelberg: Berlin, Heidelberg, 2010, pp 203–222.
- (95) Thompson, M.; Ellison, S. L. R.; Wood, R. Harmonized guidelines for single-laboratory validation of methods of analysis (IUPAC Technical Report). *Pure and Applied Chemistry* **2009**, *74*, 835–855.
- (96) De Figueiredo, T. C.; de Assis, D. C. S.; Menezes, L. D. M.; da Silva, G. R.; Lanza, I. P.; Heneine, L. G. D.; Cançado, S. d. V. HPLC–UV method validation for the identification and quantification of bioactive amines in commercial eggs. *Talanta* **2015**, *142*, 240–245.
- (97) Boqué, Y. V. H. R. The Limit of Detection. *LCGC Europe* **2009**, *22*, 82–85.
- (98) Validation of Analytical Procedures: Text and Methodology : ICH. *Validation of Analytical Procedures: Text and Methodology : ICH* **2005**.
- (99) ASTM E685 - 93(2013) - Standard Practice for Testing Fixed-Wavelength Photometric Detectors Used in Liquid Chromatography. *E685 - 93(2013)* **1993**.
- (100) Tapiero, H.; Mathé, G.; Couvreur, P.; Tew, K. D. I. Arginine. *Biomedicine & Pharmacotherapy* **2002**, *56*, 439–445.
- (101) Coquerel, G.; Sanselme, M.; Lafontaine, A. Method of measuring scattering of x-rays, its applications and implementation device. pat., WO2012136921A1, 2012.
- (102) Courvoisier, L.; Mignot, L.; Petit, M. N.; Coquerel, G. Combined Effect of Polymorphism and Process on Preferential Crystallization: Example with (±)-5(4'-Methylphenyl)-5-methylhydantoin. *Organic Process Research & Development* **2003**, *7*, 1007–1016.
- (103) Brandel, C.; Cartigny, Y.; Coquerel, G.; ter Horst, J. H.; Petit, S. Prenucleation Self-Assembly and Chiral Discrimination Mechanisms during Solution Crystallisation of Racemic Diprophylline. *Chemistry – A European Journal* **2016**, *22*, 16103–16112.
- (104) Gervais, C.; Grimbergen, R. F. P.; Markovits, I.; Ariaans, G. J. A.; Kaptein, B.; Bruggink, A.; Broxterman, Q. B. Prediction of Solid Solution Formation in a Family of Diastereomeric Salts. A Molecular Modeling Study. *Journal of the American Chemical Society* **2004**, *126*, 655–662.
- (105) Coquerel, G. In *Engineering Crystallography: From Molecule to Crystal to Functional Form*, Roberts, K. J., Docherty, R., Tamura, R., Eds.; NATO Science for Peace and Security Series A: Chemistry and Biology; Springer Netherlands: Dordrecht, 2017, pp 215–233.
- (106) Sun, H. COMPASS: An ab Initio Force-Field Optimized for Condensed-Phase Applications Overview with Details on Alkane and Benzene Compounds. *The Journal of Physical Chemistry B* **1998**, *102*, 7338–7364.
- (107) Sun, H.; Ren, P.; Fried, J. R. The COMPASS force field: parameterization and validation for phosphazenes. *Computational and Theoretical Polymer Science* **1998**, *8*, 229–246.

- (108) Ewald, P. P. Die Berechnung optischer und elektrostatischer Gitterpotentiale. *Annalen der Physik* **1921**, *369*, 253–287.
- (109) Vijayalakshmi, B. K.; Srinivasan, R. The crystal and molecular structure of dl-tryptophane ethyl ester hydrochloride. *Acta Crystallographica Section B* **1975**, *31*, 999–1003.

Appendices

A Experimental part

A.1 Materials

DL-arginine 98% was purchased from Alfa Aesar (Schiltigheim, France), L-Arginine 98%, Fumaric acid 97% and D-Methionine 98% were purchased from Acros Organics (Geel, Belgium), $^{13}\text{C}_6$ -L-Arginine 99% was purchased from Cambridge Isotope Laboratories (Andover, MA, USA). Methanol and ethanol were HPLC gradient grade and purchased from VWR (Fontenay-sous-Bois, France), formic acid, analytical grade purchased from Sigma Aldrich (Saint-Quentin Fallavier, France), Water was ultra-purified (18.2 M Ω) with a Elga system from Veolia water solution & technologies (Saint-Maurice, France).

A.2 Recrystallization of Arginine Fumarate

A volume of 35 mL of water was added to 4,35 g of fumaric acid and 6,5 g of DL-Arginine. The suspension was heated up to 80 °C until complete dissolution. The solution was stirred at 5 °C for 2 h. The solid was filtered to obtain arginine fumarate with a 77% yield.

A.3 Protocol of PE experiments

The protocol used was based on the publication of Iwama *et al.*²² Recrystallized racemic arginine fumarate was used after purification as described in Appendix A.2.

For a 850 mg scale experiment with a supersaturation $\beta=8$: a volume of 1.7 mL of water was added to 850 mg of solid at the desired enantiomeric excess, usually 5%, in a 100 mL round-bottomed flask. The suspension was heated up to 80 °C, until complete dissolution using the motor system of a rotary evaporator. Then a volume of 1.7 mL of the antisolvent, EtOH, was added at 60 °C into the solution with a syringe pump at 0.5 mL/min. The solution was cooled at 5 °C in a thermostated bath inside the cold room to avoid temperature variation. After 6 days of crystallization in *stagnant conditions* the solid was filtered. Solid phase and liquid phase were analyzed in HPLC-UV in order to determine concentrations and enantiomeric excess.

This protocol was defined as the *standard protocol*.

A.4 Preparation of samples for HPLC measurements

All samples were stored in a cold room at 5 °C before preparation. This was done to prevent the development of micro-organisms with the L-arginine.

The solid phase was completely dissolved in 100 mL HPLC grade water. The liquid phase and solution from successive dissolutions were completely diluted in 25 mL of HPLC grade water. Final dilutions were made in the vial as described in TABLE A.1. Concentrations of internal standard (D-Methionine) mother solutions were 0.500 mg/mL for HPLC-UV and 0.150 mg/mL for HPLC-MS.

TABLE A.1 – Preparation of samples

			V_{Sample} (μL)	$V_{\text{Internal Standard}}$ (μL)	$V_{\text{Mobile Phase}}$ (μL)
HPLC-UV	Solid		100	100	800
	Liquid		100	100	800
	Successive dissolutions	Washing, S1-S9 and S15-18	500	100	400
		S10-14	200	100	700
HPLC-MS	Solid		200	100	700
	Liquid		400	100	500
	Successive dissolutions	Washing, S1-S9 and S15-18	500	100	400
		S10-14	200	100	700

A.5 Experimental instruments

A.5.1 HPLC-UV

The chromatographic analyses were performed with a liquid chromatograph from Thermo Fisher Scientific (Sunnyvale, CA, USA), an Ultimate 3000 equipped with a LPG-3400SD pump, an ACC-3000 autosampler, a 5 μL loop, a VWD-3400RS UV detector and Chrom-eleon 6.80 software (Thermo Fisher Scientific, Sunnyvale, CA, USA) for acquisition and data processing.

A.5.2 HPLC-ELSD

The chromatographic analyses were performed with a liquid chromatograph from Thermo Fisher Scientific (Sunnyvale, CA, USA), which consisted of a P680 pump, an injection valve (ASI-100 automated sample injector) equipped with a 20 μL injection loop, and a UVD 340U diode-array detector (DAD) and a Polymer Laboratory PL-ELS-2100 evaporative light scattering detector (ELSD), and Chromeleon 6.80 software (Thermo Fisher Scientific, Sunnyvale, CA, USA) for acquisition and data processing.

A.5.3 HPLC-MS

The chromatographic and mass spectrometry analyses were performed with an Agilent 1200 liquid chromatograph system (Agilent, Palo Alto, CA, USA) composed of a G1312A pump, a G1329A autosampler with a 5 or 20 μL loop, a G1316A oven and a G1314B UV detector, a Bruker HCT Ultra (Bruker Daltonics, Bremen, Germany) mass spectrometer, and HyStar 3.2 software (Bruker Daltonics, Bremen, Germany) for acquisition and data processing.

A.5.4 X-ray powder diffraction

XRPD analyses were performed using a D8-Discover diffractometer (Bruker, Germany) equipped with a goniometer of geometry (θ/θ). The incident X-ray beam consisted of the Cu $K\alpha$ radiation ($\lambda=1.5418 \text{ \AA}$) with a tube voltage and amperage set at 40 kV and 40 mA respectively. The X-ray diffraction patterns were collected with a Lynx Eye[®] linear detector (Bruker, Germany). The X-ray diffraction patterns were recorded by steps of 0.04° over the angular 2θ range $3\text{-}30^\circ$ with a counting time of 0.5s per step. The position of characteristic powder diffraction peaks are expressed in degrees 2-theta.

A.5.5 In-SituX

In situ XRPD data were collected using a homemade diffractometer prototype (FIGURE A.1)¹⁰¹ This apparatus has an original goniometer with an inverted geometry ($-\theta/-\theta$). Its association with a dedicated reactor, with a bottom transparent to X-rays, provides the possibility to identify solids in suspension, all along a crystallization process (time and temperature dependent), without any sampling. The detector is a Lynx Eye[®] (Bruker, Germany) and the beam (Ni filtered) comes from an X-ray tube with a copper anticathode.

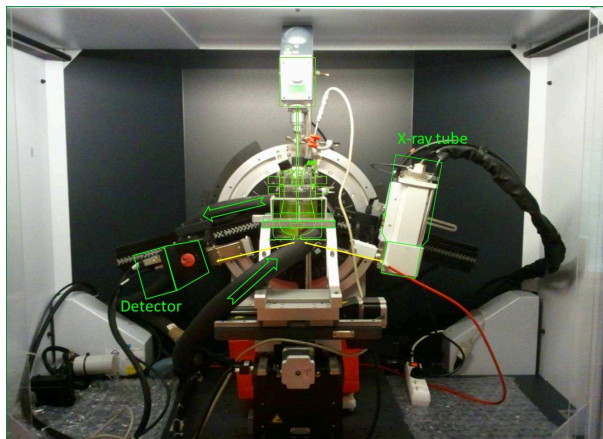


FIGURE A.1 – Photography of the In-SituX setup used in this work

A.5.6 Microscopy

Optical microscopy pictures were obtained on a Hirox (Tokyo, Japan) KH7700 digital microscope system; the lens used was the MX-2016Z. The microscope was placed into the cold room at 5 °C in order to be at the temperature of the process. PE experiments were conducted inside a UV quartz cell of 1 mm × 1 cm × 5 cm.

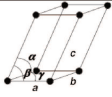
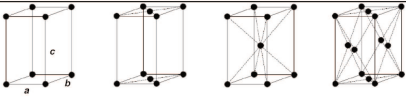
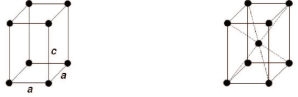
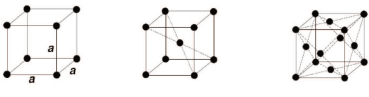
Scanning electron microscopy (SEM) pictures were obtained with a JEOL (Tokyo, Japan) JCM-5000 NeoScope instrument (secondary scattering electron) at an accelerated voltage of 10 kV.

A.6 Molecular modeling

Molecular modeling calculation were performed using Material Studio v8.0 software suite (BIOVIA Accelrys, San Diego, CA, USA). Geometry optimization was performed using Forcite plugin, with COMPASS II forcefield^{106,107} (Condensed-phase Optimized Molecular Potentials for Atomistic Simulation Studies) and the smart algorithm. Charges were calculated by the forcefield; non bonding interactions were computed with the Ewald technique.¹⁰⁸

B Bravais Lattices and Number of Associated Space Groups

TABLE B.1 – Bravais Lattices and Number of Associated Space Groups

Crystal System	Bravais Lattices and Symbols	Dimensions	Number of Space Groups
Triclinic	 P	$a \neq b \neq c$ $\alpha \neq \beta \neq \gamma$	2
Monoclinic	 P C	$a \neq b \neq c$ $\alpha = \gamma = 90^\circ \neq \beta$	13
Orthorhombic	 P C I F	$a \neq b \neq c$ $\alpha = \beta = \gamma = 90^\circ$	59
Tetragonal	 P I	$a = b \neq c$ $\alpha = \beta = \gamma = 90^\circ$	68
Hexagonal	 P	$a = b \neq c$ $\alpha = \beta = 90^\circ$ $\gamma = 120^\circ$	27
Rhomboedral	 R	$a = b = c$ $\alpha = \beta = \gamma \neq 90^\circ$	25
Cubic	 P I F	$a = b = c$ $\alpha = \beta = \gamma = 90^\circ$	36
Total			230

C Method validation supplementary tables and figures

C.1 Specificity

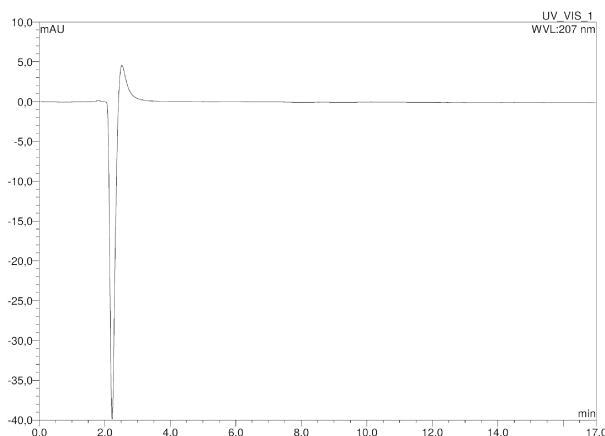


FIGURE C.1 – Chromatogram of the medium for PE experiment (**HPLC conditions 2**)

C.2 Linearity

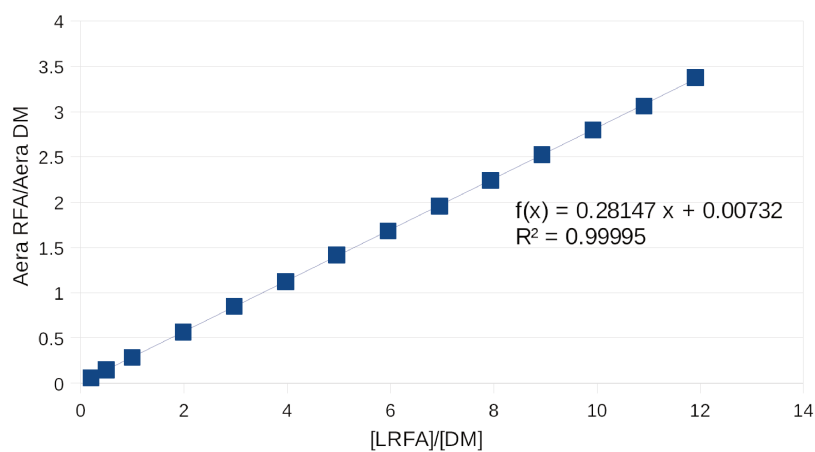


FIGURE C.2 – Calibration curve of L-arginine-fumarate (**HPLC conditions 2**)

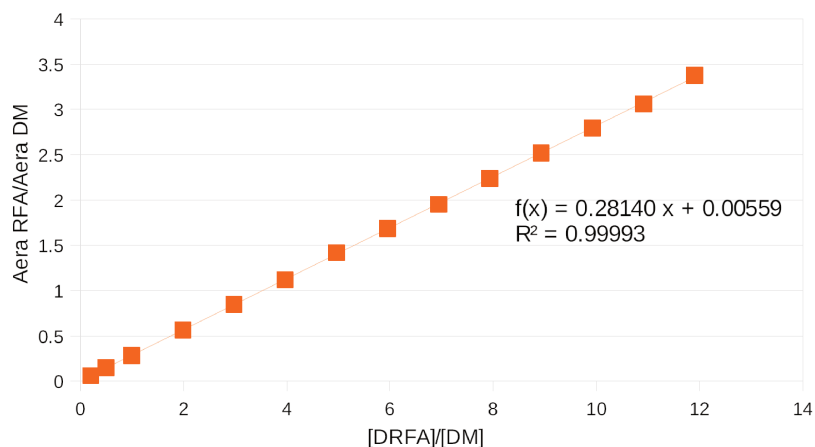


FIGURE C.3 – Calibration curve of D-arginine-fumarate (HPLC conditions 2)

C.3 Precision

C.3.1 Repeatability

TABLE C.1 – Repeatability measurements at Medium level (0.300 mg/mL)

	Area DM	Area LR	Area DR	Area LR/ Area DM	Area DR/ Area DM	e.e. (%)
E8	8.45	14.34	14.28	1.696	1.690	0.2 %
E8	8.43	14.22	14.14	1.687	1.678	0.3 %
E8	8.43	14.27	14.17	1.692	1.680	0.4 %
E8	8.45	14.26	14.22	1.688	1.683	0.2 %
E8	8.39	14.16	14.18	1.689	1.690	-0.1 %
E8	8.43	14.40	14.35	1.708	1.702	0.2 %
Average	8.43	14.28	14.22	1.693	1.687	0.2 %
RSD %	0.3%	0.6%	0.6%	0.5%	0.5%	N/A

TABLE C.2 – Repeatability measurements at High level (0.600 mg/mL)

	Area DM	Area LR	Area DR	Area LR/ Area DM	Area DR/ Area DM	e.e. (%)
E14	8.33	28.35	28.43	3.402	3.411	−0.1 %
E14	8.28	27.92	27.91	3.370	3.369	0.1 %
E14	8.27	27.82	27.84	3.365	3.367	0.0 %
E14	8.22	27.82	27.74	3.373	3.376	0.3 %
E14	8.25	27.72	27.95	3.383	3.386	0.1 %
E14	8.17	27.56	27.57	3.383	3.386	0.0 %
Average	8.25	27.88	27.90	3.379	3.383	0.1 %
RSD %	0.7 %	1.0%	1.0%	0.4 %	0.5 %	N/A

C.3.2 Ruggedness and intermediate precision

TABLE C.3 – Ruggedness measurements at Medium level (0.300 mg/mL)

	Aire DM	Aire LR	Aire DR	Aire LR/ Aire DM	Aire DR/ Aire DM	ee (%)
E8	8.32	14.03	14.03	1.686	1.686	0.0%
E8	8.30	14.05	14.01	1.693	1.688	0.1%
E8	8.40	14.29	14.29	1.701	1.700	0.0%
E8	8.33	14.02	13.93	1.683	1.672	0.3%
E8	8.33	14.03	13.98	1.684	1.679	0.1%
E8	8.28	13.92	13.91	1.682	1.680	0.0%
Average	8.33	14.06	14.02	1.688	1.684	0.1%
RSD %	0.5%	0.9%	1.00%	0.4%	0.6%	N/A

TABLE C.4 – Ruggedness calculation at Medium level (0.300 mg/mL)

	Aire DM	Aire LR	Aire DR	Aire LR/ Aire DM	Aire DR/ Aire DM	ee (%)
Average day 1	8.43	14.45	14.41	1.693	1.687	0.1%
Average day 2	8.33	14.06	14.02	1.688	1.684	0.1%
Average days 1 and 2	8.38	14.17	14.12	1.691	1.686	0.1%
RSD (%) days 1 and 2	0.8%	1.1%	1.00%	0.5%	0.5%	N/A

TABLE C.5 – Ruggedness measurements at High level (0.600 mg/mL)

	Aire DM	Aire LR	Aire DR	Aire LR/ Aire DM	Aire DR/ Aire DM	ee (%)
E14	8.38	28.23	28.20	3.369	3.367	0.0%
E14	8.26	27.85	27.86	3.372	3.372	0.0%
E14	8.35	28.17	28.18	3.374	3.375	0.0%
E14	8.26	27.71	27.71	3.355	3.356	0.0%
E14	8.37	28.21	28.23	3.371	3.372	0.0%
E14	8.33	28.19	28.18	3.383	3.382	0.0%
Average	8.33	28.06	28.06	3.371	3.371	0.0%
RSD %	0.6%	0.8%	0.8%	0.3%	0.3%	N/A

TABLE C.6 – Ruggedness calculation at High level (0.600 mg/mL)

	Aire DM	Aire LR	Aire DR	Aire LR/ Aire DM	Aire DR/ Aire DM	ee (%)
Average day 1	8.25	27.88	27.9	3.379	3.383	0.0%
Average day 2	8.33	28.06	28.06	3.371	3.371	0.0%
Average days 1 and 2	8.29	27.97	27.98	3.375	3.377	0.0%
RSD (%) days 1 and 2	0.8%	0.9%	0.9%	0.3%	0.4%	N/A

D Case of tryptophan ethyl ester hydrochloride

D.1 Preparation and chromatographic conditions

In order to find a new example, tryptophan ethyl ester hydrochloride was tested. The racemic structure was defined as a P1¹⁰⁹ in the CSD (DLTRPE).

A synthesis was performed with the following procedure (FIGURE D.1) for a 5 g scale. 6 mL of Acetyl chloride (AcCl) were added dropwise into 100 mL of EtOH. The mixture was stirred 30 min at 0 °C. A mass of 5 g of tryptophan was added, the suspension was heated at reflux for 3 hours. At the end of the process all the solid was dissolved. The solution was fully evaporated under reduced pressure. A white solid was obtained. A recrystallization was performed in water. The final yield of purified product was 75%.

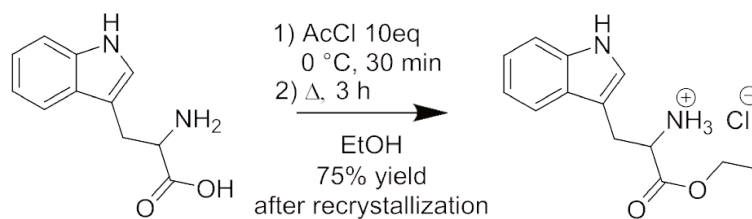


FIGURE D.1 – Synthesis of tryptophan ethyl ester hydrochloride

A chiral separation was performed in SFC with the following conditions (TABLE D.1 and FIGURE D.2) after method development.

TABLE D.1 – SFC conditions for the separation of tryptophan ethyl ester hydrochloride (**SFC Conditions**)

SFC	Waters Investigator
Column	Daicel AD-H 250 mm × 4.6 mm × 5μm
Mobile phase	80/20 CO ₂ /(i-PrOH + 0.3% i-PrNH ₂)
Flow	4 mL
Detection	DAD (λ = 220 nm)
Temperature	35 °C
BPR	120 bar
Injection Volume	10 μL

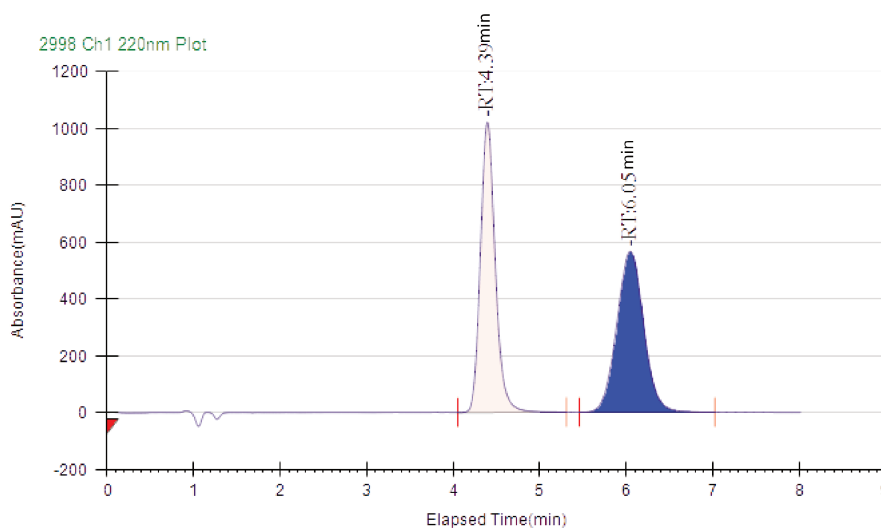


FIGURE D.2 – Separation of tryptophan ethyl ester hydrochloride at 1 mg/mL (**SFC Conditions**)

All samples were prepared with the following conditions (TABLE D.2).

TABLE D.2 – Preparation of samples of tryptophan ethyl ester hydrochloride for the SFC analyses

	$V_{\text{dissolution}}$ (mL)	V_{sample} (μL)	V_{MeOH} (μL)
Solid	100	200	800
Liquid	20	200	800

D.2 Solubility and tests of PE

Measures of solubility were performed with the **SFC Conditions** (TABLE D.3). Most frequently used solvents H₂O, MeOH, EtOH and mixture of solvents H₂O/MeOH, H₂O/EtOH (50/50 v/v) were tested.

TABLE D.3 – Solubility of hydrochloride ethyl ester of L-tryptophan (LWE) and hydrochloride ethyl ester of DL-tryptophan (DLWE) (**SFC Conditions**)

	S_{LWE} (mg/mL)	S_{DLWE} (mg/mL)	$S_{\text{LWE}}/S_{\text{DLWE}}$
H ₂ O	67	23	2.9
MeOH	185	148	1.2
EtOH	42	22	1.9
H ₂ O/MeOH	160	62	2.6
H ₂ O/EtOH	135	73	1.9

In each solvent there is a difference of solubility; the highest solubility differences were obtained in H₂O and H₂O/MeOH mixture.

After the determination of solubilities, tests of PE were performed (TABLE D.4) with the same protocol as for arginine fumarate. In each solvent the highest possible supersaturation was chosen.

TABLE D.4 – Results of preferential enrichment tries on tryptophan ethyl ester hydrochloride (**SFC Conditions**)

Solvent	Volume (mL)	β C/C*	m _{ini} (mg)	e.e.ini (%)	liquid (mg)	e.e.liquid (%)	m _{solid} (mg)	e.e.solid (%)
MeOH	3	2	900	5	189	7 ± 1	700	-0.1 ± 0.5
MeOH	3	2	900	5	90	8 ± 1	800	0.4 ± 0.5
H ₂ O/MeOH	7	2	900	5	447	5 ± 1	450	-0.1 ± 0.5
H ₂ O/MeOH	7	2	900	5	190	7 ± 1	700	0.0 ± 0.5
H ₂ O/EtOH	3	4	900	5	346	16 ± 1	550	0.0 ± 0.5
H ₂ O/EtOH	3	4	900	5	340	19 ± 1	550	0.0 ± 0.5
H ₂ O	3.5	11	900	5	100	28 ± 1	780	-0.1 ± 0.5
H ₂ O	3.5	11	900	5	105	28 ± 1	777	0.0 ± 0.5

Enantiomeric excess of final solids were always 0%, tryptophan ethyl ester hydrochloride was not enriched with PE.

E PE without Supersaturation

E.1 Further Preferential Enrichment after the End of the Process

In order to check if this “memory” is driven by the nature of the solid phase, a different procedure was applied. After 6 days (at the end of the process) of the PE experiment, the mixture was filtered. Then the enantio-enriched liquid was diluted with the saturated racemic solution. The resulting liquid with lower e.e was placed onto 750 mg of *fresh* racemic solid. After 24 hours (time required to reach 95% e.e. for standard PE), a sampling was performed. Then another addition of the saturated racemic solution was performed. At 48 h after the first filtration, the sampling and the addition were repeated. Finally at 72 hours after the first filtration, the system was filtered and analyzed (TABLE E.1 and FIGURE E.1).

TABLE E.1 – Periodic addition of the saturated non-racemic solution and subsequently the saturated racemic solution on a *fresh* racemic solid

Experiment	$m_{\text{initial}}^{\text{a}}$ (mg)	e.e. $_{\text{initial}}^{\text{b}}$ (%)	$m_{\text{solid } 6\text{d}}^{\text{c}}$ (mg)	e.e. $_{\text{solid } 6\text{d}}^{\text{d}}$ (%)	e.e. $_{\text{liquid } 6\text{d}}^{\text{e}}$ (%)	e.e. $_{\text{addition } 1}^{\text{f}}$ (%)	e.e. $_{\text{liquid } 7\text{d}}^{\text{g}}$ (%)
58	850	5.0 \pm 0.5	728 \pm 18	-5.4 \pm 0.5	98 \pm 2	94 \pm 2	97 \pm 2
59	850	5.0 \pm 0.5	541 \pm 14	-5.1 \pm 0.5	98 \pm 2	94 \pm 2	96 \pm 2

Experiment	e.e. $_{\text{addition } 2}^{\text{h}}$ (%)	e.e. $_{\text{liquid } 8\text{d}}^{\text{i}}$ (%)	e.e. $_{\text{addition } 3}^{\text{j}}$ (%)	$m_{\text{mass } 9\text{d}}^{\text{k}}$ (mg)	e.e. $_{\text{liquid } 9\text{d}}^{\text{l}}$ (%)	$m_{\text{solid } 9\text{d}}^{\text{m}}$ (mg)	e.e. $_{\text{solid } 9\text{d}}^{\text{n}}$ (%)
58	76 \pm 2	97 \pm 2	85 \pm 2	74 \pm 2	93 \pm 1	732 \pm 18	-0.2 \pm 0.5
59	86 \pm 2	94 \pm 2	84 \pm 2	74 \pm 2	94 \pm 1	789 \pm 20	-0.3 \pm 0.5

Each experiment was performed according to the protocol described above. ^aglobal mass at $t=0$; ^be.e. at $t=0$; ^cmass of filtrated deposited crystals; ^de.e. of filtrated deposited crystals; ^ee.e. of mother liquor after 6 days; ^fe.e. of mother liquor after the first addition of racemic solution (6 days); ^ge.e. of mother liquor at 7 days (24 hours after the first addition); ^he.e. of mother liquor after the second addition of racemic solution (7 days); ⁱe.e. of mother liquor at 8 days (24 hours after the second addition); ^je.e. of mother liquor after the third addition of racemic solution (8 days); ^kmass of the dissolved Arg-Fum in the mother liquor at 9 days; ^le.e. of the dissolved Arg-Fum in the mother liquor at 9 days; ^mmass of final solid at 9 days; ⁿe.e. of final solid at 9 days.

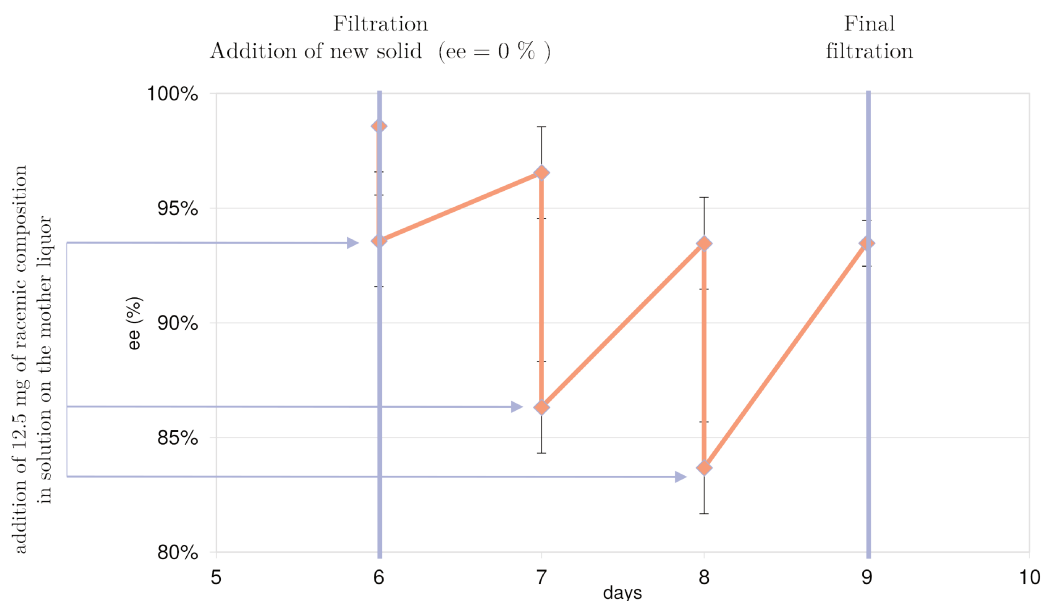


FIGURE E.1 – Periodic addition of the saturated non-racemic solution and subsequently the saturated racemic solution on a *fresh* racemic solid (experiment 59)

TABLE E.1 and FIGURE E.1 highlight that 24 h after each perturbation of the mother liquor, the e.e. in the solution goes back to 95% e.e. in spite of the presence of a fresh racemic solid.

This experiment is thus a further proof that the occurrence of PE is not related to

polymorphic transitions during crystallization and that the nature of the deposited solid does not seem correlated to the genuine PE effect.

E.2 Enrichment without Supersaturation

Since previous experiments have shown that neither the phase nor the e.e. of the crystals during PE is responsible for the success of the symmetry breaking, further experiments have been devoted to investigate the role of the liquid phase.

A fresh solution with a desired e.e. was added to a fresh racemic solid (TABLE E.2 and E.3). Under these conditions neither the solid nor the liquid have gone through PE. The overall composition of the system (Ω) can be read in the phase diagram (FIGURE E.2).

TABLE E.2 – Results of PE without supersaturation with a starting e.e._{liquid} = 80%

Conditions	Experiment	m _{solution} (mg) t=0	e.e. _{solution} (%) t=0	m _{solid} (mg) t=0	m _{solution} (mg) t=24 h	e.e. _{solution} (%) t=24 h	m _{solid} (mg) t=24 h	e.e. _{solid} (%) t=24 h
Stagnant Conditions	60	65	80	750	41 ± 8	94 ± 1	784 ± 20	-0.6 ± 0.5
	61	65	80	750	53 ± 5	87 ± 1	750 ± 19	-0.3 ± 0.5
	62	65	80	750	49 ± 5	95 ± 1	741 ± 19	0.4 ± 0.5
	63	65	80	750	52 ± 5	94 ± 1	787 ± 20	0.4 ± 0.5
30 rpm	64	65	80	750	37 ± 4	83 ± 1	746 ± 19	0.2 ± 0.5
	65	65	80	750	40 ± 4	83 ± 1	649 ± 16	-0.4 ± 0.5

One should note that the initial composition of both the liquid and solid phases correspond to the equilibrium conditions (tie line in FIGURE E.2). If agitated (30 rpm, lower part of TABLE E.2) the system keeps this equilibrium state and no notable e.e. variation is observed in the liquid and in the solid.

Surprisingly, with a starting e.e. in the liquid of 80%, and a racemic solid, if the system is left stagnant, it spontaneously evolves toward 95% e.e. in the liquid phase (there are no noticeable variations of e.e. in the solid phase). The composition point for the liquid, solid and Ω is not compatible with a regular tie line and shows that the system evolves spontaneously out of equilibrium.

TABLE E.3 – Results of PE without supersaturation with a starting e.e._{liquid} = 5%

Duration	Experiment	m _{solution} (mg) t=0	e.e. _{solution} (%) t=0	m _{solid} (mg) t=0	m _{solution} (mg) t=final	e.e. _{solution} (%) t=final	m _{solid} (mg) t=final	e.e. _{solid} (%) t=final
24 h	66	65	5	750	28 ± 3	12 ± 1	801 ± 20	0.0 ± 0.5
	67	65	5	750	26 ± 3	12 ± 1	819 ± 20	0.1 ± 0.5
	68	65	5	750	27 ± 3	11 ± 1	810 ± 20	0.2 ± 0.5
144 h	49	65	5	750	29 ± 3	8.3 ± 0.5	798 ± 20	0.2 ± 0.5
	70	65	5	750	28 ± 3	9.2 ± 0.5	785 ± 20	0.2 ± 0.5
	71	65	5	750	28 ± 3	9.2 ± 0.5	784 ± 20	0.1 ± 0.5

With a starting e.e. in the liquid of 5%, and a racemic solid, the system trends to 10% e.e. in the liquid phase. In this case Ω is around 0.5% e.e. and with a liquid/solid ratio representing an initial β of 8. The system crystallized almost 0% e.e. solid from the solution.

Increase of e.e. in the liquid phase is limited by the position of the Ω point; for e.e. in the liquid phase of 5%, the Ω point was too close to the racemic composition line.

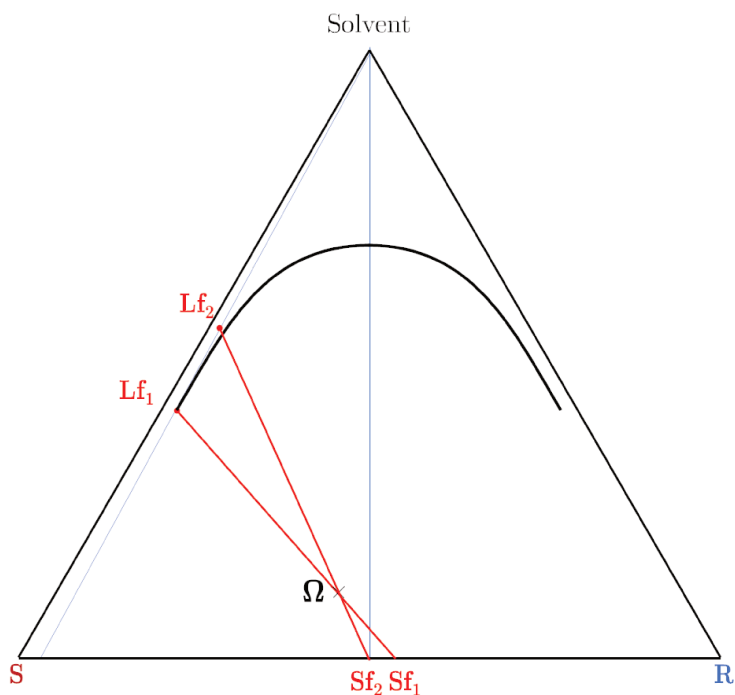


FIGURE E.2 – Theoretical diagram representing: 1) classical PE, 2) PE without supersaturation

Abstract

Preferential Enrichment (PE) is an unusual spontaneous symmetry breaking phenomenon developed by Prof. Tamura's group in the late nineties. Starting with a slightly enriched in one enantiomer, highly supersaturated solution, this out of equilibrium process permits the system to deviate from standard crystallization, in stagnant conditions, in order to obtain a highly enriched mother liquor and deposited crystals slightly enriched in the opposite enantiomer.

The objective of this thesis is to assess the process of PE with the case study of Arginine Fumarate in water/ethanol mixture to obtain a better understanding of its mechanism.

The main results of this work can be summarized as:

- Using time monitoring performed by stopping experiments at 11 different times, PE appeared as a continuous process;
- In situ X-Ray powder diffraction experiments showed that polymorphic transitions are not required for PE, different phases or successions of phases can achieve identical results of preferential enrichment;
- Exchanges between enantiomers of mother liquor and the deposited crystals were demonstrated by addition of labeled-L-Arginine as counter enantiomer during experiments starting with an excess of D-Arginine.

To conclude this work a revised mechanism for PE as a continuous process is proposed. Criteria to achieve PE are reduced to four: i) a strong difference of solubility between pure enantiomers and racemic compound; ii) the racemic compound should crystallize with a solid solution domain; iii) the system should stay stagnant during the complete process; iv) the initial composition should be in the appropriate zone of the phase diagram (*e.g.* for Arg-Fum system a e.e. $< 12\%$ and a $\beta \geq 4$).

Résumé

L'enrichissement préférentiel (PE) est un procédé de brisure de symétrie spontanée non-usuel développé par le groupe du Pr Tamura à la fin des années 90. En commençant avec une solution avec un léger excès énantiomérique et une haute sursaturation, le système dévie de la cristallisation classique, en conditions stagnantes (hors équilibre) vers une solution très enrichie et des cristaux légèrement enrichis dans le contre énantiomère.

L'objectif de cette thèse est d'évaluer le procédé de PE avec le cas d'étude du Fumarate d'Arginine dans un mélange eau/éthanol, pour obtenir une meilleure compréhension de son mécanisme.

Les principaux résultats de ce travail peuvent être résumés ainsi :

- En réalisant un suivi temporel conduit par l'arrêt d'expérience à 11 différents temps le PE apparaît être un procédé continu ;
- Les expériences de diffraction des rayons X montrent que les transitions polymorphiques ne sont pas requises pour le procédé de PE, différentes phases ou successions de phases peuvent conduire à des résultats identiques de PE ;
- Des échanges entre énantiomères de la solution mère et des cristaux déposés ont été démontrés par addition de L-Arginine marquée comme contre énantiomère durant des expériences commençant avec un excès de D-Arginine.

Pour conclure ce manuscrit un mécanisme révisé du PE comme procédé continu est proposé. Les critères pour faire fonctionner le PE sont réduits à quatre : i) une forte différence de solubilité entre les énantiomères purs et le composé racémique ; ii) le composé racémique doit avoir un domaine de solution solide ; iii) le système doit rester stagnant durant tout le procédé ; iv) la composition initiale doit être dans une zone appropriée du diagramme de phase (pour le cas du Arg-Fum : un e.e. $< 12\%$ et un $\beta \geq 4$).